METHANE ACTIVATION VIA BROMINATION
OVER SULFATED ZIRCONIA/SBA-15 CATALYSTS

A THESIS SUBMITTED TO
THE GRADUATE SCHOOL OF NATURAL AND APPLIED SCIENCES
OF
MIDDLE EAST TECHNICAL UNIVERSITY

BY

VOLKAN DEĞİRMENCİ

IN PARTIAL FULFILLMENT OF THE REQUIREMENTS
FOR
THE DEGREE OF DOCTOR OF PHILOSOPHY
IN
CHEMICAL ENGINEERING

NOVEMBER 2007

Approval of the Thesis

"METHANE ACTIVATION VIA BROMINATION OVER SULFATED ZIRCONIA/SBA-15 CATALYSTS"

submitted by **VOLKAN DEĞİRMENCİ** in partial fulfillment of the requirements for the degree of **Doctor of Philosophy in Chemical Engineering Department, Middle East Technical University** by,

Prof. Dr. Canan Özgen
Dean, Graduate School of **Natural and Applied Sciences** _____

Prof. Dr. Gürkan Karakaş
Head of Department, **Chemical Engineering** _____

Prof. Dr. Deniz Üner
Supervisor, **Chemical Engineering Dept., METU** _____

Assist. Prof. Dr. Ayşen Yılmaz
Co-supervisor, **Chemistry Dept., METU** _____

Examining Committee Members:

Prof. Dr. Timur Doğu
Chemical Engineering Dept., METU _____

Prof. Dr. Deniz Üner
Chemical Engineering Dept., METU _____

Prof. Dr. Işık Önal
Chemical Engineering Dept., METU _____

Prof. Dr. Gürkan Karakaş
Chemical Engineering Dept., METU _____

Assist. Prof. Dr. Emiel J.M. Hensen
Chemical Engineering and Chemistry Dept.,
Eindhoven University of Technology, The Netherlands _____

Date: _____

I hereby declare that all information in this document has been obtained and presented in accordance with academic rules and ethical conduct. I also declare that, as required by these rules and conduct, I have fully cited and referenced all material and results that are not original to this work.

Name, Last name:

Signature:

ABSTRACT

METHANE ACTIVATION VIA BROMINATION
OVER SULFATED ZIRCONIA/SBA-15 CATALYSTS

Değirmenci, Volkan

Ph.D., Department of Chemical Engineering

Supervisor   : Prof. Dr. Deniz Üner

Co-supervisor : Assoc. Prof. Dr. Ayşen Yılmaz

November 2007, 157 pages

Methane activation with bromine followed by the condensation of the methyl bromide into higher hydrocarbons or oxygenates is a novel route. However, the selective production of monobrominated methane (CH_3Br) at high conversions is a crucial prerequisite.

A reaction model was developed according to the kinetic data available in the literature and thoroughly studied to investigate the optimum reactor conditions for selective methane bromination in gas phase. It was concluded that at high methane (>90%) conversions dibromomethane synthesis was favored at high selectivity (~90%) under the following conditions: T=330 °C, τ = 3 s, Br:CH_4 = 3.

Sulfated zirconia included SBA-15 catalysts were prepared and characterized for the catalytic methane activation via bromination. The SBA-15 sol-gel preparation technique was followed and the zirconium was added during the preparation in the form of $ZrOCl_2 \cdot 8H_2O$ with 5-30 mol % ZrO_2 with

respect to the SiO_2 content simultaneously with the silicon source (TEOS). The catalysts were sulfated in 0.25 M H_2SO_4 solution.

The zirconium contents of the catalysts were determined by elemental analysis and 15 wt. % Zr was determined as the highest amount. XRD analysis showed the crystalline zirconia peaks only for high zirconia loadings (>25 mol % ZrO_2) indicating the good distribution of Zr in silica framework at lower loadings. BET surface areas of the sulfated catalysts are in the range of 313-246 m^2/g. The porous structures of the catalysts were determined by TEM pictures, which revealed that the increase in Zr content decreased the long range order of pore structure of SBA-15 in agreement with XRD results.

The acidities of the catalysts were determined by ^{1}H MAS NMR experiments. Brønsted acidity was identified by a sharp ^{1}H MAS NMR line at 10.6 ppm. The highest acidity was observed at 5.2 wt. % Zr loading according to ^{1}H MAS NMR experiments. ^{29}Si MAS NMR analysis showed the formation of Si-O-X linkages (X=H, Zr). Further characterization of Brønsted acidity was performed by FT-IR spectroscopy of adsorbed CO at 82 K. The analysis revealed that the Brønsted acidity of sulfated catalysts were similar to the acid strength of the conventional sulfated zirconia. In TPD experiments, the basic molecule isopropylamine (IPAm) was adsorbed and decomposition temperature of IPAm was monitored. The temperature decreased from 340 °C to 310 °C in sulfated catalysts, indicating the acidic character of these samples.

Catalytic methane bromination reaction tests were performed in a quartz tubular reactor. The results showed that 69% methane conversion was attainable over SZr(25)SBA-15 catalyst at 340 °C. The liquid ^{1}H NMR measurements of the products revealed that >99% methyl bromide selectivity was achieved.

ÖZ

SÜLFATLANMIŞ ZİRKONYA/SBA-15 KATALİZÖRLERİ ÜZERİNDE BROMLAMA İLE METAN AKTİVASYONU

Değirmenci, Volkan

Doktora, Kimya Mühendisliği Bölümü

Tez Yöneticisi   : Prof. Dr. Deniz Üner

Ortak Tez Yöneticisi : Yard. Doç. Dr. Ayşen Yılmaz

Kasım 2007, 157 sayfa

Metan aktivasyonunda brom kullanılarak, takibinde metil bromürün hidrokarbon ya da oksijenli bileşiklere dönüşümünün sağlanması yeni bir yöntemdir. Fakat, monobromometan'nın (CH_3Br) yüksek dönüşüm değerlerinde seçici üretimi kritik önceliktir.

Literatürdeki mevcut reaksiyonun kinetiği verileri kullanılarak bir reaksiyon modeli geliştirilmiş ve seçici metan bromlama'nın optimum reaksiyon koşulları incelenmiştir. Yüksek metan dönüşümlerinde (>90%) yüksek dibromometan seçiciliklerine (~90%) şu koşullar yol açmaktadır: T=330 °C, τ = 3 s, Br:CH_4 = 3.

Bromlama ile katalitik metan aktivasyonu için sülfatlanmış zirkonya içeren SBA-15 katalizörleri hazırlanmış ve karakterize edilmiştir. SBA-15 sol-gel hazırlama tekniği takip edilmiş ve zirkonyum hazırlama sırasında $ZrOCl_2 \cdot 8H_2O$ olarak SiO_2'ye göre 5-30 mol % ZrO_2 içerecek şekilde silikon

kaynağı (TEOS) ile birlikte eklenmiştir. Katalizörlerin sülfatlama işlemi 0.25 M H_2SO_4 çözeltisinde yapılmıştır.

Katalizörlerdeki zirkon miktarı elementel analiz ile belirlenmiş ve en fazla 15 wt. % Zr koyulabildiği görülmüştür. XRD sonuçları kristal zircon piklerini yüksek zirkonyum içeriklerinde göstermiş ve düşük içeriklerde SiO_2 yapısı içinde iyi Zr dağılımını işaret etmiştir. Sülfatlanmış katalizörlerin BET yüzey alanları 313-246 m^2/g aralığındadır. TEM fotoğrafları ile belirlenen katalizörlerin gözenek yapısı, artan Zr miktarının SBA-15'in uzun gözenek düzenini bozduğunu göstermiştir.

Asit merkezler ^{1}H MAS NMR deneyleri ile belirlenmiştir. Brønsted asitliği 10.6 ppm'de görülen ^{1}H-MAS NMR piki ile belirlenmiştir. ^{1}H MAS NMR deneylerine göre en yüksek asitlik 5.2 wt. % Zr katalizöründe görülmüştür. ^{29}Si MAS NMR analizleri Si-O-X (X=H, Zr) bağlarının kurulduğunu göstermiştir. CO katalizörler üzerine 82 K'de adsoblanarak FT-IR spektrumları kaydedilmiştir. Analizler katalizörlerin Brønsted asitliğinin konvansiyonel sülfatlanmış zirkonya ile benzer kuvvette olduğunu göstermiştir. TPD deneylerinde bazik bir molekül olan isopropylamine (IPAm) adsorplanmış ve bozunma sıcaklığı gözlenmiştir. Sıcaklık sülfatlanmış katalizörlerde 340 °C'den 310 °C'ye inerek asitlik artışına işaret etmiştir.

Katalitik metan bromlama reaksiyonu sınamaları quartz tüp reaktörlerde yapılmıştır. Sonuçlar 69% metan dönüşümünün SZr(25)SBA-15 katalizörü üzerinde erişilebilir olduğunu göstermiştir. Ürünlerin sıvı ^{1}H NMR ölçümleri >99% seviyesinde metil bromür seçiciliği elde edildiğini göstermiştir.

Anahtar kelimeler: Metan Aktivasyonu, Bromlama, Sülfatlanmış Zirkonya, SBA-15, ^{1}H MAS NMR

To my dearest parents for their perpetual love and support

ACKNOWLEDGMENTS

acknowledged gratefully, as well as their friendship in Eindhoven University of Technology.

The author is thankful to Dr. Jie Fan and Prof. Galen Stucky for providing the TEM images of the catalysts, otherwise a great deficiency in the thesis.

The technical assistance of Mr. Murat Üner in the very beginning of the author's days in the laboratory, for assistance in the microcalorimetry and chemisorption setup, and practical information about how to build up the experimental set-up is well appreciated. Also special thanks are to Bora Atalik who helped through the operation of HP-GC (although not used) and acquaintance at lunch, and studying the "kinetic theory of the geese" in the laboratory for relaxation.

Colleagues in the research group, "Cactus Group" for their patience for the scrupulously tidiness (enduring sometimes) of the author, and creating a friendly environment in the laboratory and sharing unforgettable memories, namely; Murat Üner, Bora Atalik, Volkan Genç, Hakan Önder Olcay, Özlem Özcan, Burcu Akça, Özge Güner, Ebru Erünal, Hilal Demir, Mukaddes Can, Orçun Ergün, Osman Karslıoğlu, Başar Çağlar, Mehmet Kaptan and Mert Oymak. The authors kind regards are not enough to colleges Neelesh, Dilip, Vittorio, Allessandro, Michel, Pieter, and Evgeny in Eindhoven.

Colleagues from the neighboring groups, Belma Soydaş and Ela Eroğlu are kindly appreciated for sharing the depressing environment of the E block in the department. Özlem Dede requires additional emphasis which was a great reason to come to the department enthusiastically and a fresh start everyday to see her pure face. Her presence was marvelous. Indeed, it was invaluable to know that there is somebody to do her best for you without any expectation if you are in need of something.

The technical assistance by Gülten Orakçı in BET measurements, glass worker İsa Çağlar, electrician Nevzat Bekçi (special thanks for assistance in

producing home made tubular ovens), and technicians Adil Demir, Süleyman Arslan, and Ertuğrul Özdemir is appreciated.

TABLE OF CONTENTS

LIST OF TABLES

LIST OF FIGURES

LIST OF SYMBOLS

Å	Angstrom, length unit
ATR	Autothermal Reforming
bbl	Barrel, volumetric unit
bbls	Barrels, volumetric unit
BET	Brunauer-Emmett-Teller
BJH	Barrett-Joyner-Halenda
C_p	Constant Pressure Heat Capacity, J/mol
C_{pp}	Temperature Constants for C_p
cc	Cubic Centimeters, cm^3
CFCs	Chlorofluorocarbons
CSTR	Continuously Stirred Tank Reactor
$\Delta G°$	Gibbs Free Energy of Formation, J/mol
ΔG_{rxn}	Gibbs Free Energy Change on Reaction, kJ/mol
ΔG_{0rxn}	Gibbs Free Energy Change on Reaction at STP, kJ/mol
$\Delta G_{rxn}^°$	Gibbs Free Energy Change on Reaction at STP, kJ/mol
$\Delta H°$	Enthalpy of Formation, kJ/mol
ΔH_{rxn}	Enthalpy Change on Reaction, kJ/mol
ΔH_{0rxn}	Enthalpy Change on Reaction at STP, kJ/mol
$\Delta H_c^°$	Standard Heat of Combustion, kJ/mol
F-T	Fischer-Tropsch
FT-IR	Fourier Transform Infrared
ICDD	International Centre for Diffraction Data
ICP	Inductively Coupled Plasma
ID	Internal Diameter, mm
IEA	International Energy Agency
IPAm	Iso-propylamine

IUPAC	The International Union of Pure and Applied Chemistry
k	Rate Constant of the Reaction, s^{-1}
K_{eq}	Equilibrium Constant
K_0	Equilibrium Constant at Standard States
LNG	Liquefied Natural Gas
LPG	Liquefied Petroleum Gases
M	Molarity, mol/liter
MAS	Magic Angle Spinning
MCM-41	Mobil Composition of Matter No 41
M_n	Molecular Weight, g/mol
MTG	Methanol to Gasoline
MTO	Methanol to Olefins
Mtoe	Million tones oil equivalent
NMR	Nuclear Magnetic Resonance
ppm	Parts per million
R	Universal Gas Constant
R/P ratio	Reserve-to-Production ratio
rxn	Reaction
SBA-15	Santa Barbara Number 15
SMR	Steam Methane Reforming
STP	Standard Temperature and Pressure
Syn-gas	Synthesis Gas, H_2/CO mixture
SZ	Sulfated Zirconia
T	Temperature, K
τ	Residence Time, s
TEM	Transmission Electron Microscopy
TEOS	Tetra Ethyl Ortho Silicate
θ	Reactant Concentration Ratio
TMS	Tetra Methyl Silane
TPD	Temperature Programmed Desorption

TPO	Temperature Programmed Oxidation
XRD	X-ray Diffraction
w.r.t.	With Respect To
ZSM	Zeolite Socony-Mobil

CHAPTER 1

INTRODUCTION AND SCOPE

1.1 HYDROCARBON CONVERSION

In 1956, M King Hubbert proposed a life cycle model for petroleum widely known as ''Hubbert's Model'' [1]. His prediction that oil production in U.S. would peak around 1969, actually happened in 1970, which was only off by one year. The extension of this model towards the 1980s predicted that the rate of world crude oil production would start to decrease after 2000 and petroleum would be exhausted by about 2060 [2]. The insufficient oil production would probably increase the oil price unless the demand for oil decreases. As a consequence, the decline in the crude oil reserves increases the importance of alternative hydrocarbon sources. Natural gas is another large hydrocarbon reserve of the World (as well as coal), which could be a substitute for crude oil. The typical composition of natural gas consists of 70-90% methane and the rest is higher volatile hydrocarbons. However, the end use of natural gas is almost completely methane, above 99% after the extraction of other hydrocarbons.

The dependency on crude oil does not only stem from the energy needs. Olefins are primarily raw materials for most of the available chemicals, from polymers to solvents, through plasticizers, adhesives, detergents and additives, crucial in modern societies. Conventionally, olefins are produced from crude

oil by high temperature, energy consuming processes such as dehydrogenation or cracking. Thus, the utilization of alternative hydrocarbon sources such as coal, and natural gas into ethylene or value-added petrochemicals in the absence of abundant and cheap crude oil would exploit a large hydrocarbon feedstock in a more efficient fashion for the use of our modern society [3].

Natural gas burns cleaner because it is aromatic free rather than coal. In addition, coal mining requires giant extraction activities which make natural gas a more preferred feedstock with present piping infrastructure. Coal and natural gas could be converted into liquid fuels and valuable hydrocarbons in industrial scale currently by either methanol to olefins route or Fischer-Tropsch (F-T) synthesis route. Both methods involve the production of a mixture of carbon monoxide and hydrogen, the mixture of which is called synthesis gas as an initial step. The installation of a synthesis gas production facility requires high investment costs, and thus many different methane conversion methods have been proposed to bypass the high cost of synthesis gas production step.

The processes proposed and studied extensively for methane conversion involve the use of oxygen. It is focused on the formation of ethylene by oxidative coupling of methane or oxygenates – mainly methanol, formaldehyde and dimethylether – by partial oxidation of methane [4-6]. The activation of C–H bond can be achieved by the use of oxygen; however, it reveals the problem of low product selectivity. Although it was the subject of a lot of studies in the beginning of 80's, the remaining selectivity and coking problems decreased the research interest on the oxidative coupling of methane. Another approach is methane conversion under non-oxidative processes [7, 8]. Zeolites and metal or metal oxide modified zeolites are studied extensively [8-10]. Different transition metal catalysts were reported for direct methane conversion into liquid fuels [7, 11]. Similar to the oxidative coupling studies low conversion and selectivity problems remained a challenge for non-oxidative processes.

In addition to the applications mentioned, novel processes were also proposed. One of them is the photo catalytic conversion of methane, which is not yet economical due to the low yields as compared to the high demands of the petrochemical or fuel market [12, 13]. Another novel application is the use of pulsed discharge plasma reactors. Although high methane conversions have been reached, the low energy efficiency remains a great drawback for the commercial applications [14]. Another method is the use of halogens for methane activation, which is discussed in the following section.

1.2 METHANE HALOGENATION

In addition to the methods mentioned above, the utilization of halogens to activate the C–H bond of a methane molecule was proposed for methane conversion [15-19]. The advantage of this method is the high activities of halogen radicals. Instead of producing synthesis gas and the conversion of synthesis gas into methanol, highly reactive halogen radicals can be used to obtain a methanol like molecule easily for further conversions into higher hydrocarbons or oxygenates similar to Mobil's Methanol to Olefins (MTO) or Methanol to Gasoline (MTG) processes. Although it is easy to activate the C–H bond with a radical, it is not easy to control the degree of halogenation. In other words all hydrogen atoms in the methane molecule can be substituted by halogen atoms. The corrosion of the equipment and the probability of explosion due to the use of halogen radicals are the operational difficulties. Since the environmental concerns about halogens results in strict regulations, their release out of the system is not possible. In spite of the disadvantages regarding the industrial operations, among all of the methods, halogenation is a promising way to convert methane into valuable chemicals if high product selectivity can be achieved.

The bromination of methane was reported in the patents of Gas Reaction Technologies Inc. [20, 21] and in the studies of McFarland and coworkers [22-26]. In these studies the partial oxidation of alkanes to alcohols, ethers, or olefins via halogenation were realized. In this route, alkane was brominated in the first part of a reactor followed by a reaction with solid metal oxide to generate oxygenated products in the second part [20]. The second reactor was fed either methanol or methyl bromide. The product distributions for these two different feeds were very similar. However, in the presence of CH_2Br_2, formation of adsorbed carbon and the cross-coupling between CH_2Br_2 and CH_3Br was seen with higher output of aromatics when both reactants were present. The presence of CH_2Br_2 in the feed stream of CH_3Br resulted in formation of aromatics and excessive amount of surface carbon deposition leading to coking. Because of favorable product distribution towards olefins under conditions of low CH_2Br_2 and high CH_3Br concentrations, it is important to obtain high selectivity for CH_3Br in the methane bromination reaction in order to replace the MTO route (Figure 2.6).

In the activation of methane with a halogen atom, other than the gas phase reactions, heterogeneous systems require acid centers to scissor the carbon hydrogen bond (Equation 1.1).

Methane activation in the presence of Brønsted acid:

$$CH_4 \xrightarrow{H^+} \left[H_3C \cdots \begin{matrix} \cdot H \\ \\ \cdot H \end{matrix} \right]^+ \xrightarrow{Br_2} CH_3Br + HBr \qquad (1.1)$$
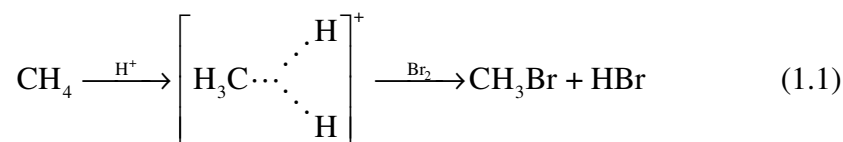
Sulfated zirconia (SZ) is a good candidate, because it shows high catalytic activity in the isomerization of small hydrocarbon molecules at low temperatures, which requires strong acid sites. On the other hand, the relatively small surface area and the low pore volume of the SZ limit its applications.

Therefore, the combination of the advantages of a mesoporous molecular sieve and sulfated zirconia should greatly expand the catalytic activity. Such a material will have the advantages of high acidity, high surface area, uniform pores with adjustable pore diameters. A good distribution of active centers in the mesoporous structure can separate the adsorbed reactants from each other on the catalyst surface. This can inhibit further contact of the adsorbed species, which eventually results in the inhibition of further halogenation. In other words, by the separation of active centers it can be possible to obtain high selectivity towards mono brominated methane molecule.

1.3 MESOPOROUS SILICA AND SULFATED ZIRCONIA

Zeolites are probably the most common materials used as catalysts for oil refining, petrochemistry, and in the production of fine and specialty chemicals as well as their role as a molecular sieve for gas separation. They are well ordered crystalline structures of alumina silicates containing exchangeable cations with pore openings between 3-10 Å. Despite their widespread use in different applications because of their catalytically desirable properties, they can not be used in reactions involving reactants with dimensions above the pore openings of the zeolites [27]. Therefore the synthesis of porous materials with well ordered structures with larger pore diameters than zeolites was investigated thoroughly.

The International Union of Pure and Applied Chemistry (IUPAC) accepted a classification of porous materials according to their pore diameters. According to this classification, porous materials with pore diameters smaller than 2 nm are called microporous, between 2-50 nm are called mesoporous, and with openings above 50 nm are called macroporous materials. The effort to increase the pore diameters of the zeolites were achieved by the discovery of

ordered mesoporous silicas by Mobil scientists in 1992 [28]. The MCM-41 (Mobil Composition of Matter No. 41) is a highly ordered hexagonal array of pores with amorphous silica walls. It has a very narrow pore size distribution with one-dimensional pore openings (Figure 1.1).
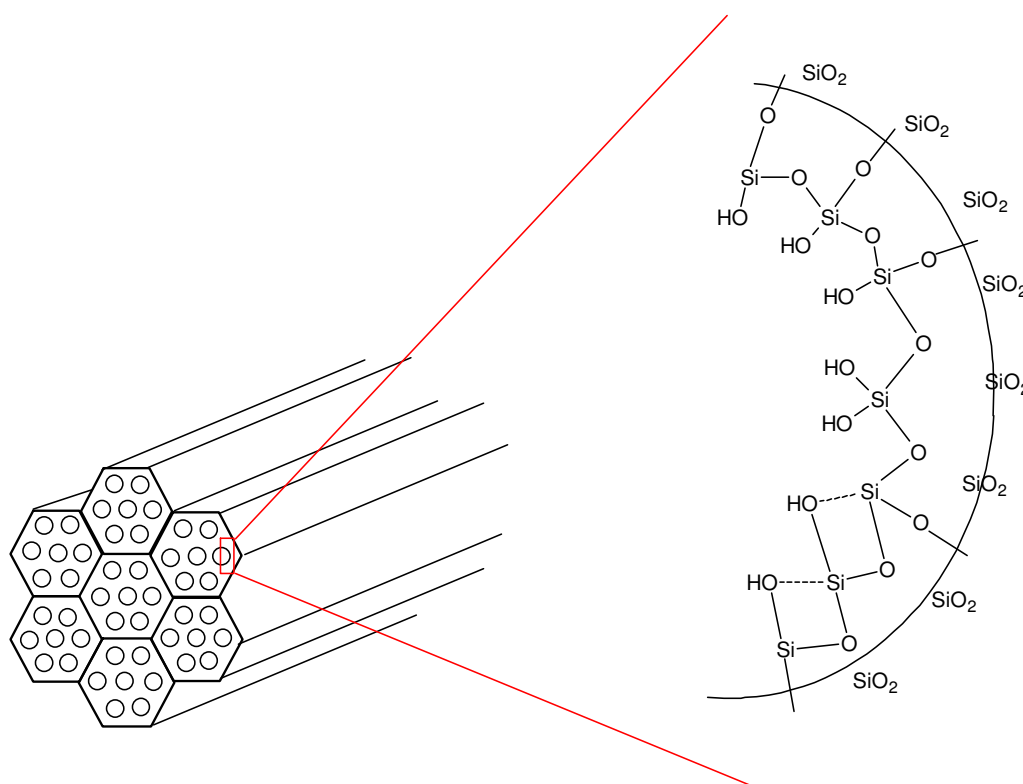
Figure 1.1 Hexagonally arrayed uniform mesoporous structure of SBA-15 and MCM-41 and silanol groups on their inner pore surface.

These mesoporous materials exhibit high surface areas in the range of 600-1300 m^2/g. Their potential in catalytic applications with higher pore diameters as compared to zeolites causes the interest on the successful synthesis of similar materials [29]. Nonetheless, these mesoporous materials have low catalytic activity, which severely hinders their practical applications in catalysis [27]. They are composed of silica (SiO_2) walls and the inner

surface of the material is formed by the neutral or slightly acidic silanol (Si-OH) groups. The lack of the active centers is the reason behind the absence of catalytic activity in catalytic applications and different metals and oxides were included in the mesostructure by different methods [30]. The SBA-15 (Santa Barbara Number 15) mesoporous silica show higher thermal and hydrothermal stability than the other mesoporous silicas due to its thicker pore walls. The higher stability and thick walls thus well hosts the additional atoms in the structure.

The introduction of sulfated zirconia in SBA-15 should provide higher catalytic activity to SBA-15. The conventional sulfated zirconia was prepared by sulfating the zirconium hydroxide. First a zirconium salt (i.e. $ZrOCl_2$, $ZrO(NO_3)_2$) is hydrolyzed with aqueous ammonia to produce zirconium hydroxide. Then the sulfation is performed with a H_2SO_4 or $(NH_4)_2SO_4$ solution [31]. The low pore volume of the conventional sulfated zirconia stimulates search for a higher pore volume structure. In order to obtain higher pore volumes, amorphous silica and γ-alumina were used as a support for sulfated zirconia, and sulfated zirconia was impregnated by incipient wetness technique [32]. Another way was to impregnate a zirconium precursor (i.e. zirconium nitrate) into the support followed by sulfation [33]. MCM-41 [34] and SBA-15 [35-37] were also used as a support for sulfated zirconia. The direct synthesis techniques resulted in catalysts with higher metal loadings and more dispersed active centers on mesoporous silica materials [37-39]. Direct methods involve the introduction of the metal precursor during the synthesis of the SBA-15.

1.4 SCOPE OF THESIS

In this thesis, homogenous gas phase reactions of methane and bromine were modeled, the catalyst – sulfated zirconia included in SBA-15 – was synthesized and characterized and over this catalyst the selective conversion of methane into methyl bromide was investigated. The objective of the study was to develop a deeper understanding of the sulfated zirconia in SBA-15 and its activity on the selective methyl bromide production, which is the most important step in methane activation through halogenation. The ultimate aim of this route is a two-step process, which involves first the conversion of methane into a brominated molecule and second the conversion of this halogenated molecule into a desired hydrocarbon or a mixture of higher hydrocarbons successively. The bromination reaction is the crucial step since the formation of higher substituted brominated methane compounds results in the formation of aromatic compounds and subsequent coke.

As we approach to the inevitable end of abundant oil reserves, global efforts enhance the research on alternatives to crude oil. The summary about the proposed methods for the replacement of oil dependency is given in chapter 2. The gas phase kinetics of the bromination of methane was reported in the 1950s. In Chapter 3 the possibilities of the gas phase selective production of brominated methane were investigated by developing a reactor model based on the kinetic data available in the literature. The characterization of the sulfated zirconia in SBA-15 catalysts were achieved by different techniques, namely ICP, XRD, TEM, BET, ^{1}H and ^{29}Si MAS NMR, FT-IR, and TPD, for which the details are reported in Chapter 4. The methane bromine reaction was studied on a packed bed reactor over the catalyst of sulfated zirconia in SBA-15, the results of which can be found in chapter 5.

CHAPTER 2

METHANE ACTIVATION

2.1 ENERGY MARKET

Energy is a necessity for our civilization. The major source of energy is fossil fuels including crude oil, natural gas, and coal. Hydroelectricity and nuclear energy follows the fossil fuels. 35.8% of the energy needs are supplied by crude oil in the year 2006 (Figure 2.1). It is projected that the energy demand in the world will increase by 1.8% annually, reaching 117.7 billion tones of oil equivalent in the year 2030 [40]. The geothermal and other sources including solar and wind only supply 1.3% of the present energy requirements [41]. Although there is a great interest and utilization of new methods on the renewable resources, they do not much exceed the current levels in the following decade according to recent forecasts [41]. The share of oil (35%) in the total energy use has shrunk over the past several decades as a result of conservation efforts, but it will remain the major energy source (32%) and fossil fuels will remain dominant by the year 2030 [40].

The uses of crude oil are diverse. The products obtained from crude oil fall into three major categories: fuels such as gasoline and diesel fuel; finished non-fuel products such as solvents and lubricating oils; and feedstocks for the petrochemical industry such as naphtha and various refinery gases. 60% of the crude oil is consumed for the production of transportation fuels in refineries

annually (Table 2.1). Developments are progressing in hydrogen, liquefied natural gas (LNG), bioethanol and bio-diesel technologies, but dominant share of oil in transportation fuels has not been overcome yet. Agriculture, residential and commercial uses comprises a big portion with industrial uses in crude oil consumption.

Table 2.1 Percent shares of the fossil fuel uses by sector in 2005. Tabulated from the report of IEA: "Key World Energy Statistics 2007" [42].

	Oil	Natural Gas	Coal
Transport	60.3	5.7	0.6
Industry	9.4	35.1	78.0
Other Sectors[b]	14.5	48.5	17.1
Non-Energy Use[c]	15.8	10.7	4.3

[b] Other sectors comprises agriculture, residential, commercial, public service and non-specified uses.
[c] Non-Energy Use covers the petrochemical feedstocks and uses of other petroleum products such as, paraffin waxes, lubricants, etc.

As follows from Table 2.1, our dependence on oil does not only stem from the energy needs. The non energy use of crude oil involves the finished products in refineries as well as the production of raw materials for petrochemical industry (~5%). Except for the finished products, the feedstocks for petrochemical industry have a share which is much lower than the energy related needs. Nonetheless, they are crucial for supplying, because it invokes the manufacturing of plastics, elastomers, pharmaceuticals, paints and many other chemicals essential for our daily use.
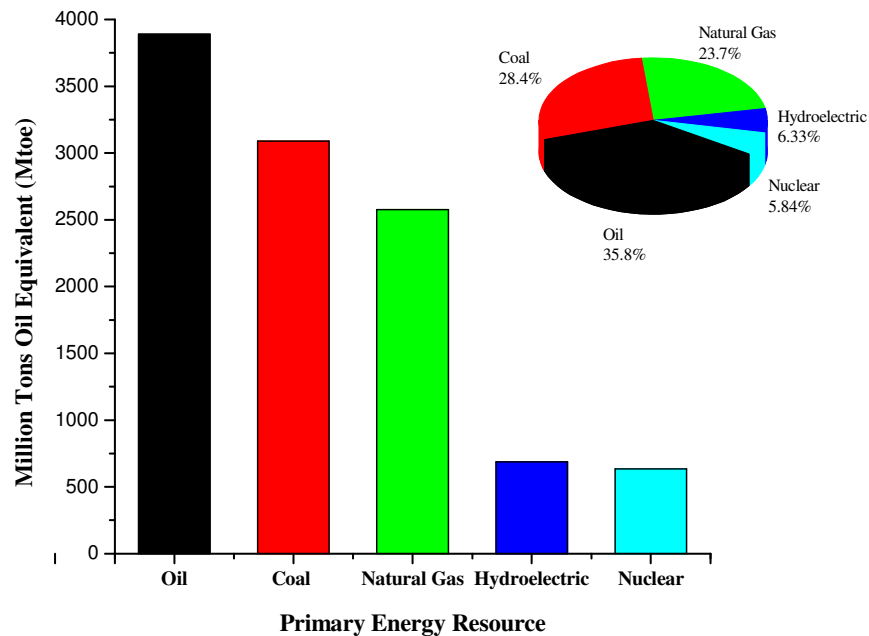
Figure 2.1 World primary energy consumption in 2006. Insert: Percentage of the world energy consumption by primary resource. Obtained from the British Petroleum (BP) report: "Statistical review of world energy June 2007" [43].

2.2 FUTURE PERSPECTIVES

The projection of the future energy trend is not so simple. Thus it can not be foreseen by dividing the initial total reserve to the consumption rate in order to find out the date that we would run out of petroleum. The global energy market is so versatile that the demand and the production rates would change regularly and shifted unexpectedly in some years. During the two Middle East crises in 1973 and 1979 the oil prices tripled and doubled. However, they were not permanent situations, and did not have any relation to the remaining reserves of our planet. It is certain that fossil fuel resources are

nonrenewable. We are running out of oil, so the next increase in the oil prices would be permanent causing the end of the cheap and abundant crude oil era. But, the question is: *"when?"*

M. King Hubbert a geologist from Shell Development Company proposed a life cycle model for petroleum in 1956. It is known widely as "Hubbert's peak" [1]. This model was based on three assumptions. First, a total certain potential petroleum production capacity was assumed, 1250 billions of barrels. The second one is related to the production rate. Due to feasibility reasons it is known that the production rate in a well reaches to a maximum in the operating life time of the well, more likely when the remaining reserve reaches half of the initial amount, than it decreases. Overall oil production was assumed to follow this trend. Third, it was assumed that the production rate is symmetrical according to the maximum point in the timescale. In other words, production rate increases up to a maximum point followed by a symmetrical decrease. In summary, the life cycle of oil production rate follows a bell shaped trend with respect to time.

By using the empirical data of the U.S. oil production statistics, he predicted in 1956 that the oil production in U.S. would peak in year 1969. It actually happened in 1970, only one year off the prediction of Hubbert. The power of the correct prediction gives its fame, and the extension of this model to the world oil market makes it more popular for the evidence of the global oil scenarios for the future. Hubbert himself predicted in 1956 that the world peak would occur near 2000 (Figure 2.2). The predictions are revised continuously by different authors by the accumulation of additional empirical data about world oil production [44]. The world peak is now pushed towards 2010 and the petroleum will be exhausted by about 2060 [2].

Reserve-to-production (R/P) ratios are also predictive for the situation in fossil fuels. Reserves-to-production ratio is an indication of the time that resource lasts. It is obtained by dividing the reserves remaining at the end of any year by the production in that year. Therefore, it indicates the length of

time that those remaining reserves would last if the production rate remains unchanged. R/P ratios of 2006 indicate that the remaining oil would last about 40 years. The situation is 50% better in natural gas, around 65 years. However, coal remains the most abundant fossil fuel in the following decades, about 150 years (Table 2.2).
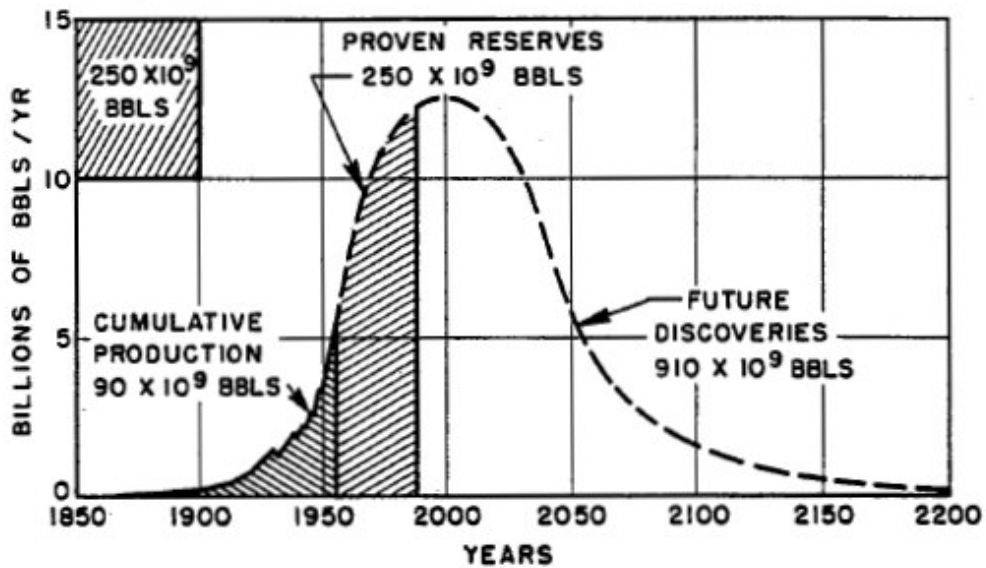
Figure 2.2 Hubbert curve for world crude oil production [1].

In addition to the threats due to the depletion of the reserves and the dependency on petroleum, environmental issues are also important. The public awareness of the environmental problems increases the global concerns, stimulating government incentives for cleaner technologies. Once considered as a nuisance, natural gas is now more preferred to coal and oil in order to decrease air pollution. The constituent of natural gas is primarily methane, and thus the combustion products are carbon dioxide, carbon monoxide and water. In contrast to coal and oil, the emissions of natural gas combustion does not

constitute higher hydrocarbon compounds, particulate matter, nitrogen oxides (NO_x) and sulfur oxides (SO_x) [45].

Table 2.2 R/P ratios of fossil fuels for 2006. Tabulated from the British Petroleum (BP) report: "Statistical review of world energy June 2007" [43].

	Oil	Natural Gas	Coal
R/P ratios	40.5	63.3	147

The increasing demand for natural gas accounts for the increase in the exploration activities. Natural gas is more probable to be formed in greater depths than oil (oil decompose to natural gas at higher temperatures and pressures in the earth's crust) and thus, the improvements in drilling technology also increased the discovery of new reserves. Another untapped natural gas reserve is methane gas hydrates deposited under the deep ocean ground and in Siberia and Alaska in sandstone and siltstone beds [24]. Methane gas hydrates are compounds of methane in different crystal cages of water in different composition with the formula of $CH_4 \cdot nH_2O$. Their amount is estimated to exceed known conventional reserves. Their economical utilization however, has not been achieved yet [46, 47]. Apart from methane gas hydrates, an alternative method of obtaining methane is via biogas generated by the fermentation of organic matter such as wastewater sludge, municipal solid waste (landfills), or any other biodegradable feedstock.

New discoveries, utilization of tar sands, and the technologies with more efficient use of oil are the efforts to extend the abundant and cheap oil era. The current increase in the oil prices could be due to the increase in demand from India and China; however, we will certainly enter a permanent situation that oil would not be abundant and cheap. Thus, the natural gas and coal technologies are becoming increasingly popular with the depletion of oil

reserves. Natural gas is a preferred energy source due to its clean burning, with optimism about the possibility of future discoveries of new resources, utilizing the unconventional reserves, and the production prospects through renewable bio routes.

2.3 INDUSTRIAL OIL ALTERNATIVES

The end of available abundant and cheap oil increases the importance of alternative hydrocarbon sources. Coal and natural gas could be a substitute for crude oil to produce liquid fuels and petrochemicals.

The recent coal and natural gas conversion technologies date back to the beginning of 20th century. The industrial applications of coal and natural gas conversion technologies involve the energy intensive synthesis gas production as a first step. Natural gas is a more preferred resource than coal because it burns cleaner and does not require huge excavation activities. The overview of the recent technology and the research trends for coal and natural gas conversion are explained in the following sections.

2.3.1 Synthesis Gas Production

2.3.1.1 Coal Conversion

Different coal conversion technologies involve direct hydrogenation at elevated temperatures and pressures, solvent extraction, and pyrolysis. Novel technologies for coal conversion were developed for the production of liquid hydrocarbons by different companies (Exxon, Amoco) but could not be realized other than the pilot plant applications [48]. The indirect coal

liquefaction process can only be put into practice, namely synthesis gas production in the first step generally followed by a Fischer-Tropsch synthesis.

Initially, the synthesis gas is produced in a gasifier, using coal as a feedstock. In the coal gasification system, the process is the partial combustion of coal with a mixture of oxygen and steam. Different designs were present with different operating conditions but all are high temperature (1000-1800 °C) and moderate pressure (25-40 atm) systems [48]. The raw synthesis gas coming out of the gasifier contains other constituents such as ash, H_2S, other hydrocarbons and CO_2. It is passed through processes for ash and sulfur removal. The hydrogen to carbon monoxide ratio (~2.0 for F-T synthesis [49]) is adjusted by the use of water gas shift reaction (Equation 2.1) if necessary.

$$CO + H_2O \rightleftharpoons CO_2 + H_2 \qquad \Delta H^o_{rxn} = -41.2 \text{ kJ/mol} \qquad (2.1)$$

2.3.1.2 Natural Gas Conversion

Industrial applications of natural gas conversion are similar to coal based technologies if natural gas is used to produce synthesis gas in the first step. Gas-to-liquid (GTL) is the conversion of natural gas (primarily methane) into liquid fuels, mainly diesel oil and involves the conversion into other hydrocarbons also (naphtha, and LPG). Recently, this is a more preferred method than coal based technology followed by the improvements in the natural gas extraction and piping activities. Synthesis gas can be produced by methane through steam methane reforming (SMR) (Equation 2.2), partial oxidation of methane (Equation 2.3), or the combination, which is called the autothermal reforming (ATR).

Steam methane reforming:

$$CH_4 + H_2O \rightleftharpoons CO + 3H_2 \qquad \Delta H^o_{rxn} = 205.8 \text{ kJ/mol} \qquad (2.2)$$

Partial oxidation of methane:

$$CH_4 + \tfrac{1}{2}O_2 \rightleftharpoons CO + 2H_2 \qquad \Delta H^o_{rxn} = -36 \text{ kJ/mol} \qquad (2.3)$$

Steam methane reforming, and the autothermal reforming are the most common methods of producing commercial bulk hydrogen. It is also the way to produce the hydrogen for the use of the industrial synthesis of ammonia. Water gas shift reaction (Equation 2.1) also takes place during ATR, and an additional shift reactor is placed after the synthesis gas production similar to coal based technology both in SMR and ATR methods.

The natural gas based syn-gas production step is a high temperature (700-1100 °C) and moderate pressure process (~ 35 atm in SMR, and ~60 atm in ATR) in the presence of a nickel based catalyst. The partial oxidation reactors are operated at temperatures between 1300 °C and 1500 °C and pressures up to 70 atm. They require water gas shift reaction taking place either at high temperature (350-550 °C) or low temperature (<300 °C) converters operating at pressures of 30 to 55 atm respectively. The synthesis gas production including the shift reaction accounts for the 50-75% of the total investment in a GTL plant [50]. Therefore, new reactor designs and novel catalysts were pursued to reduce the investment costs. An alternative to SMR and ATR is the direct catalytic partial oxidation of methane (CPO), in which no air blown burner is used. Carbon dioxide reforming of methane is another alternative, which is under investigation [51]. Promising results were reported over Pt and Rh surfaces on a ceramic monolithic reactor, but low H_2 to CO ratio was still a disadvantage [52, 53].

CO_2 reforming of methane:

$$CH_4 + CO_2 \rightleftharpoons 2\,CO + 2\,H_2 \qquad \Delta H_{rxn}^{o} = 247 \text{ kJ/mol} \qquad (2.4)$$

2.3.2 Fischer-Tropsch Synthesis

The hydrocarbon synthesis starts after the production of syn-gas either from coal or natural gas. The synthesis gas produced by coal requires the removal of sulfur and particulate matter. The sulfur and the aromatic free nature of the natural gas enable the production in a simpler system and the use of sulfur intolerant catalysts.

The formation of methane from a mixture of CO and H_2 over a nickel catalyst was described by Sabatier and Senderens in 1902 [54]. Two decades later, in 1920s Fischer and Tropsch reported the formation of higher hydrocarbons over an iron catalyst [55-57]. The procedure was patented in their names in 1926 and the hydrocarbon synthesis based on this method is called by their names afterwards.

The generated synthesis gas with required H_2/CO ratio (~2.0 for F-T synthesis) depending on the application is sent to the synthesis reactor, where it is converted into hydrocarbons at moderate temperature and pressure, typically 225-340 °C and 15 to 60 atm. Depending on the operating conditions, the catalyst employed, and the reactor design, the Fischer-Tropsch synthesis reactor yields a range of products with high molecular weights.

The efforts for the mechanistic explanation of Fischer-Tropsch synthesis lead to different models which are controversial [47, 58]. One early explanation proposed by Fischer involves the dissociation of CO into its elements at first. Then the conversion takes places via adsorbed CH and CH_2 species. The hydrocarbon chain growth by the addition of CH_x species may lead to a chain length distribution of products. The product distributions of the

Fischer-Tropsch synthesis may be predicted using an appropriate mathematical formula. Anderson-Schulz-Flory equation derived for polymerization kinetics was applied to the Fischer-Tropsch synthesis (Equation 2.5).

$$\log\left(\frac{W_n}{n}\right) = n\log\alpha + \log\left(\frac{(1-\alpha)^2}{\alpha}\right) \tag{2.5}$$

W_n is the weight fraction of the products with carbon numer n, and α is the probability that a carbon chain grows by adding another carbon atom rather than termination. When α is zero only CH_4 is formed and wax is the main product as α approaches to one. In between, as a consequence of Anderson-Schulz-Flory statistics, it is not possible to realize 100% selectivity but a fraction of hydrocarbons are obtained with a range in carbon number.

The main products from the process are paraffins (C_1-C_{50} and higher), oxygenates (methanol, higher alcohols, ethers), and olefins. The reactor could be targeted to produce C_2-C_4 olefins or, alternatively, C_{10}-C_{20} paraffins which could then be utilized to produce gasoline.

Examples of reactions take place in Fischer-Tropsch synthesis [48, 58]:

Paraffins:
$$(2n+1)H_2 + nCO \longrightarrow C_nH_{2n+2} + nH_2O \tag{2.6}$$

Olefins:
$$2nH_2 + nCO \longrightarrow C_nH_{2n} + nH_2O \tag{2.7}$$

Oxygenates:
$$2nH_2 + nCO \longrightarrow C_nH_{2n+1}OH + (n-1)H_2O \tag{2.8}$$
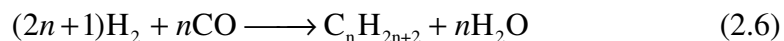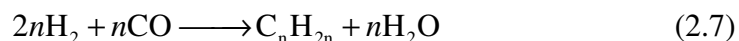
Polymerization:
$$R_n + m\,(CO + 2H_2) \longrightarrow R_{n+m} + mH_2O \tag{2.9}$$
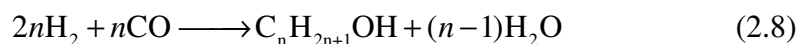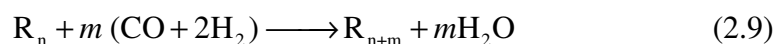
The first commercial catalyst in 1930s was cobalt and thoria based, operated at atmospheric pressure and 200 °C in a fixed bed reactor [47]. It has changed into an iron based catalysts in 1950s. The only and the ever-largest coal based operating plant in South Africa (Sasol) uses an iron on silica catalyst in fixed bed reactor and a fused iron catalyst in a slurry phase reactor. Other than iron, cobalt is also very active in Fischer-Tropsch synthesis, especially for obtaining high yields of parrafinic hydrocarbons, which is used in GTL plants [59]. The research activities on Fischer-Tropsch synthesis were boosted in 1970s due to the two petroleum crises in the beginning and at the end of 1970s. The research interest decreased but still continues by funding through research agencies and governments, and it increases in the years with the peaks in the oil prices. Generally, metal catalysts were under investigation for the Fischer-Tropsch synthesis. The metals were cobalt, nickel, iron and ruthenium impregnated on supports ranging from metal oxides to zeolites [60].

2.3.3 Methanol; Synthesis and Conversion

Methanol synthesis is of enormous industrial importance with an annual production of about 30 million tones all around the world. The largest use of methanol by far, is its use in making other chemicals. The importance in this context is due to the efficient way of converting synthesis gas into valuable chemicals through methanol. The shares of the methanol uses for the production of chemicals in U.S. are given in Figure 2.3.

Globally 40% of methanol is converted into formaldehyde, and from there the products as diverse as plastics, paints, explosives, and textiles were manufactured. Other chemical derivatives of methanol include dimethyl ether, which has replaced chlorofluorocarbons as an aerosol spray propellant.

BASF developed a process to convert syn-gas into methanol in 1923 [61]. Zinc oxide – chromia was used as the catalyst. The process requires

temperature at about 350 °C, and pressures as high as 300-1000 atm [62]. Today, the most widely used catalyst is $Cu/ZnO/Al_2O_3$ first used by the Imperial Chemical Industries in 1966. It is a low pressure process, and at 50-100 atm and at temperatures around 260 °C, it can catalyze the production of methanol from carbon monoxide and hydrogen (Equation 2.10-2.11) with high selectivity (99%) [63].
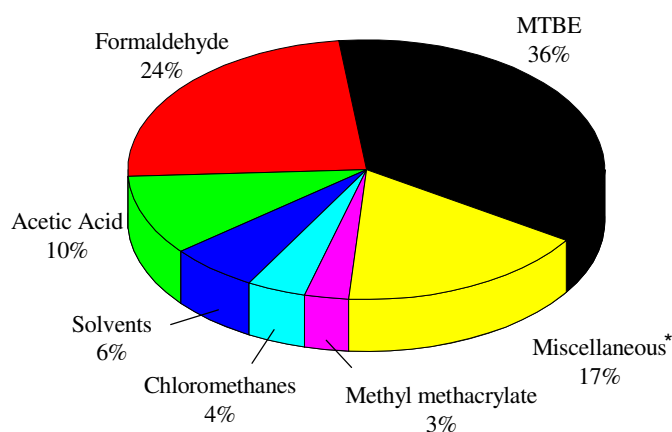
Figure 2.3 The shares of the chemicals synthesized from methanol in U.S. in 1998. The data was tabulated from reference [64]. *Miscellaneous includes methylamines, glycol methyl ethers, dimethyl terephthalate, antifreeze and fuels.

Reactions in methanol synthesis:

$$CO + 2H_2 \rightleftharpoons CH_3OH \qquad (2.10)$$

$$CO_2 + 3H_2 \rightleftharpoons CH_3OH + H_2O \qquad (2.11)$$

However the copper based catalysts are not sulfur and chlorine tolerant, and thus high purity syn-gas produced by methane is used, which dominates the current world wide methanol production technology. Since the early 1980s, less efficient small facilities are being replaced by larger plants using new efficient low pressure technologies.

Methanol can be converted into hydrocarbons over acidic catalysts [65-69]. The general reaction in methanol conversion is the elimination of oxygen (Equation 2.12). Except for the zeolites the catalysts deactivate rapidly.

Methanol conversion reaction:

$$n\text{CH}_3\text{OH} \longrightarrow (CH_2)_n + n\text{H}_2\text{O} \qquad (2.12)$$
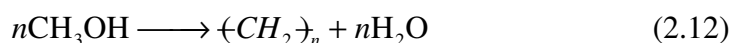
In early 1970s Methanol to gasoline (MTG) and Methanol to olefin (MTO) processes were developed by Mobil with the discovery of ZSM-5 (MFI) catalysts [70]. The development of MTG opens an alternative way for the efficient utilization of syn-gas through methanol. The ZSM-5 is a zeolite, i.e. a member of a class of crystalline aluminasilicates which is comprised of well defined microporous channels. In ZSM-5 (MFI) the channels were 10-ring windows with diameters of 5.5 Å, providing to control the product selectivity depending on the molecular size [71, 72]. Bifunctional catalysts without the shape selectivity properties such as, WO_3/Al_2O_3 are also active in methanol conversion. Despite the intensive research on the mechanism of the methanol transformation into hydrocarbons, many of the details remain unresolved [47]. The development of another zeolite, SAPO-34, enables the selective production of ethylene and propylene. The channel opening of SAPO-34 is smaller (4 Å) than ZSM-5, which restricts the diffusion of higher or branched hydrocarbons, and thus increasing the light olefin yield [73]. The MTO processes can convert methanol into ethylene and propylene at about 75-80% selectivity [74], which is promising for the large scale commercial applications.

2.3.4 Commercial Applications

2.3.4.1 Coal Conversion Plants

The first nine industrial plants for coal conversion were established in Germany in 1930s just after the discovery of Fischer and Tropsch and operated till the end of the World War II. The lack of oil reserves in Germany made the coal based technologies the only alternative for running the war machines during World War II. In that time feasibility was probably out of question, but afterwards the abundant Middle East's oil become incomparably more economical as a source of gasoline and diesel oil. In addition to the plants operated in Germany before World War II [48], a demonstration plant was established in The United States (Missisipi, Luisiana) between 1951 and 1957 (Carthage Hydrocol) [47]. The only plant still in operation for the production of transportation fuels and higher hydrocarbons was established in South Africa in 1950s when the county was faced with a worldwide embargo. Sasol I with the additional two plants (Sasol II and Sasol III) established in 1980s is now producing the ~29% of the oil requirements of South Africa [75], as well as more than 200 different chemicals (mainly diesel oil, naphta and LPG). However, the production capacity is almost 523 times smaller than the world oil consumption in 2006 [43] with a 160,000 bbl/day, requiring coal of about 50 million tons/year. As far as the Sasol's plants and the huge production operations are concerned for coal excavation, transportation and pretreatment, this technology alone seems inadequate for supplying the oil needs of the world in future.

2.3.4.2 Natural Gas Conversion Plants

In 1985, Mobil commercialized its Methanol-to-Gasoline (MTG) technology in New Zealand [76], natural gas being the feedstock. This fixed bed process converts synthesis gas to 4400 tons of methanol per day; the methanol can then be converted to 14,400 bbl/day gasoline. However the plant is used only to produce methanol now.

Shell has a Fischer-Tropsch plant in Bintulu (Malaysia), opened in 1993, with a current production capacity of 14,700 bbl/day. The plant uses The Shell Middle Distillate Synthesis (SMDS) process, which is a modernized way of hydrocarbon production through Fischer-Tropsch technology. First, synthesis gas is obtained by partial oxidation of natural gas with pure oxygen in the Shell Gasification Process. Second, the synthesis gas is converted into liquid hydrocarbons (Heavy Paraffin Synthesis) with a low temperature GTL technology over a cobalt based catalyst. Third, the waxy product is selectively hydrocracked to the desired middle distillate products (Heavy Paraffin Conversion) [77].

Today new projects are launched for integrated processes involving the natural gas conversion into liquid fuels or olefins through either methanol or Fischer-Tropsch technology. Oryx Sasol GTL plant started operation in June 2006 in Quatar. It is based on the syn-gas production through the ATR technology of Topsøe followed by the slurry phase F-T technology of Sasol. It has a capacity of 34,000 bbl/day with a product range of diesel oil, naphtha, and LPG [75]. The joint venture of Sasol and Chevron is planning to increase this capacity by two additional plants with a capacity of 66,000 bbl/day and 130,000 bbl/day. The same joint venture obtained the bid for their GTL project in Nigeria to construct a plant which converts Nigeria's gas into liquid fuels through F-T synthesis with a capacity of 34,000 bbl/day [78].

The most daring investment on the GTL technology is from Shell with their Pearl project in Quatar. The Pearl GTL plant will produce 140,000

bbl/day of GTL products as well as approximately 120,000 bbl/day of associated condensate and liquefied petroleum gas planned for the second stage. The 140,000 barrels per day Pearl GTL plant will be the size of some of the world's largest refineries. The project will be developed in two phases with the first phase operational around the end of the current decade.

2.4 ALTERNATIVES OF METHANE CONVERSION

In an effort to replace crude oil dependency, the motivation of the intensive research is to find an easy way to produce chemicals that we strongly depend on currently. As mentioned in previous sections, there are two commercial methane conversion methods, namely the methanol to hydrocarbons and Fischer-Tropsch synthesis. Both of them involve the production of synthesis gas as a first step and indirectly produce the valuable chemicals for our society (Figure 2.4). Investment and operating cost of the synthesis gas production is very high (50-75% of the total cost in GTL [50]). Therefore, many different methane conversion methods have been proposed to overcome the high cost of syn-gas route and to achieve the direct conversion of methane into ethylene, formaldehyde, methanol or liquid fuels. The economic incentive has stimulated large amount of research in oxidative techniques. Oxidative coupling of methane into higher hydrocarbons or partial oxidation into oxygenates were investigated in previous decades in great detail by many researchers. Nonoxidative methods and novel technologies were also developed; however, none of them were so successful to be commercialized. As far as the activation of methane is concerned, breaking the carbon-hydrogen bond in the molecule revealed to be the necessary step.
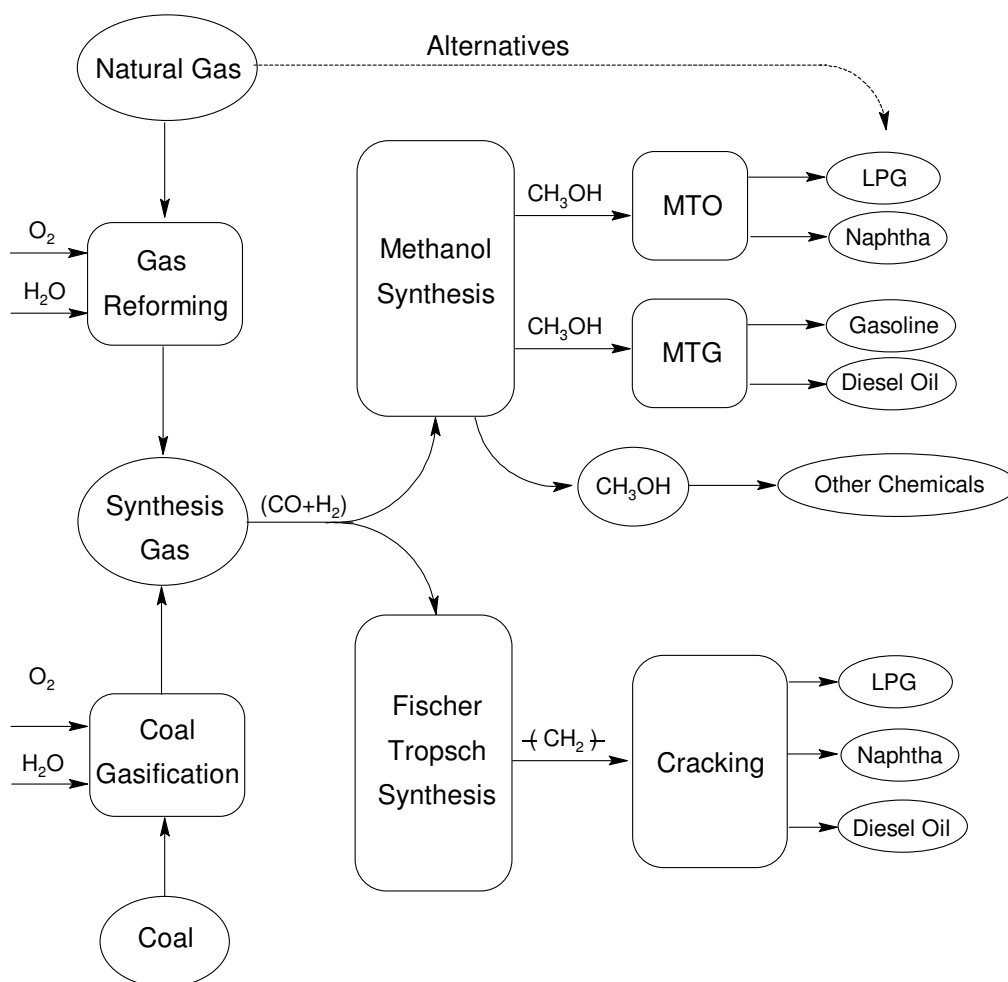
Figure 2.4 Hydrocarbon synthesis from alternative natural resources.

2.4.1 The structure of Methane Molecule

The simplest saturated hydrocarbon is methane. It is formed by a single carbon atom bonded to four hydrogen atoms. The highest possible H:C ratio is realized in methane molecule [79]. The 1s and three 2p ground state orbitals of carbon atom are combined to form four sp^3 hybridized orbitals. The overlap of the sp^3 orbitals of one carbon atom with the 1s orbitals of four hydrogen atoms forms the carbon-hydrogen σ bonds in methane molecule. The maximum

separation of the four pairs of electrons induces the tetrahedral orientation of methane in 3D space [80].
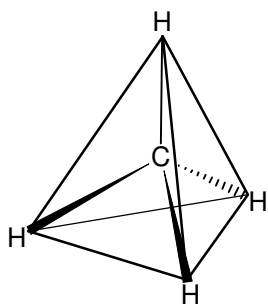
Figure 2.5 The structure of methane molecule.

The structure of the methane molecule (Figure 2.5) with four identical hydrogens is responsible for its stability ($\Delta H_c^\circ = 802.3\,\text{kJ/mol}$). Once it is oxidize, the removal of one of the identical hydrogens goes into complete combustion of methane, which we utilize to produce energy in large amounts. However, the intervention to the pathway for the partial removal of hydrogens in order to produce the desired chemical is difficult to achieve. The examples of the intensive research devoted to this difficult goal are given in the following sections.

2.4.2 Oxidative Coupling of Methane

The quest for an easy way for direct methane conversion stimulates the extensive research and oxidative coupling could be the most attractive one in 1990s. The thermodynamic disadvantages of methane conversion can be overcome by the introduction of an oxidant (Equation 2.13-2.15) [81, 82]. The formation of ethane and water from methane and oxygen mixture is known as

oxidative coupling, which involves the in situ conversion of ethane into ethylene [83].

Methane oxidation into hydrocarbons:

$$2CH_4 \rightleftharpoons C_2H_6 + H_2 \qquad \Delta G_{rxn}^{\circ} = 69.1\,\text{kJ/mol} \qquad (2.13)$$

$$2CH_4 + \tfrac{1}{2}O_2 \rightleftharpoons C_2H_6 + H_2O \qquad \Delta G_{rxn}^{\circ} = -159.5\,\text{kJ/mol} \qquad (2.14)$$

$$2CH_4 + O_2 \rightleftharpoons C_2H_4 + 2H_2O \qquad \Delta G_{rxn}^{\circ} = -287.7\,\text{kJ/mol} \qquad (2.15)$$
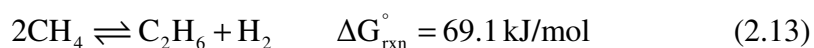
The target molecule is the ethylene, which is one of the largest volume organic chemical produced worldwide. However, in the presence of oxygen methane conversion into C_2 hydrocarbons is generally accompanied by the thermodynamically favorable conversion of CH_4 into CO_2 or CO (Equation 2.16-2.17). In addition, the gas phase kinetics of the reaction does not favor the formation of methanol or higher hydrocarbons [84]. This limits the productivity. Besides, the exothermic nature of the reactions results in a substantial temperature increase of the catalyst zone, which must be handled carefully. Other than methane conversion, selectivity is the important criterion under investigation at modest methane conversions. Different catalysts have shown to be more or less active in oxidative coupling with 20% methane conversion at 80% C_{2+} selectivity [85].

Deep methane oxidation reactions:

$$CH_4 + 2O_2 \rightleftharpoons CO_2 + 2H_2O \qquad \Delta G_{rxn}^{\circ} = -801.1\,\text{kJ/mol} \qquad (2.16)$$

$$CH_4 + \tfrac{3}{2}O_2 \rightleftharpoons CO + 2H_2O \qquad \Delta G_{rxn}^{\circ} = -543.9\,\text{kJ/mol} \qquad (2.17)$$

The oxidation studies revealed the radical mechanism of the reactions. The oxygen species on the catalyst surface forms the methyl radicals by interacting with methane. The coupling of the methyl species either in gas

phase or on the surface will lead to the formation of ethane. Further dehydrogenation of ethane will form ethylene. Methyl radicals, ethane and ethylene may react with oxygen for complete oxidation into carbon dioxide or carbon monoxide. Experiments performed by isotope labeling revealed the sources of CO_2. Methane is the major source at small conversion levels, whereas at high conversion levels, ethylene is the dominant source of CO_2 [83].

2.4.3 Partial Oxidation of Methane

Methanol is a major bulk chemical for the industry, because it is a starting material of many different chemicals, i.e. formaldehyde (which goes into polymers), toluene (major solvent), acetic acid and liquid fuels (through MTO) [58, 86]. Therefore it is a desired target molecule, and research was stimulated to find and easier way other than syn-gas to produce methanol from methane. One additional advantage of CH_4 conversion into CH_3OH is that, it is a liquid, which can be transferred through long distances easier than methane.

The direct conversion of methane into methanol is studied through the partial oxidation of methane. The main target products were not only methanol but also formaldehyde, which is another bulk chemical for the industry. Different metal oxides (i.e., W/SiO_2, V_2O_5/SiO_2, $FePO_4/SiO_2$, $Cu-Fe/ZnO$, and $V/MCM-41$) were investigated for this purpose and MoO_3/SiO_2 was reported to be one of the best catalysts [87, 88]. Except for the few reports on outstanding yields of methanol and formaldehyde, at 5-10% methane conversions, CH_3OH selectivity of around 35% were observed at ca. 450 °C. The partial oxidation of methane reactions were the subject of the studies with CH_4/O_2 feed both in the presence and absence of H_2O. The results indicate that formaldehyde is produced by the further oxidation of methanol. The CO and CO_2 formation reduces the selectivity. At 350 °C the overall selectivity for CH_3OH and HCOH is about 40% at 15% methane conversion in the presence of 80% vol.

of feed gas [88]. The yields of formaldehyde or methanol are too low for possible industrial applications. Mo/ZSM-5 catalysts were investigated for methane oxidation towards formaldehyde. Generally, Mo=O sites of terminal atoms in molybdenum oxide is accepted as the specific sites for HCOH production, whereas, Mo–O–Mo and ZSM-5 sites would lead to total oxidation products [89]. Other than oxygenates, although the selectivity and conversion remains low, the oxidation of methane over metal loaded ZSM-5 catalyst was reported to be active in liquid hydrocarbon production [90]. Liquid hydrocarbons could be produced from methane oxidation if CH_4 or C_2H_6 dehydrogenation and olefin oxidation of the metals in the metal–ZSM-5 catalysts are in balance.

The activity of MoO_3/SiO_2 and V_2O_5/SiO_2 in methane oxidation to formaldehyde were reported [91]. The state of the silica support is much dependent on the preparation procedure; however, the presence of available lattice oxygen leads to further oxidation of the desired compounds. High concentration and high dispersion of Fe^{3+} over silica surface was reported to show superior activity [92]. The high activity of $FePO_4/SiO_2$ catalyst was explained by the isolation of the tetrahedrally coordinated Fe^{3+} ions from each other by the phosphate groups that act as proton donors for methanol formation via the methoxy intermediate [93]. The high stability of methane molecule required high temperatures for oxidation, which cause the necessity for the catalyst to have high dispersion of isolated sites over a matrix of weak Brønsted acidity [92].

2.4.4 Non-oxidative Methane Conversion

In the absence of oxygen the equilibrium conversion of methane is ca. 12% at 700 °C and naphthalene and benzene are the major products [94]. 100% benzene selectivity was achieved at 7% methane conversion over Mo/ZSM-5 at

700 °C [95]. XPS results indicate the formation of Mo_2C species after exposure of a 2 wt% Mo/ZSM-5 catalyst to CH_4 at 700 °C. About 60 to 80% of Mo species are present in the form of Mo_2C indicating that carbidic molybdenum species are the active centers to initiate the formation of CH_x species, which oligomerized on ZSM-5 support having proper acidity to produce aromatic hydrocarbons [94]. This is supported by comparing the methane aromatization reactions on MoO_2, MoO_3, Mo and Mo on ZSM-5. Mo and molybdenum oxides results in mainly H_2O, CO_2, trace amount of ethane and the catalyst was poisoned due to coke formation. On the other hand, Mo/ZSM-5 shows ethane, ethylene and benzene and Mo_2C/ZSM-5 clearly increases the benzene yield (80% selectivity at 6% conversion) [96]. W/ZSM-5 was reported to be an active catalyst in the same reaction at 800 °C with methane conversion of ca. 20% and ca. 50% selectivity to aromatic hydrocarbons. Cu/ZSM-5 is better for liquid hydrocarbon production with a C_5-C_{10} selectivity and 15% methane conversion [97]. The absence of oxygen, introduce the fact that the temperatures are as high as 700-800 °C. Although, oxygen is not present, the product distribution is not limited to a certain hydrocarbon but a range of hydrocarbons, probably due to the effect of high temperature. Therefore, this method does not seem to solve the problems of oxidative processes.

2.4.5 Homogeneous Routes

One of the main drawbacks in oxidative coupling and partial oxidation approaches is the over oxidation of methane into CO_2 and CO at elevated temperatures. Therefore, homogeneous catalytic conversions of methane to liquid products under milder conditions were investigated. The molten salt prepared by $AgNO_3$-KNO_3 system was reported for direct methane conversion into acetone under milder conditions. The autoclave was used as a reactor at 160 °C and at ca. 60 atm. The addition of $Cu(CF_3CO_2)_2$ in the reaction medium

results in the best selectivity for acetone (78%) with 2.3% methane conversion. Other component is the $CF_3CO_2CH_3$ and the reaction time is about 15 h [98]. The temperature is lower than oxidative coupling or partial oxidation studies but pressure is higher in this process and the reaction time and conversion is far from industrial applications.

The direct formation of acetic acid is another desired target, which is currently produced from methanol. The mixture of methane, oxygen and CO were reported to be converted into acetic acid by dissolving in water in the presence of $RhCl_3$ as the catalyst at 100 °C [99]. The formation of acetic acid was accompanied by the formation of methanol and formic acid. The yield of acetic acid was, however, very low (1.2%).

In order to overcome the formation of CO_2 and CO at elevated temperatures, other oxidants were proposed. The methane oxidation with O_2 and hydroperoxide as oxidants was reported at ambient temperature over phthalocyanines of Fe, Cu and Co encapsulated in zeolites X and Y [100]. The products were CH_3OH, HCOH and HCOOH. The oxygenate selectivity to CO_2 is promising; however, the methane conversion is between 0.3-5% in a reaction in an autoclave reactor after 12 h.

Oxidative addition of methane to an iridium based organometallic complex $[(\eta\text{-}C_5Me_5)Ir(CO)(H)CH]$ to form a characterized product was reported by Hoyano et. al [101]. Different metal complexes were known to be active in C–H bond cleavage [102]. The promising studies on low temperature C–H bond activation were reviewed by Wolf [103], as indicating remarkable high yields of methanol by Pt complexes in fuming sulfuric acid.

The reaction scheme of another homogeneously catalyzed process is given in Equation 2.18 [11], with high selectivity (at ca. 95%) towards the methyl ester, CH_3OSO_3H. Au, Hg, and Tl, salts and W, Ti, Ir, Rh, Pd, and Pt complexes tried, and Pt in the form of bipyrimidine–$PtCl_2$ complex gives the best result [11, 104, 105]. According to Periana et al. [11], the rate constant of the oxidation step of CH_4 to methyl bisulfate is 100 times higher than that of

the further oxidation of methyl bisulfate and thus methanol is trapped in esterification in the form of CH_3OSO_3H, which prevents overoxidation to CO_2. Although the overoxidation of methane is prevented in this route at temperatures as low as 100 °C, the homogeneous nature of the scheme remains a challenge for industrial applications.

Reaction scheme for methane activation in fuming sulfuric acid:

$$CH_4 + HX + SO_3 \rightarrow CH_3X + H_2O + SO_2$$
$$CH_3X + H_2O \rightarrow CH_3OH + HX$$
$$\underline{SO_2 + \tfrac{1}{2}O_2 \rightarrow SO_3}$$
$$\text{net rxn: } CH_4 + \tfrac{1}{2}O_2 \rightarrow CH_3OH \text{ where } X = OSO_3H$$

(2.18)
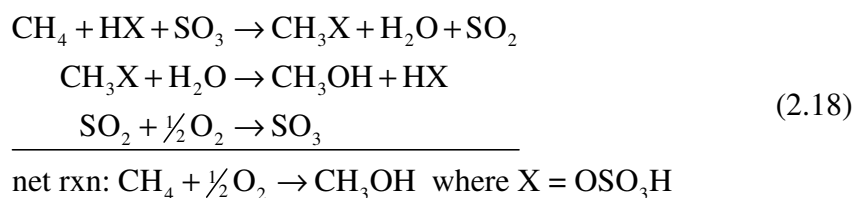
2.4.6 Photocatalytic Methane Conversion

One method proposed for the methanol production is to use light, water, and CH_4 through photocatalytic reactions. The catalytic photolysis of water forms hydroxyl radicals. The interaction between the hydroxyl radical and the methane molecule forms a methyl radical. Preferably the former reaction of methyl radical with water forms an additional hydroxyl radical and methanol. The chain reactions between water, methane, hydroxyl radicals and methyl radicals will lead to the formation of methanol from methane in a very clean procedure. The experiment was performed in a quartz reactor at ca. 90 °C. The catalyst is suspended in the reactor and methane is bubbled in a carrier (He). The experiments were performed either under UV or visible light radiation controlling by special lamps and filters. Tungsten oxide catalysts were revealed a maximum of 4% methane conversion with different dopants as La, Co, Pt, La/Co. The products include H_2, CO and CH_3OH. Pt and La/Co addition diminishes the catalytic effect, and La promotes and Co inhibits the methanol

production [106]. Although the possibility of methane conversion into methanol by photocatalytic systems, the reaction is slow and the conversions are much lower than the desired conversions for commercial applications.

2.4.7 Methane Oxidation with CO_2

The conversion of CO_2 is also a much desired reaction, because a large amount of CO_2 is dissipated into the atmosphere, which is blamed to cause greenhouse effect. The current indirect methane conversion technology is based on steam reforming of methane; however, CO_2 reforming is much investigated to use CO_2 instead of steam to produce synthesis gas. This approach does not substitute the high cost synthesis gas production route. Therefore, alternatively, direct conversion of CH_4 and CO_2 at low temperatures (100-400 °C) into hydrocarbons and oxygenates were proposed. Cu/Co based catalysts were used for hydrogenation of CO and CO_2 were applied in methane activation studies [107]. The product distribution involves the formation of acetic acid, methanol, formic acid, formaldehyde, butanone and cyclopentane derivatives. It was shown that the production of valuable oxygenates from CH_4 and CO_2 were possible, but the product selectivity was not promising.

2.4.8 Plasma Reactors for Methane Oxidation

The conversion of methane into higher hydrocarbons was also investigated by using a plasma reactor. The operating pressure was generally the atmospheric pressure. In this method, the excitation of methane – dehydrogenative coupling – is achieved in the absence of oxygen. Different types of plasmas were investigated. C_2 hydrocarbons, mainly acetylene, were obtained in pulsed corona discharges with high selectivities (70–90%) [108]. In

microwave plasmas the product distribution is dependent on the input energy. At low energies ethane is the main product, whereas at high energies acetylene is produced [109]. Microwave can easily penetrate through materials. Depending on the energy it can be absorbed by the whole volume of an irradiated object. Therefore the irradiated object is heated fast and homogeneously. One approach is based on the idea of selective heating of an active metal supported on a porous matrix. A ceramic catalyst support therewith does not absorb microwaves and remains cold thus providing fast quenching of the products. The combinations of the microwave plasma technology over different catalysts were reported. Over Ni, Cu and CuO catalysts C_2-C_3 hydrocarbons were dominant. Benzene formation is observed over Mo/ZSM-5 [110]. In another study Al–Ni–Ti alloy, ThO_2/Al_2O_3, Fe/Al_2O_3, Ni/Al_2O_3 were investigated. Ni/Al_2O_3 was found to be the best catalyst with 50% conversion is obtained for methane conversion with a very similar high temperature product distribution of methane pyrolysis [111]. Coke formation is a critical drawback in microwave assisted plasma reactors. In dielectric barrier discharge plasmas, ethane formation is dominant [112, 113]. The effect of this type of plasma is different than the microwave. The nonthermal plasma creates a high electron temperature as high as 10^5 K; on the other hand, bulk gas temperature is as low as ambient temperature. The CO_2 and CH_4 co-feed results in the formation of higher hydrocarbons and oxygenates with low selectivities, but CH_4 and CO_2 conversions were high (64% and 43% respectively) [114]. The plasma technology is far from practical applications, because it is a very energy intensive process. 10-17 eV is required per methane molecule converted.

In addition to the mentioned methods above, the use of halogens for methane conversion is a promising alternative. This method constitutes a major part in the thesis is, for which the recent research trends are summarized in a separate section below.

2.5 HALOGENATION ROUTE

Similar ways of natural gas conversion was proposed by Olah [15-17] and Benson [18, 19], both of which involves the use of halogens (chlorine and bromine) in catalytic and noncatalytic processes respectively. By extracting hydrogen from methane and producing methyl halide (a methanol like molecule) under relatively mild conditions, then the condensation of methyl halide to achieve the production of higher hydrocarbons or oxygenates is an alternative route for commercial methane conversion into hydrocarbons through syn-gas route (Figure 2.6).

Reactions for methane conversion into hydrocarbons through halogens are given below:

$$CH_4 + X_2 \rightarrow CH_3X + HX \qquad\qquad (2.19)$$

$$nCH_3X \rightarrow \left(CH_2\right)_n + nHX \qquad (X: Either\ Br\ or\ Cl) \qquad (2.20)$$
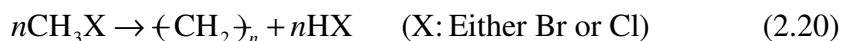
After the formation of methyl halide, methyl chloride or bromide can be condensed onto hydrocarbons over acidic catalysts (Equation 2.19-2.20). However, monochlorination or monobromination of methane is the necessary condition for the application of the halogenation route to synthesize hydrocarbons from methane [47]. Gas phase radical chlorination of methane is not selective. In order to minimize the formation of higher halogenated methanes limited amount of halogen should be sent with methane for the reaction. Halogenation of methane towards higher hydrocarbons has been extensively studied in the past by Benson [18, 19]. The Benson process required the use of chlorine for methylchloride production. Further pyrolysis of methylchloride at high temperature (1000 °C) into hydrocarbons is the basis of the process. Detailed kinetic mechanism of the methyl chloride pyrolysis was described in literature [115, 116]. However, the selectivity problems and the

corrosive nature of the reactants and the products were the major drawbacks of the commercialization.
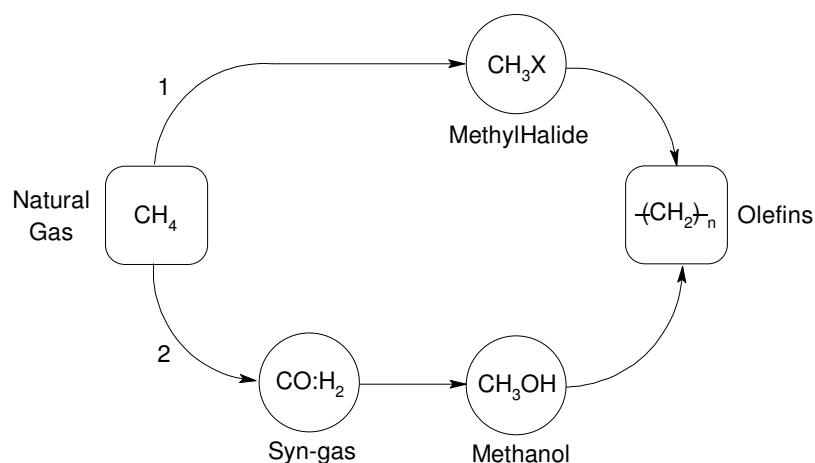
Figure 2.6 Alternative methane conversion into higher hydrocarbons through halogenation: 1. Halogenation route, 2. Commercial methanol to olefins (MTO) route.

On the contrary to the gas phase halogenation of methane, catalytic methane halogenation was reported to show high selectivity [16]. Olah proposed the catalytic dehydrohalogenation of methane by extracting hydrogen from methane molecule and producing methyl halides under relatively mild conditions [15]. He studied a set of catalysts, which are known as superacids. The supported Lewis acid oxyhalide (or halide) catalysts, $FeOCl/Al_2O_3$, $TaOF_3/Al_2O_3$, $NbOF_3/Al_2O_3$, $ZrOF_2/Al_2O_3$, SbF_5–graphite, and TaF_5–Nafion-H and Nafion-H were studied for mono chlorination and $SbOF_3/Al_2O_3$ and $TaOF_3/Al_2O_3$ were investigated for mono bromination of methane. In addition to these, $Pd/BaSO_4$ and Pt/Al_2O_3 catalyzed chlorination reactions were also reported. The results showed that $ZrOF_2$–Al_2O_3 is the best catalyst which gives 96% selectivity for monochloromethane at 34% methane conversion. On the

other hand, in bromination $SbOF_3$–Al_2O_3 is the best with 99% selectivity for monobromomethane at 20% methane conversion. $Pd/BaSO_4$ and Pt/Al_2O_3 catalysts were also reported to be very effective with selectivities also exceeding 90% but not reproduced elsewhere yet.

The hydrolysis of methyl halides to oxygenates (dimethyleter (CH_3OCH_3) and methanol) were reported over γ-alumina and γ-alumina-supported metal oxide/hydroxide catalysts. The metal oxides were, V_2O_5, MnO_2, Cr_2O_3, MgO, ZrO_2, BaO, TiO_2, ZnO, and Fe_2O_3 and 25% conversion were obtained over $ZnO/Al(OH_3)/γ$-Al_2O_3 catalyst revealed an alternative way to produce methyl alcohol and dimethyl ether instead of the synthesis gas route used in industry currently [16, 17].

Furthermore, hydrocarbon formation from methyl chloride was reported over different catalysts. The reaction on ZSM-5 gives a product distribution of 43.1% aliphatics and 57.1% aromatics at 369 °C, which is similar to product distribution of methanol conversion [117]. The methyl chloride and methyl bromide conversion into higher hydrocarbons over H-SAPO-34 catalyst resulted in similar product distribution with methanol feed [118]. WO_3/Al_2O_3 results in 42.8% selectivity for C_2-C_5 hydrocarbons at 327 °C with a methyl chloride conversion of 36% [119, 120].

Lorkovic et al. studied methane bromination for the formation of higher hydrocarbons or oxygenates [22-26]. In this route, methane is either brominated in a separate reactor first at 500-525 °C [22] or the bromination takes places in the first part of a dual zone reactor followed by condensation over a solid metal oxide to products in the second part [25]. The pure CH_3Br feed over CaO/ZSM-5 catalyst at 400 °C results in the formation of C_2 (6%), C_3 (37%), C_4 (26%), C_5 (9%), aromatics (5%), C_5-C_7 aliphatics (12%), and adsorbed carbon (5%) [22]. This product distribution is almost identical to the methanol transformation [23]. However, in the presence of CH_2Br_2 in the feed, the product distribution is altered to C_2 (7%), C_3 (26%), C_4 (11%), C_5 (4%), aromatics (16%), C_5-C_7 aliphatics (14%), and adsorbed carbon (22%) [22]. The

amount of adsorbed carbon in the product distribution makes the big difference between CH_3Br and CH_2Br_2 feeds. Thus it was concluded that CH_2Br_2 condenses predominantly to carbonaceous material. Dibromomethane also favors the formation of aromatics other than C_2-C_5 hydrocarbons [25]. Therefore, the production of monobromomethane selectively reveals to be the necessary step for natural gas conversion through halogenation.

The formation of oxygenates from CH_3Br were also reported over metal oxide catalysts. Methane was brominated in a dual zone reactor; homogeneous gas phase bromination in the first zone was followed by the coupling over the 50/50 CuO/ZrO_2 catalyst in the second zone. At 8.1% methane conversion the products were CH_3OH (37%), CO_2 (35%) and unconverted CH_3Br (29%). Application of another catalyst, 43/7/50 $Co_3O_4/Sm_2O_3/ZrO_2$, resulted in the products of CH_3OH (20%), $(CH_3)_2O$ (20%), CO_2 (5%), and unconverted CH_3Br (40%) and CH_2Br_2 (15%) [25]. $AlBr_3$ is another catalyst studied for the condensation of CH_3Br. The product distribution was predominantly saturated C_1-C_3 hydrocarbons, not too attractive for the petrochemical industry [121].

The halogenated products ($CH_{4-n}X_n$) and Hydrogen bromide (chloride) were not environmentally benign materials. The desired product of methane bromination reaction is methyl bromide and unfortunately it is an ozone depleting material. The production and distribution of CH_3Br was abandoned by Montreal Protocol. Therefore the halogenated products should be handled carefully. The HBr (HCl) could be neutralized by bubbling the exit gas through a NaOH solution. After the hydrocarbon synthesis in the overall reaction scheme, the unconverted product (i.e., CH_3Br) must be recycled. This could be done by a Hofmann elimination type reaction (Equation 2.21). This remains to be difficult to achieve, but required for the overall synthesis route to be applicable [47].

$$2C_2H_5O^-Na^+ + 2CH_3Br \rightarrow 2C_2H_5OH + C_2H_4 + 2NaBr \qquad (2.21)$$

CHAPTER 3

GAS PHASE BROMINATION OF METHANE

3.1 INTRODUCTION

The direct conversion of methane to liquid fuels has been the subject of the catalysis community in the past couple of decades. Direct oxidative coupling of methane drew a lot of attention. Although several catalysts were investigated, low yield and low selectivity problems could not be overcome. Any catalyst that could reach yields higher than 25% and selectivity over 80% could not be put into practice for economical reasons [8, 103]. Studies focusing on one-step partial oxidation of methane to methanol or formaldehyde were confronted with the problems of low selectivity accompanied by long residence times [4]. The utilization of HZSM-5 and metal supported HZSM-5 zeolites in the direct conversion of methane to liquid hydrocarbons have not achieved high selectivity values [90]. Pulsed discharge plasma processes also applied to methane conversion with the advantage of low gas phase temperature. But, low energy efficiencies revealed a drawback for this approach [14]. Besides, the photo catalytic reactions managed to activate methane, however they do not result in high yields [12, 13].

High stability of the methane molecule is the biggest obstacle against the way from the smallest hydrocarbon to fuels or petrochemicals. As far as the activation of methane is concerned, breaking the carbon-hydrogen bond in the

molecule under either oxidative or non-oxidative condition is revealed to be the necessary step. Gas phase chlorination of methane towards higher hydrocarbons has been extensively studied in the past by Benson [18, 19] . The Benson process required the use of chlorine as an intermediate. However, the corrosive nature of the reactants and the products, oxidation of HCl, and the low product selectivity were the major drawbacks of the commercialization. Lorkovic *et al.* [25] studied methane activation through bromination in a two step process. First methane was brominated in gas phase in a reactor and the reactants were sent to another reactor for condensation into hydrocarbons. They reported that in the presence of dibromomethane the product distribution was not favorable in the second reactor. Thus, the selective CH_3Br production become important, and 63% selectivity was reported at 70% methane conversion in gas phase at 500 °C with 60 s space time in a homogeneous reactor [23].

Olah [16, 17] proposed catalytic oxidation of methane by halogens. Producing methyl halides under relatively milder conditions than syn-gas, and further catalytic hydrolysis of methyl halides into olefins or oxygenates is a promising way for methane activation. He achieved over 90% selectivity for CH_3Br and CH_3Cl over superacid catalysts, i.e, $TaOF_3/Al_2O_3$, $SbOF_3/Al_2O_3$, $ZrOF_2/Al_2O_3$, SbF_5–graphite, and TaF_5–Nafion-H. Moreover, Olah [16] reported the hydrolysis of methyl halides to methyl alcohol and dimethyl ether, over γ-alumina and γ-alumina-supported metal oxide/hydroxide catalysts and Lorkovic reported the formation of higher hydrocarbons over CaO/ZSM-5 [23] and dimethyl ether and methanol over CuO/ZrO_2 and $Co_3O_4/Sm_2O_3/ZrO_2$ catalysts [25].

In the next part of the thesis, the thermodynamics and kinetics of gas phase homogenous halogenation reactions are reported. The hydrolysis of methyl halide into a favorable product distribution reveals the importance of selective methyl bromide production. Therefore, a reaction model was developed according to the kinetic data available in the literature and this

model was thoroughly studied to investigate the optimum reactor conditions for selective methane bromination in gas phase.

3.2 KINETICS AND THERMODYNAMICS OF HOMOGENEOUS METHANE HALOGENATION

The enthalpy and free energy of formation of all halogenation reactions are presented in Table 3.1. The low activation energy for the chain propagating steps and the large overall heat of reaction makes fluorine highly reactive towards methane. Highly exothermic fluorine-methane reactions are not easy to control and even cause explosions. The use of chlorine is not preferable in industry due to its corrosive effects. In addition, the reaction of methane with chlorine results in polychlorinated products easily which makes it difficult to stop the reaction from further chlorination when one or two substituted methane halides are desired. Methane-iodine reactions are thermodynamically limited to the equilibrium conversions of 10% even at 650 °C. Finally, the low reactivity of iodine leaves bromine as the most suitable halogen for methane activation. Slightly exothermic reaction of bromine and methane has the advantage to control the degree of halogenation. As summarized briefly above, bromine revealed to be the most suitable halogen for methane activation.

Table 3.1 Enthalpy and free energy of formation of methane-halogen reactions [122].

$CH_4 + X_2 \longrightarrow CH_3X + HX$		
X	$\Delta H°$ (kJ/mol)	$\Delta G°$ (kJ/mol)
F	-427.0	~ -430.0
Cl	-99.8	-107.9
Br	-28.3	-32.3
I	53.2	49.1

The enthalpy and free energy of formation of bromination reactions at standard states are presented in Table 3.2. It is seen that the formation of CH_2Br_2 is most exothermic reaction and are all spontaneous and the formation of CBr_4 is the least favorable. The temperature dependencies of Gibbs free energies of reactions presented in Table 3.2 were calculated and plotted in Figure 3.1 (The details of the calculations are given in Appendix A). It was observed that the formation of CH_2Br_2 becomes non-spontaneous at 450 °C.

Table 3.2 Enthalpy and free energy of formation of methane-bromine reactions at standard states [122].

	Reaction	$\Delta H°$ (kJ/mol)	$\Delta G°$ (kJ/mol)
1	$CH_4 + Br_2 \rightarrow CH_3Br + HBr$	-28.3	-32.3
2	$CH_3Br + Br_2 \rightarrow CH_2Br_2 + HBr$	-70.6	-40.8
3	$CH_2Br_2 + Br_2 \rightarrow CHBr_3 + HBr$	-11.3	-37.91
4	$CHBr_3 + Br_2 \rightarrow CBr_4 + HBr$	-5.2	-2.5

In the literature, bromination reaction rates have been studied by either direct bromination reaction method [123], i.e. the reaction system composed of single reactant CH_4 and Br_2 or a competitive bromination reaction method [124], i.e. a reference compound is brominated simultaneously with CH_4, which results in similar reaction rates. Kistiakowski and van Artsdalen [123] studied the thermal bromination of methane at 570 K and Amphlett and Whittle [124] resulted in the similar reaction rate results by competitive reaction analysis.
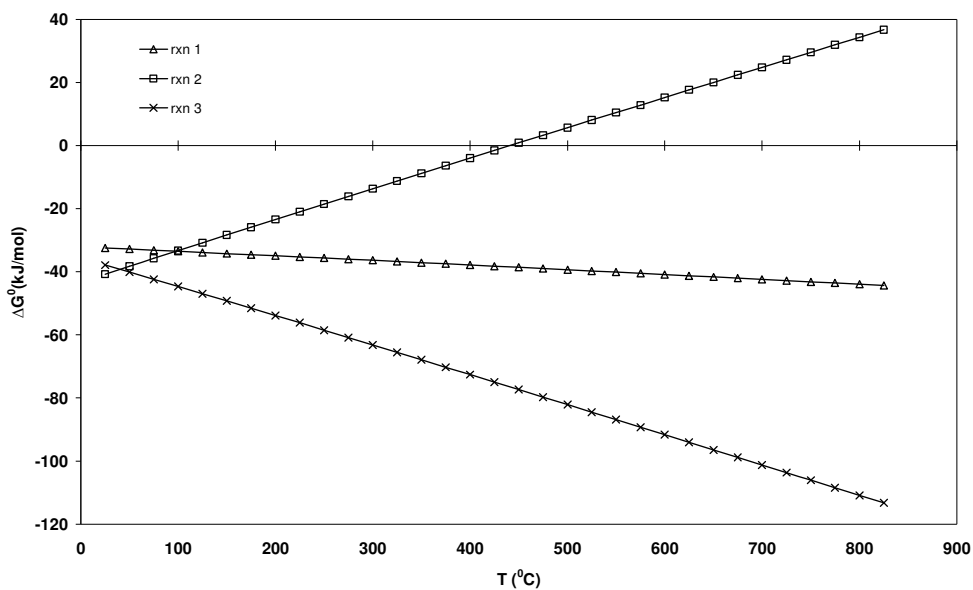
Figure 3.1 Free energy of formation of methane-bromine reactions as a function of temperature.

The rate of formation of methyl bromide and rate of consumption of methane was obtained [123] for the accepted mechanism of free radical halogenation reactions of alkanes, which are shown below.

Reaction Mechanism:

$$Br_2 \underset{}{\overset{K_{eq}}{\rightleftharpoons}} 2\,Br\bullet \qquad\qquad \text{Initiation, Termination} \qquad (3.1)$$

$$CH_4 + Br\bullet \xrightarrow{k_2} CH_3\bullet + HBr \qquad\qquad \text{Propagation} \qquad (3.2)$$

$$CH_3\bullet + Br_2 \xrightarrow{k_3} CH_3Br + Br\bullet \qquad\qquad\qquad (3.3)$$

$$CH_3\bullet + HBr \xrightarrow{k_4} CH_4 + Br\bullet \qquad\qquad \text{Inhibition} \qquad (3.4)$$

$$CH_3Br + Br\bullet \xrightarrow{k_5} CH_2Br\bullet + HBr \qquad\qquad\qquad (3.5)$$

$$CH_2Br\bullet + Br_2 \xrightarrow{k_6} CH_2Br_2 + Br\bullet \qquad\qquad \text{Poly Bromination} \qquad (3.6)$$
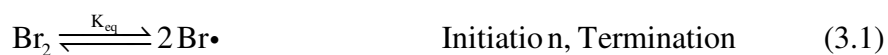
Rate Equations:

$$\frac{d}{dt}[CH_3Br] = \frac{k_2 K_{eq}^{1/2}[CH_4][Br_2]^{1/2}}{1+\frac{k_4[HBr]}{k_3[Br_2]}} - k_5 K_{eq}^{1/2}[CH_3Br][Br_2]^{1/2} \qquad (3.7)$$

$$-\frac{d}{dt}[CH_4] = \frac{k_2 K_{eq}^{1/2}[CH_4][Br_2]^{1/2}}{1+\frac{k_4[HBr]}{k_3[Br_2]}} \qquad (3.8)$$

$$k_2 = 6\times10^{13} \exp\left[\frac{-76060(J/mol)}{RT}\right] \qquad [123, 125] \qquad (3.9)$$

$$k_5 = 1.67\times10^{13} \exp\left[\frac{-66320(J/mol)}{RT}\right] \qquad [123, 126] \qquad (3.10)$$

Kistiakowski and van Artsdalen [123] determined the equilibrium constant for the dissociation of bromine from the thermodynamic data of Gordon and Barnes [127]. The effect of inhibition step of radical reactions was involved in relations in terms of rate constant (k_4). The assumption of k_4/k_3=0.1 did not bring about any significant errors [128]. Radical reactions continued until all the hydrogen atoms in the methane molecule were replaced by a halogen, a situation commonly encountered in chlorine reactions. However, low reactivity of bromine towards alkanes prevented the formation of three or four substituted carbon molecules [125].

In this part of the study the bromination reaction was modeled to take place in a well mixed reactor (CSTR). The reaction rates mentioned above were used. Methane conversion and the product selectivity were obtained at different temperatures (Figure 3.2) by using MATLAB® software (The code of the program is given in Appendix B). In Figure 3.2, it can be seen that as the reactor temperature increases methane conversions and dibromomethane selectivities increase.
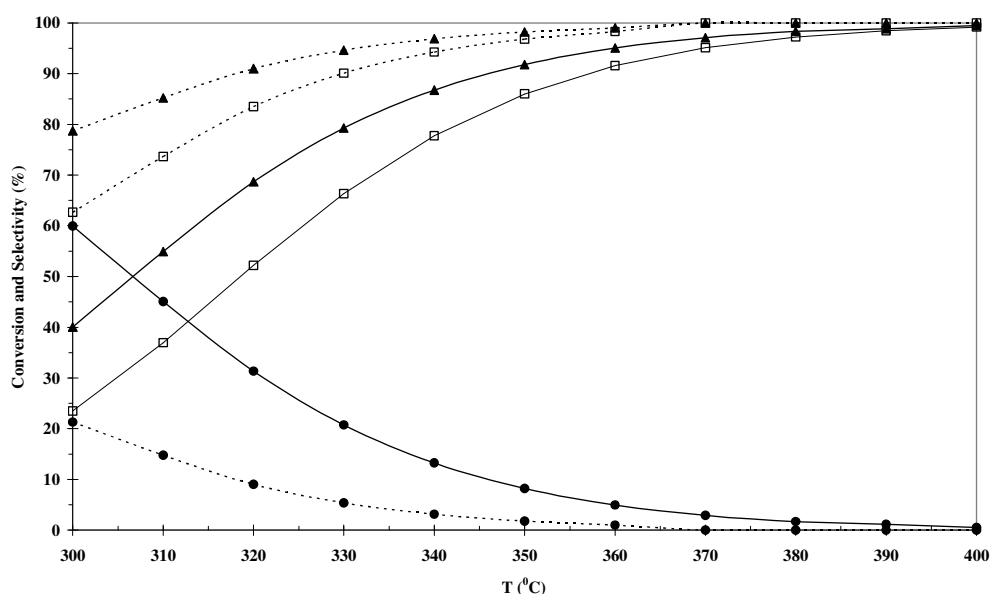
Figure 3.2 Conversion of CH_4 (□) and Selectivity of CH_3Br (●) and CH_2Br_2 (▲) for two different residence times: (0.5 s:__ ,and 3 s:_ _) for $C_{Br_2}/C_{CH_4} = 3$ at different temperatures.

Methane conversions and product selectivities can also be manipulated by changing the reactor feed conditions. If the amount of bromine is decreased in the feed both the conversion of methane and the selectivity of CH_2Br_2 decrease. Conversely, both conversion and selectivity increases with excess amount of bromine in the feed.

In the reaction model, it was observed that monobromination reaction is difficult to control. However, dibromination reaction can run with high methane conversions and with high dibromomethane selectivity. For instance, it is possible to obtain methane conversions above 90% accompanied by high CH_2Br_2 selectivity above 90% at 330 °C at a residence time of 3 s (Figure 3.3 T=330 °C, τ = 3 s, Br:CH_4 = 3).
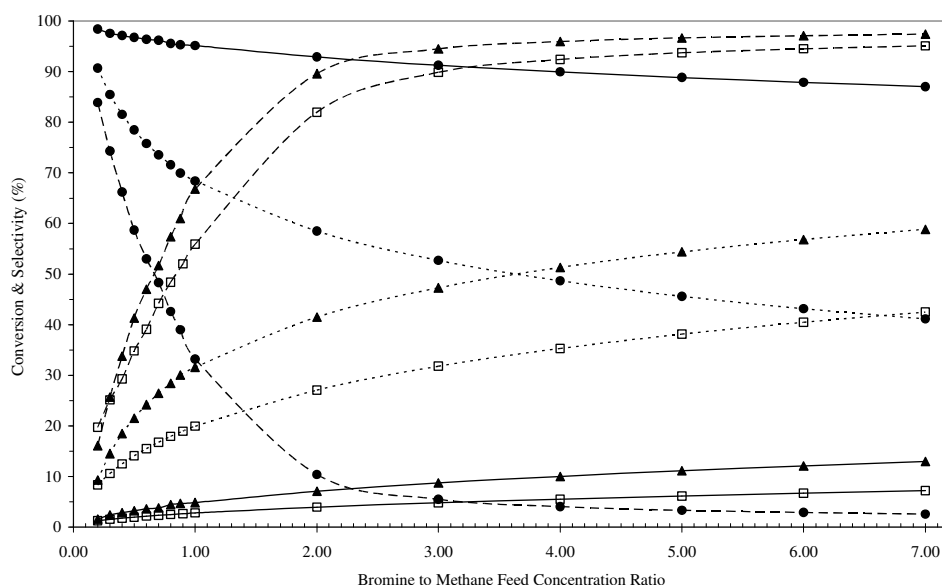
Figure 3.3 Conversion of CH_4 (□) and selectivity of CH_3Br (●) and CH_2Br_2 (▲) at three different residence times: (0.01 s:__ ,0.1 s: …. ,and 3 s:_ _) at 330 °C.

3.3 SUMMARY OF THE KINETIC ANALYSIS STUDY

In this part of the study, it was observed that selective production of methyl bromide is not favored under homogeneous conditions and dibromomethane synthesis route can be favorable in terms of methane conversions and dibromomethane selectivity. The analysis briefly presented above indicated that it is possible to activate methane at relatively low temperatures and pressures than that required by the synthesis gas requiring routes. The activated halo-methane compounds can further react over appropriate catalysts to produce higher hydrocarbons and/or oxygenates. This feature, in addition to the low separation requirements due to the high selectivity of dibromomethane may significantly decrease the operating costs, provided that coke formations in the subsequent dibromomethane reactions [22-26] are inhibited.

CHAPTER 4

CATALYST: SULFATED ZIRCONIA IN SBA-15

4.1 INTRODUCTION

The catalytic halogenation of methane requires an acid center (Equation 1.1). There have been many studies on the solid acid catalysts, and novel materials are continuously reported. Different types of strong solid acids are, (i) supported acids (liquid acids on high surface area solids), (ii) synergism of metal halides and metal salts (e.g. $AlCl_3$–$CuCl_2$; $AlCl_3$– $CuSO_4$); (iii) sulfate-promoted metal oxides (S-ZrO_2), (iv) metal-promoted superacids and (v) polymeric superacid, Nafion-H [129]. Although there is still debate on whether sulfated zirconia is classified as a superacid [130], it can catalyze the reactions that need strong acidity such as n-butane isomerization at sufficiently low temperatures [131].

Sulfated zirconia (SZ) has been extensively studied due to its high catalytic activity for the activation of C–C and C–H bonds of alkanes [47, 132] and especially for the isomerization of small hydrocarbons, which requires strong acid sites [133-140]. However, there is a debate on the interpretation of the origin of the strong acidic property ascribed to sulfated zirconia. Different surface models (Table 4.1) were proposed to elucidate the origin of the strong acidity or high activity in isomerization reactions of sulfated zirconia [141].

Table 4.1 Sulfated zirconia surface models proposed by different authors [141].

Model	Author	Technique	Surface Structure
1	Yamaguchi T. et. al [142]	FT-IR XPS	
2	Arata K. et. al [143]	Pyridine adsorbed IR XPS	
3	Bensitel M. et. al [144]	FT-IR	
4	Clearfield A. et. al [145]	IR ^{1}H MAS NMR TGA	
5	Kustov L.M. et. al [146]	FT-IR	
6	Adeeva V. et. al [147]	FT-IR ^{1}H MAS NMR TPD TPO	

Yamaguchi and coworkers [142] proposed the formation of a chelating bidentate structure on the metal oxide surface based on their XPS and IR data. They proposed that the reason of the strong acidity could be the electron inductive effect of the S=O double bonds, which withdraw electrons from the

metal atom, and thus created a more strong Lewis acid center. However, the isomerization reaction proceeds via carbocation mechanism, which involves the protonation of the hydrocarbon. Therefore the creation of Brønsted acid sites was proposed by Arata et. al [143] through the interaction of the Lewis acid center by adsorbed water (Table 4.1, model 3). Bensitel et. al [144] proposed another structural model by ^{18}O exchange IR measurements (Table 4.1, model 2). Single S=O were observed in the structure for the dehydrated sulfated zirconia with low sulfate contents. The structure transforms into a bridged bisulfate (-OSO$_3$H) complex by the introduction of water (Figure 4.1).
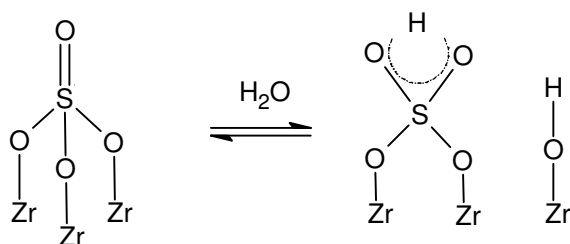
Figure 4.1 Formation of bridged bidentate structure [148].

The bisulfate involved models achieved a general acceptance by introducing another view point to the structure of the sulfated zirconia. Clearfield et. al [145] stated that in the structures with a chelating sulfate group zirconium is saturated and thus can not form low coordinated Zr centers, which act as a Lewis acid center. Therefore, he proposed the model, which involves Lewis acid and Brønsted acid centers together (Table 4.1, model 4). During calcination the removal of water results in the formation of unsaturated Zr centers, which acts as a Lewis acid center. Due to the electron withdrawing effect of the Lewis acid center the proton of the bisulfate group (-OSO$_3$H) attached to a Zr$^+$ center shows strong Brønsted acidity. The strong acidity of sulfated zirconia is then ascribed to the nature of the presence of both Brønsted

and Lewis acid centers [148]. Following the bidentate model a monodentate model was proposed by Kustov et. al [146] and Aeedeva et. al [147] (Table 4.1, models 5 and 6). Kustov and coworkers concluded that the sulfation eliminates the isolated Zr-OH species. Sulfation enhances the strength of the Lewis acidity by electron withdrawing effect of bisulfate group or by the hydrogen bonding between the proton of the bisulfate group and the oxygen attached to a low coordinated zirconium. Adeeva et. al observed that the proton responsible for the strong acidity could not be identified and concluded that it is hydrogen bonded to the surface.

Adeeva and coworkers also suggested that the catalyst does not possess acid strength [148, 149] that can be identified as a superacid because the IR redshifts by CD_3CN adsorption was in comparable range with zeolites (HY). The high catalytic activity could be due to the reaction path via a less energy intensive bi-molecular mechanism in n-butane isomerization [150-152]. In other words, the hypothetical reaction mechanism involves the formation of C_4 carbenium ion, which reacts with butene and forms the intermediate structure C_8. Further cracking of the C_8 complex yields iso-butane. The reason of the higher activity of the sulfated zirconia as compared to zeolites can be explained by the stabilization of the adsorbed intermediates, which results in a transition state with a lower Gibbs free energy [147, 150].
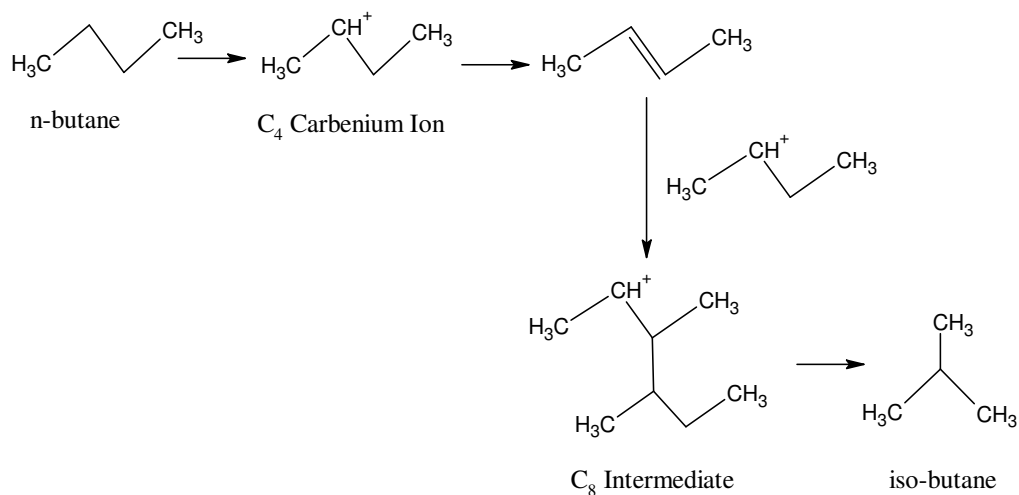
Figure 4.2 Bi-molecular oligomerization-cracking n-butane isomerization reaction mechanism [148].

The conventional sulfated zirconia lacks pore volume with typical surface areas of ca. 100 m^2/g. Since the catalytic activity strongly depends on the surface area, much effort has been spent in order to prepare a high surface area sulfated zirconia. In this respect, mesoporous silicas have attracted increasing interest due to their high surface areas (ca. 1000 m^2/g), large pore volumes, and uniform hexagonal arrays of mesopores [27, 153-156]. Thus, they have potential applications in catalysis, adsorption and separation of molecules because of their high surface areas, large pore volume, and tunable uniform pore structures, but they show relatively weak acid strengths. The silanol groups on the surface of these materials are non-acidic or slightly acidic. To increase the acid strength of mesoporous materials, sulfated zirconia was introduced into the structures such as MCM-41, FSM-16, and SBA-15. The potential combinations of the mesoporous silicas and the highly active sulfated zirconia should greatly enhance the catalytic capabilities of both materials for the applications where strong acidity is essential. The SO_4^{2-}/ZrO_2 incorporation approach has successfully generated materials that show stronger acid strength than conventional mesoporous materials.

Different techniques have been reported to achieve a combination of sulfated zirconia and MCM-41 type mesoporous silicas [157, 158]. MCM-41 is prepared in a basic medium and it is difficult to maintain the crystal structure in strong acidic media [159-161]. SBA-15 type mesoporous materials have higher stability than other mesoporous silicas due to their thicker walls, which enables the introduction of other metals into the framework. Therefore, it is a suitable material to host zirconium. It has been reported that sulfated zirconia may be impregnated into SBA-15 by means of the incipient wetness method [107, 162]. The impregnation of zirconia into the SBA-15 support is a straightforward technique, but it is difficult to obtain uniformly distributed zirconia on the support. The introduction of the zirconia precursor simultaneously with the silicon precursor in the preparation of SBA-15 is a better way to obtain a fine distribution of zirconia [37, 163].

In this part of the study, the synthesis and the characterizations of the catalyst are presented. ICP, XRD, N_2 adsorption (BET), TEM, ^{1}H and ^{29}Si MAS NMR, low temperature CO adsorption FT-IR, and IPAm TPD, are the techniques used for this purpose. The degree of the metal loading into the silica structure was determined by ICP technique. The crystal structures of the catalysts were determined by X-Ray diffraction method. The surface areas were determined by BET method, applied to the isotherms obtained by N_2 adsorption experiments. The pore structure was investigated by TEM. The effect of the inclusion of sulfated zirconia to SBA-15 on the acidic properties is investigated by means of ^{1}H MAS NMR spectroscopy, because the proton chemical shift is sensitive to the electronic environment [164, 165] and the ^{1}H chemical shifts are known to be correlated with the acidic strength of the surface OH groups [166-168]. Another important technique to investigate the acidic structure of the catalysts is FT-IR. CO is known to be a weak base, and by the use of FT-IR and CO adsorption acid sites can be probed. The strength of the acid sites was determined by IPAm decomposition method. IPAm is a basic molecule, which is adsorbed on the acidic sites, and it decomposes into

ammonia and propene above 300 °C depending on the strength of the acid sites.

4.2 EXPERIMENTAL

4.2.1 Synthesis of Catalysts

Pure, ZrO_2 included, and SO_4^{2-}/ZrO_2 modified SBA-15 type catalysts were prepared according to literature [169, 170] and a schematic representation of the followed procedure is given in Figure 4.3.

In order to prepare pure SBA-15 molecular sieve, first 4 g of triblock co-polymer; poly(ethyleneoxide)–poly(propyleneoxide)–poly(ethyleneoxide) ($EO_{20}PO_{70}EO_{20}$, average M_n=5,800 g/mol, Aldrich) was weighed in a beaker. Then, 150 ml of 1.6 M HCl solution was added. The clear solution with co-polymer was mixed with stirrer at ambient temperature until the triblock co-polymer dissolves completely (around 1h). Next, the temperature of the solution was raised to 40 °C. Then, 8.75 g (42 mmol, 9.46 ml) of tetra ethyl ortho silicate (TEOS, $C_8H_{20}O_4Si$, 98% Merck) was added in the solution as the silicon source. The mixture was stirred for ca. 24 h at 40 °C. The solution was transferred into Teflon bottles and the gelation was allowed to take place at 90 °C overnight. Afterwards, the solid material was obtained by filtration. The sample was dried at room temperature overnight. The sample was calcined at 500 °C in airflow for 5 h after a pre-heating period at 400 °C for 1 h. The temperature of the catalyst was raised with a rate of 5 °C/min during calcination.

When preparing the ZrO_2 included SBA-15, zirconium was introduced in solution simultaneously with TEOS in the form of zirconiumoxychloride ($ZrOCl_2·8H_2O$, 99.9998%, Strem Chemicals). The zirconium salt was added in

solution in proper amounts in order to obtain catalysts with zirconia contents of 5, 10, 15, 20, 25, and 30 mol % ZrO_2 with respect to (w.r.t.) the content of SiO_2 and denoted as Zr(X)SBA-15, X=ZrO_2 mol %. In other words, the Zr/Si atomic ratios were in between 0.05 and 0.3 (The corresponding weight percentages were given in Table 4.2).

Table 4.2 Zirconia contents of the catalysts in solution during the synthesis of the catalysts.

Catalyst	ZrO_2 mol % w.r.t. SiO_2 Content	Zr/Si Atomic Ratio	Zr Weight %
SBA-15	0	0	0
Zr(5)SBA-15	5	0.05	6.89
Zr(10)SBA-15	10	0.1	12.60
Zr(15)SBA-15	15	0.15	17.42
Zr(20)SBA-15	20	0.2	21.54
Zr(25)SBA-15	25	0.25	25.10
Zr(30)SBA-15	30	0.3	28.20

Finally, calcined zirconia included catalysts were sulfated: 15 mg of the catalyst was placed in a beaker and 15 ml of 0.25 M H_2SO_4 solution was dropped over. After waiting 15 min at ambient temperature, the catalyst was transferred into an oven at ca. 80 °C. After 24h the dried sulfated catalysts were obtained and denoted as SZr(X)SBA-15, X=ZrO_2 mol %. SBA-15 also sulfated by the same procedure after calcination and denoted as S-SBA-15.
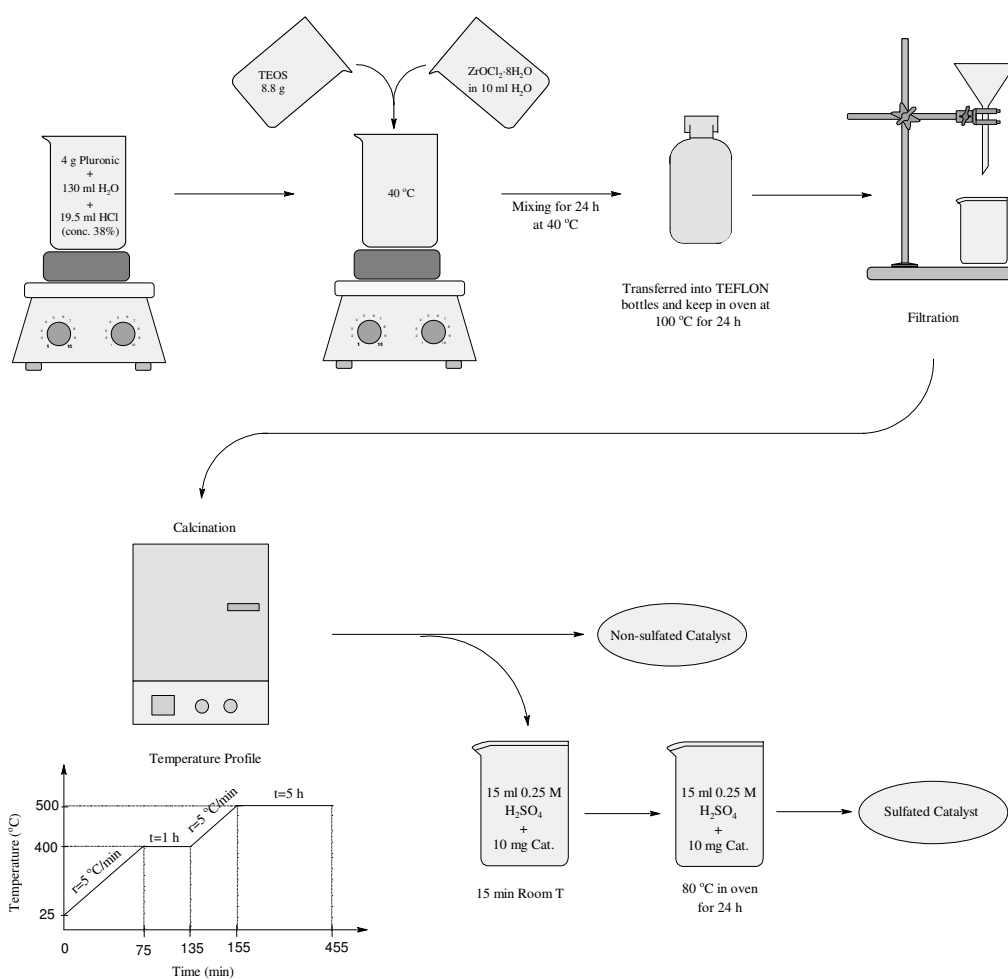
Figure 4.3 Schematic representation of the catalyst preparation procedure.

4.2.2 Characterization of Catalysts

Zirconium and sulfur contents of the samples were determined by Spectro Ciros CCD ICP optical emission spectrometer with axial plasma viewing. For ICP experiments all samples were weighed (~35 mg) and dissolved in a 1.5 ml solution of $HF/HNO_3/H_2O$ (1:1:1) acid mixture.

The X-ray diffractograms were recorded by means of a Rigaku X-ray diffractometer (30 kV, 15 mA) with a miniflex counter using a Cu Kα radiation

($\lambda=1.54$ Å). Diffraction patterns were collected at ambient temperature in the 2θ range of 1-3° at a scanning rate of 0.2° min^{-1} in steps of 0.005° and in the 2θ range of 10–70° at a scanning rate of 1° min^{-1} in steps of 0.05°.

TEM images were taken on a FEI T20 electron microscope operating at 200 V. The specimens were dispersed in ethanol and placed on holey copper grids.

The surface areas were measured using nitrogen adsorption isotherms at −196 °C on a Micromeritics ASAP 2000 gas sorption and porosimetry system. The samples were prepared for measurement by degassing at 150 °C for 24 h. Surface areas were calculated by the BET (Brunauer-Emmett-Teller) method and the pore size distributions were determined by using the BJH (Barrett-Joyner-Halenda) method.

^{1}H MAS NMR experiments were performed at a 400 MHz Bruker AVANCE spectrometer using a MAS probe with an outer rotor diameter of 7 mm. The measurements were performed at 300 K using the solid echo pulse sequence; the proton 90° pulse length was 3.4 µs. ^{1}H MAS NMR spectra of the samples were collected for the hydrated and dehydrated materials and the chemical shifts were recorded relative to Tetra Methyl Silane (TMS). The ^{1}H MAS NMR experiments of the catalysts in the hydrated state were performed by directly filling the catalysts into the 7 mm MAS rotor without any prior treatment. In order to dehydrate the samples, they were placed in special NMR tubes suitable for MAS, connected to a vacuum line, and then heated up to 473 K in steps of 10 K. After a vacuum of 10^{-3} bar is achieved, the system was heated up to 573 K where it was kept there for 24 h. After this pretreatment *in vacuo,* the cylindrical glass tubes were sealed off under vacuum conditions. The sealing symmetry was carefully controlled in a way that a fast sample rotation was possible. Then the sealed glass tubes containing the dehydrated samples were placed into the 7 mm MAS rotor (Figure 4.4). Details of this special preparation of NMR samples suitable for MAS are described, for instance, in Ref. [171, 172].

^{29}Si MAS NMR experiments were realised at 79.6 MHz on AVANCE-400 spectrometer with 4 mm MAS sample tubes. The MAS frequency was 10 kHz and a single pulse sequence was applied. The measurements were performed at 297 K and the chemical shifts were recorded relative to TMS.
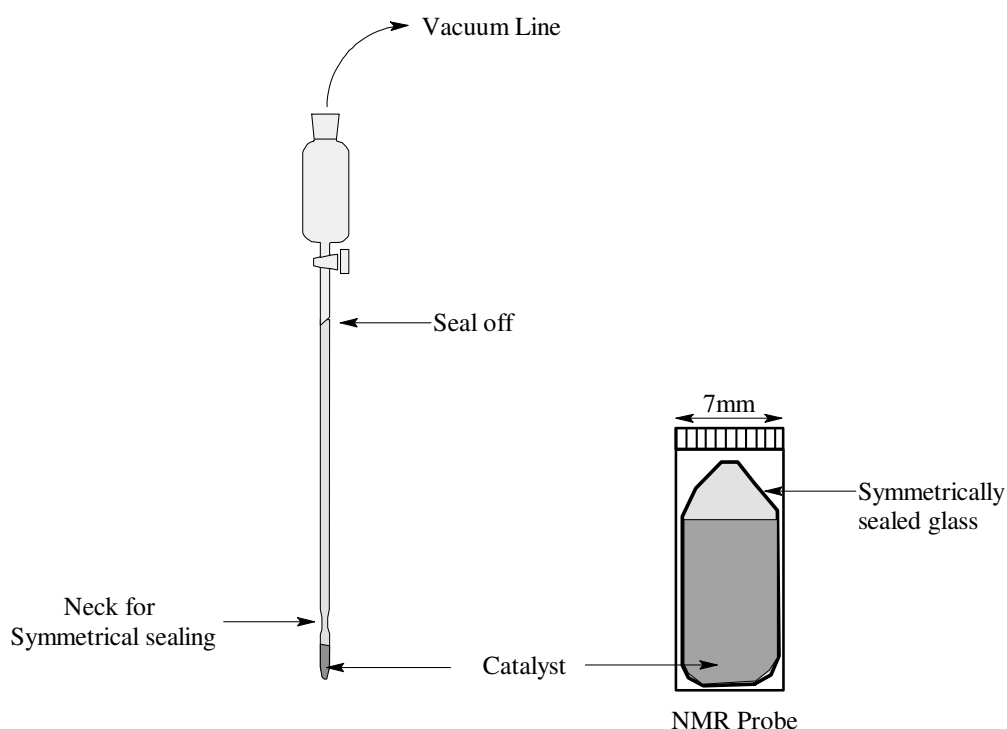
Figure 4.4 Schematic representation of the dehydration setup and the sealed catalyst in 7mm NMR probe.

FTIR spectra of the samples were recorded in the range of 4000-400 cm^{-1} by a Bruker IFS 113v instrument. The spectra were acquired at a 2 cm^{-1} resolution and averaged over 20 scans. The samples were prepared as thin self-supporting wafers of 5-10 mg/cm^2 and placed inside a controlled environment infrared transmission cell, capable of heating and cooling, gas dosing and evacuation (Figure 4.5). Prior to CO adsorption, the catalyst wafer was heated to 823 K at a rate of 10 K/min in an oxygen atmosphere. Subsequently, the cell

was out-gassed at the final temperature until the residual pressure was below 5×10^{-5} mbar. The sulfated samples were activated at a lower temperature (573 K) for 1 h. The sample was then cooled to 82 K. CO was introduced into the cell via a dosing valve (0.4 μmol per dose).
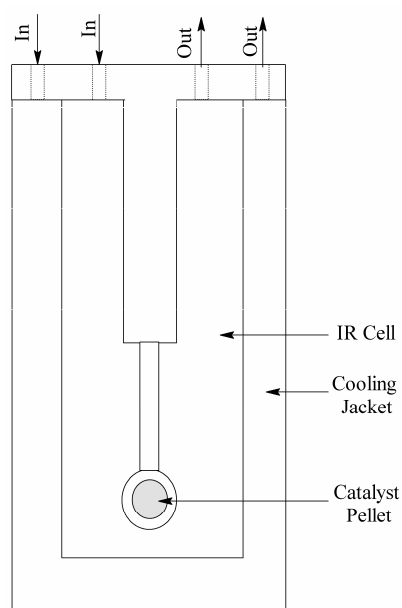
Figure 4.5 Schematic representation of the IR cell used in CO adsorption FT-IR experiments.

TPD analysis of IPAm decomposition was performed in a packed bed quartz reactor. The effluent gases were analyzed by a Balzers quadrupole mass spectrometer. In each experiment, an amount of 100 mg of catalyst was heated at a rate of 5 K/min to 523 K in a He flow of 100 ml/min. The sample was then cooled to 373 K and exposed to excess IPAm (99.5%, Aldrich) for 10 min. Physisorbed IPAm was removed at 373 K by purging in 100 ml/min He for 24 h. TPD of IPAm was carried out by heating the sample to 823 K at a rate of 5 K/min in 200 ml/min He. The formation of propene (m/e = 41) and ammonia (m/e = 17), i.e. the decomposition products of IPAm, as well as the amount of

desorbed IPAm (m/e = 44, 41, and 17) were followed and compared to well-calibrated standards.

4.3 RESULTS AND DISCUSSION

4.3.1 ICP Analysis

The zirconium and sulfur contents of the catalysts are shown in Table 4.3. The zirconium contents of the catalysts were lower than the amounts added in solution during the synthesis. Therefore, it was certain that, all of the zirconium could not be included in the structure. The remaining zirconium probably stayed in the aqueous phase when the precursor – zirconium salt (zirconiumoxychloride) – was dissolved and the zirconium was filtered out in the filtration step of the catalyst preparation. The actual Zr amount in the catalyst Zr(5)SBA-15 with 6.9 wt. % Zr in solution was 2.3 wt. % and as much as 13.4 wt. % of Zr was inserted into the Zr(30)SBA-15 catalyst with 30 mol % Zr in solution (28.2 wt. % in solution). The actual amount of zirconia in catalysts is not same for different preparation sets. The catalysts used for ^{1}H MAS NMR measurements and FT-IR experiments differ in terms of zirconia contents although the intended amounts in solutions were equal to each other (Table 4.4).

In the preparation of the sulfated catalysts, the last step was the sulfation of the catalysts after calcination. For this purpose 0.25 M sulfuric acid solution was prepared from concentrated sulfuric acid (95-98%, Merck). The sulfation takes place at room temperature in 0.25 M H_2SO_4 and the removal of the sulfuric acid solution was performed at ca. 80 °C overnight. The sulfur contents of the catalysts were in range between 9.3 to 2.9 wt %. The sulfur content is much higher than expected for the catalyst with low zirconia content

(Zr(5)SBA-15). Sulfuric acid could be adsorbed in the structure as well as water. Therefore, in order to remove the physisorbed sulfur, the samples were heated at ca. 350 °C in oven for 4h. As a result the decrease in the sulfur content was observed as expected. The average sulfur content of the samples after heat treatment is about 3.3 wt. %.

Table 4.3 Zirconium and Sulfur contents of the catalysts used for FT-IR and TPD measurements.

| | Zr (wt. %) | | S (wt. %) | |
| Catalyst | Intended Loading | Actual Loading | *Heat Treatment at ca. 350 °C 4h* | |
			Before	*After*
SZr(5)SBA-15	6.9	4.3	9.3	3.5
SZr(10)SBA-15	12.6	3.7	5.9	N/A
SZr(15)SBA-15	17.4	5.2	5.8	3.4
SZr(20)SBA-15	21.5	8.9	4.1	N/A
SZr(25)SBA-15	25.1	10.8	3.6	N/A
SZr(30)SBA-15	28.2	13.4	2.9	3.1

Table 4.4 Zirconium contents of the catalysts used for ^{1}H MAS NMR measurements and activity tests.

| | Zr (wt. %) | |
Catalyst	Intended Loading	Actual Loading
SZr(5)SBA-15	6.9	2.0
SZr(15)SBA-15	17.4	4.8
SZr(25)SBA-15	25.1	8.5
SZr(30)SBA-15	28.2	15.2

4.3.2 X-Ray Diffraction

The small angle X-ray diffraction patterns of SBA-15 and non-sulfated zirconia included SBA-15 samples are shown in Figure 4.6. SBA-15 exhibits two peaks at ca. $2\theta = 1.51°$ and $1.71°$ corresponding to diffraction lines from (110) and (200) planes. The line at ca. $1.2°$ (diffraction from 100 planes) was not clearly dissolved due to instrumental limitations; however, its presence is seen as an intense starting of the XRD spectrum at $1.25°$. In zirconia included catalysts the peaks at $1.51°$ and $1.71°$ were shifted to $1.39°$ and $1.56°$ respectively up to Zr(20)SBA-15 and disappeared above this loading. The shift towards lower degrees and the disappearance of the peaks in the small-angle region at higher zirconia loadings indicates the gradual loss of uniform mesostructure with respect to the increase in the zirconia content.
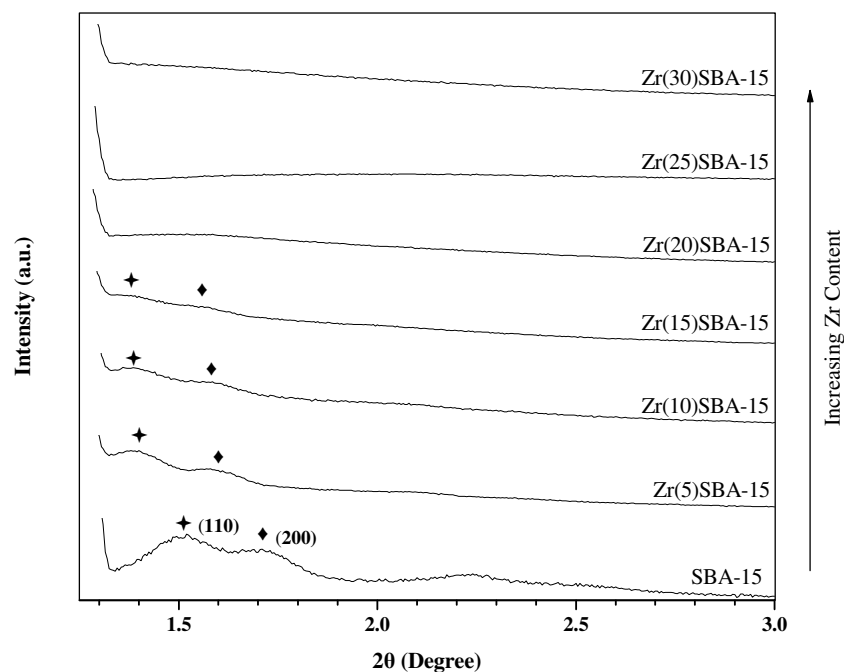
Figure 4.6 Small angle XRD patterns of SBA-15 and non-sulfated SBA-15 with ZrO_2 loadings of 5-30 mol % showing diffraction peaks from 110 and 200 planes of SBA-15.
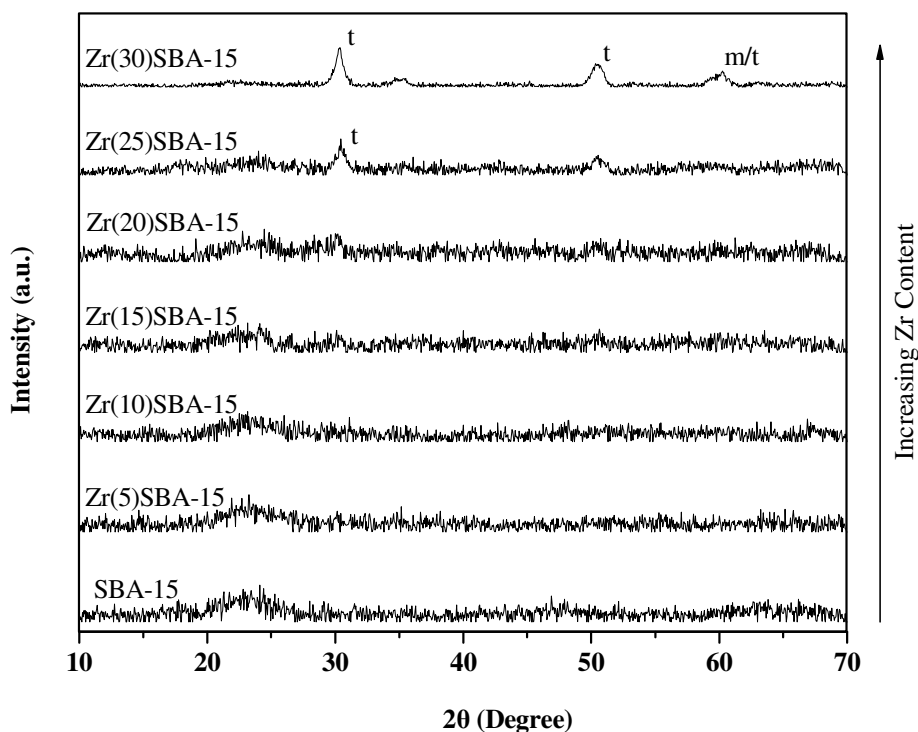
Figure 4.7 Wide angle XRD patterns of SBA-15 and non-sulfated SBA-15 with ZrO$_2$ loadings of 5-30 mol % showing crystalline tetragonal (t) and monoclinic (m) zirconia phases.

X-ray diffraction patterns in the wide angle region (10-70°) are shown in Figure 4.7. In the wide angle region, the catalysts below 25 mol % ZrO$_2$ loading exhibit no diffraction lines, indicating that zirconia is distributed uniformly within the structure. However, the catalyst with 25 mol % ZrO$_2$ content revealed a diffraction peak at $2\theta = 30°$. This peak corresponds to the tetragonal crystalline zirconia (ICDD No: 17-0923). In 30 mol % ZrO$_2$ loading, two additional peaks at ca. 50° and 58° were also appeared, corresponding to the tetragonal (ICDD No: 17-0923) and monoclinic (ICDD No: 74-0815) zirconia crystals. The XRD lines of crystalline zirconia appeared only in the catalysts with high zirconia contents (at ca. $\geq$ 25 mol %). Therefore, for

catalysts at ca. 25 mol % ZrO_2 contents, zirconia is not distributed finely within the structure, but the zirconia crystals were formed. At these loadings, small angle XRD lines at $2\theta = 1.51°$ and $1.71°$ also disappeared, indicating that the long range order of the pores was lost upon the agglomeration of zirconia precursor to form crystalline phases.

4.3.3 Transmission Electron Microscopy

The TEM images of SBA-15 are shown in Figure 4.8. The uniform hexagonal arrays of mesopores were detected in the first row of the pictures. The parallel extension of the pores in 2D space is clearly seen in the second row.
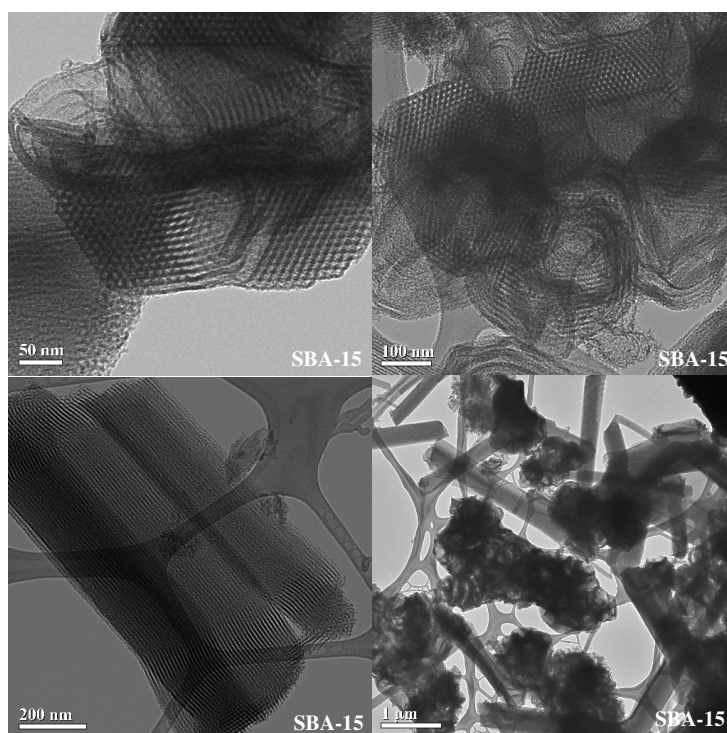
Figure 4.8 TEM images of SBA-15 structure with hexagonally arrayed parallel mesopores.

SBA-15 was also sulfated to control the effect of sulfation to the SiO_2 matrix. The TEM image of S-SBA-15 revealed that the sulfation treatment did not bring about significant influence on the framework (Figure 4.9).
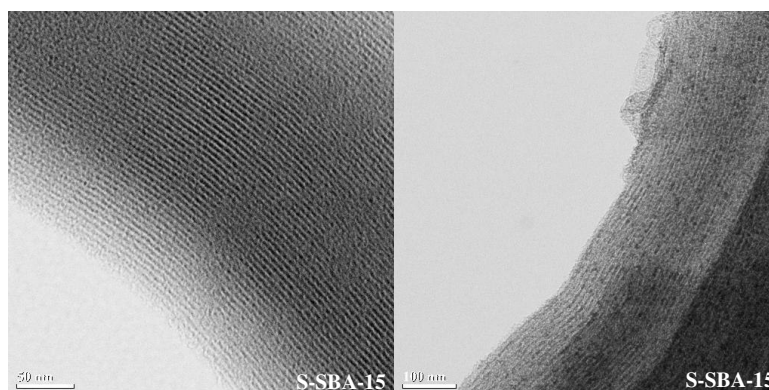
Figure 4.9 TEM images of sulfated SBA-15 structure with parallel mesopores.

TEM images of non-sulfated catalysts with 15 and 25 mol % ZrO_2 loadings are given in Figure 4.10. When zirconia was introduced to the SBA-15 structure at 15 mol % loading, the mesostructure was retained. Zirconia could not be distinguished in the TEM images at this loading, which indicates a high dispersion of zirconia in the mesostructure, in agreement with the wide angle XRD patterns at these loadings. For catalyst with 25 mol % zirconia loading long range order has been lost, although ordered structure could be observed locally to some extent. A phase separation of zirconia; however, could not be distinguished indicating the high dispersion of zirconia.
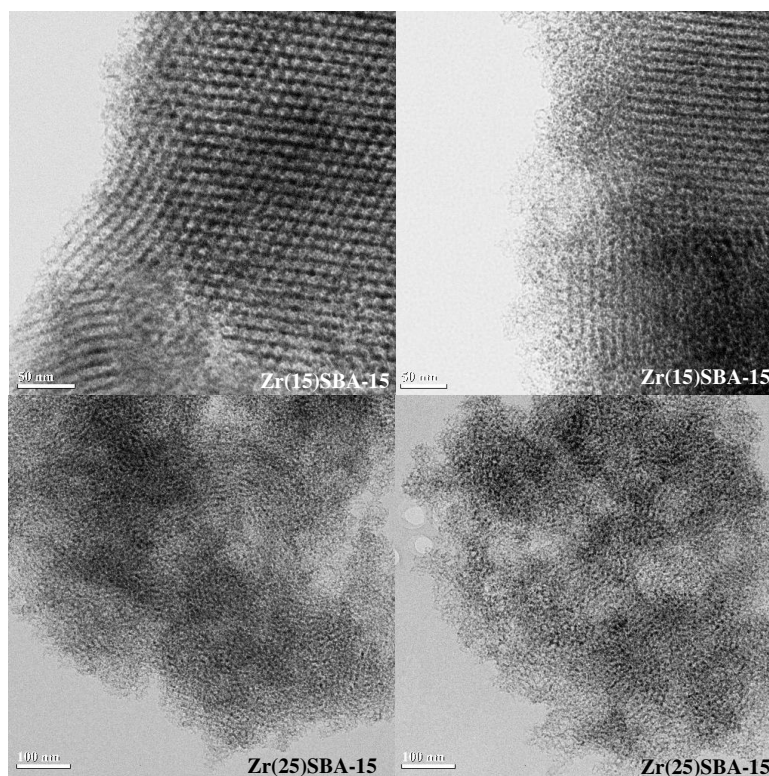
Figure 4.10 TEM images of zirconia included SBA-15 catalysts with hexagonally arrayed mesopores extending parallel to each other.

After sulfation of the 15 mol % ZrO_2 included catalyst, the structure exhibited uniformity (Figure 4.11). The long range order of mesopores was not seen in the sulfated catalyst with 25 mol % loading.
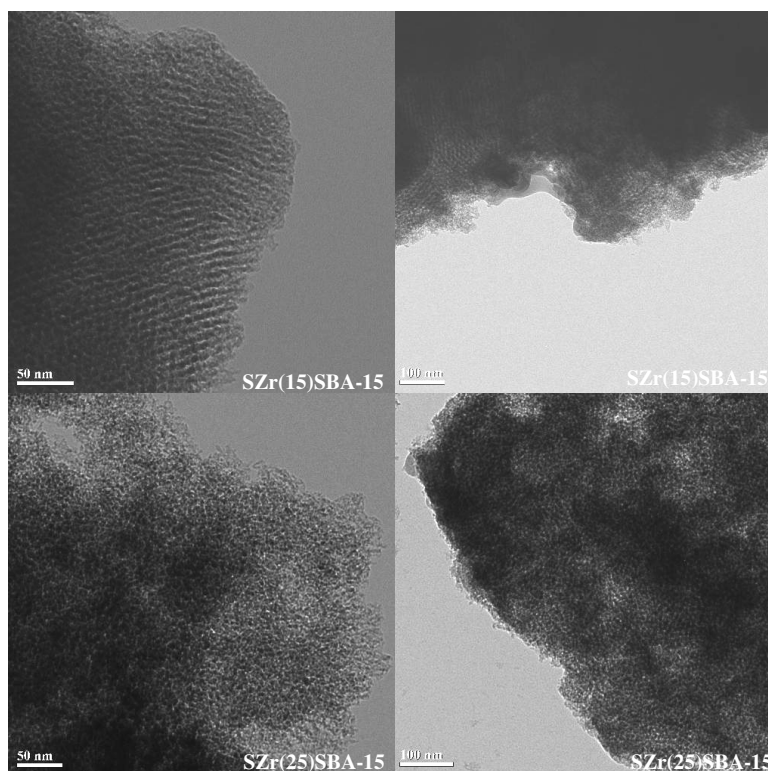
Figure 4.11 TEM images of sulfated zirconia included SBA-15 catalysts.

4.3.4 N$_2$ Adsorption

The surface areas of the catalysts were given in Figure 4.12. SBA-15 exhibits a BET surface area of 773 m^2/g, confirming the highly ordered mesostructure in good agreement with the TEM and XRD results. Zirconia included catalysts have lower surface areas than pure SBA-15 ranging between 733 to 456 m^2/g. The introduction of zirconia in SBA-15 formed a less ordered structure than pure SBA-15, which reduces the surface area as well as the long range order. The decrease in the surface area is more drastic in sulfated catalysts, which show BET areas in between 313-246 m^2/g.
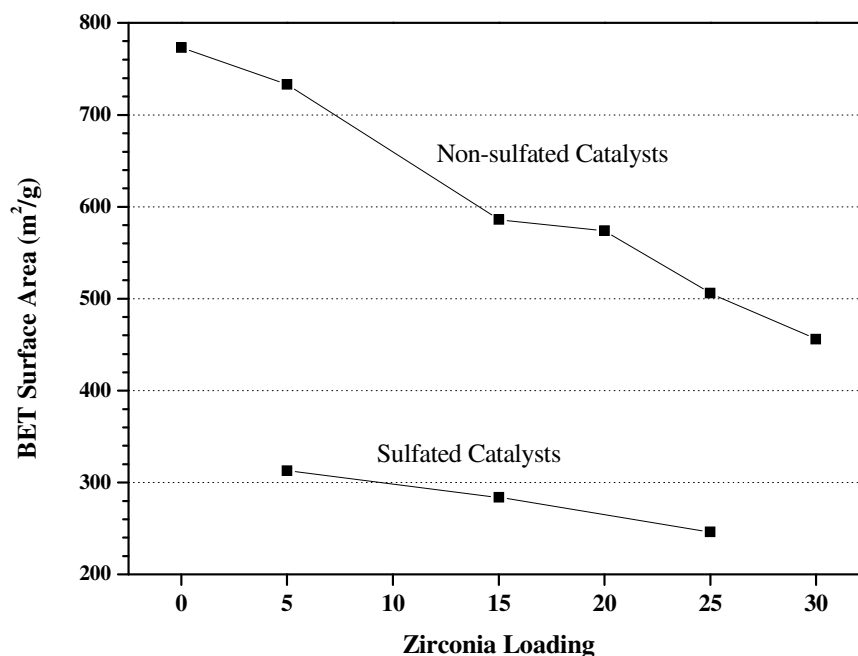
Figure 4.12 BET surface areas of SBA-15, non-sulfated and sulfated Zr included SBA-15.

The structural parameters of the catalysts obtained from BET analysis were presented in Table 4.5. Pore diameters of the non-sulfated catalysts are in between 66.3 and 103.5 Å. The average pore diameter of SBA-15 is 71.2 Å and the introduction of zirconia increases the average pore diameter up to 20 mol % loading. Nevertheless, the pore diameter decreases to 66.3 Å at 30 mol % loading. The effect of zirconia in the SBA-15 structure is the enlargement of the pore openings; however, at higher loadings the catalysts does not exhibit long range uniformity of the mesostructure and thus a decrease in pore diameter was observed. The pore volumes of the catalysts follow a similar trend.

Table 4.5 BET single point total volume of pores and average pore diameters of the non sulfated and sulfated Zr-SBA-15.

Catalysts	Pore diameter (Å)	Pore volume (cc/g)
SBA-15	71.2	1.18
Zr(5)SBA-15	77.5	1.34
Zr(15)SBA-15	82.9	1.46
Zr(20)SBA-15	103.5	1.55
Zr(25)SBA-15	94.4	1.15
Zr(30)SBA-15	66.3	0.96
SZr(5)SBA-15	54.5	0.43
SZr(15)SBA-15	55.9	0.40
SZr(25)SBA-15	55.5	0.34

Figure 4.13 shows the pore size distributions of SBA-15 and 5, 25 mol % zirconia included SBA-15 catalysts without sulfation (the distributions of the rest of the catalyst are given in Appedix C). The narrow pore size distribution of SBA-15 around 10 nm indicates its highly ordered mesostructure. As the zirconia content increased, the pore size distribution was broadened. This is in agreement with the XRD patterns and the TEM images that the increase in zirconia content reduces the uniformity of the structure. The pore size distribution of the sulfated samples is broader, in 2-8 nm pore size range (Figure 4.14). These pore structure data can be interpreted only as the long range order was lost.

The nitrogen adsorption-desorption isotherms of the catalyst were given in Appendix C (Figure C.4 and Figure C.12). All the catalysts show type IV adsorption isotherms. Type A hysteresis loop was observed for all catalysts, which was related to the capillary condensation associated with porous

structure of the catalyst. The adsorption and desorption isotherms were closer to each other with the increase in zirconia content, and in sulfated catalysts. This indicates in accordance with the TEM images that SBA-15 has more uniform structure than zirconia included catalyst and they have more uniform mesopores than the sulfated catalysts.
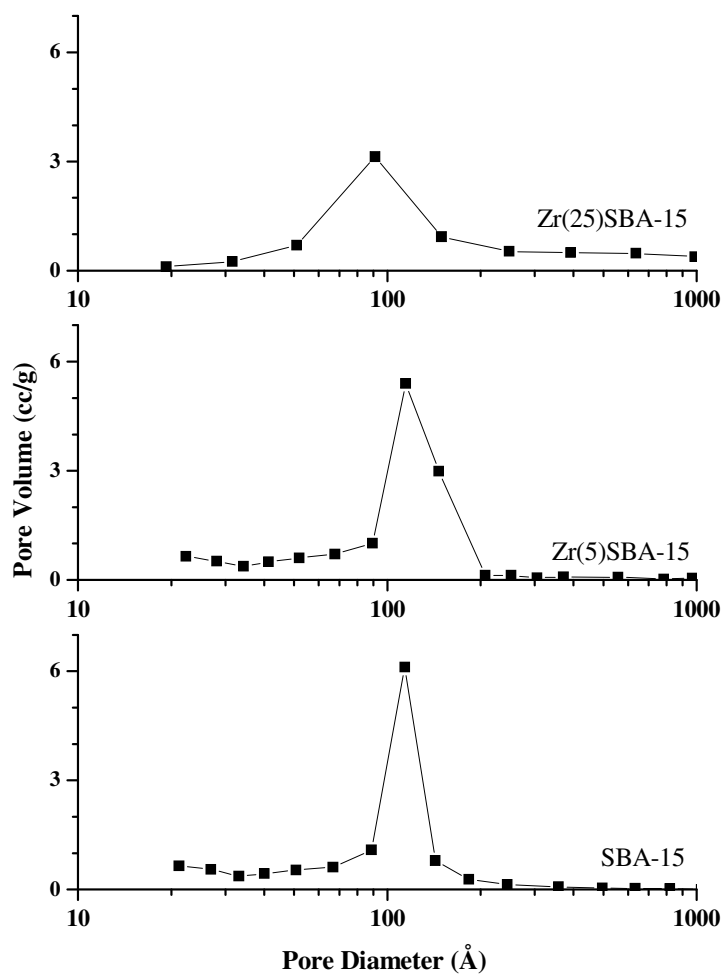
Figure 4.13 BJH pore size distribution of SBA-15 and zirconia included SBA-15 at 5 and 25 mol % Zr loading.
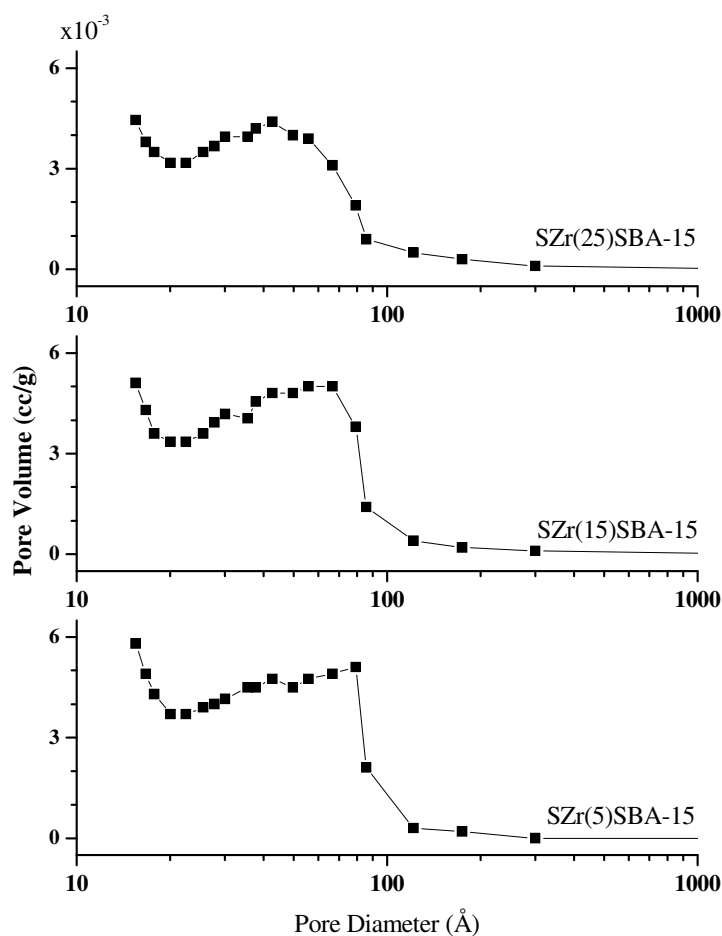
Figure 4.14 BJH pore size distribution of sulfated SBA-15 at 5,15 and 25 mol % zirconia loading.

4.3.5 ^{1}H MAS NMR Spectroscopy

^{1}H MAS NMR investigations on conventional zirconia and sulfated zirconia samples have been reported by Riemer et al. [173]. It is reported that sulfate-free ZrO_2 shows a ^{1}H NMR line at 3.86 ppm and a weaker signal at 1.60 ppm. On the other hand, the conventional sulfated zirconia sample was found to be dominated by a single line at 5.85 ppm. Thus, the sulfate modification induces a significant downfield shift of at ca. 2 ppm that

suggested a strongly enhanced proton acid strength relative to pure ZrO_2, i. e. the OH groups developed a high protonic acidity owing to the high electronegativity of Zr^{4+}.

In the present ^1H MAS NMR measurements, we compared the spectra of hydrated, dehydrated and modified SBA-15 catalysts. In the absence of any heat treatment the catalysts adsorb water in ambient conditions and present in a hydrated state. The modifications include co-precipitation with zirconia and then the sulfation of the zirconia samples with H_2SO_4 as described above. In Figure 4.15 a and b the proton NMR spectra are shown for hydrated and dehydrated SBA-15 materials without any further modification. The dehydrated samples reveal an overlap of various resonance lines. In the shift range of structural OH groups, the deconvoluted ^1H MAS NMR spectra reveal four distinct resonance lines at -0.5, 0.7 (very weak shoulder), 1.2, and 1.8 ppm relative to liquid TMS. Prior to dehydration, an additional line at ca. 3.5 ppm, attributed to bound water [174], was also observed. It is known from the previous work [164, 175, 176] on MCM-41 that the asymmetric shape of these signals is a hint for the presence of different types of silanol groups, such as isolated and geminal SiOH groups and internal SiOH groups.

The chemical shift range between 1.2 and 2.2 ppm is typical for silanol groups in most of the zeolites (Hunger et al. [176] and references therein). According to Trèbosc et al. [164], the isolated, i.e. non-hydrogen bonded, single and/or geminal SiOH groups are not detectable directly at their usual position around 1.8 ppm due to the fast proton exchange. In SBA-15 material, the intensity of 1.2 ppm line does not change appreciably, but the intensity of the line at 1.8 ppm is increased upon removal of water (Figure 4.15 a and b). This situation can be interpreted as the decrease of intensity at 1.8 ppm line under hydrated conditions due to the fast exchange with bound water. On the other hand, species giving rise to 1.2 ppm line is not interacting with adsorbed water. The intensities and the shift of the weak line at 0.7 ppm and the peak at -

0.5 ppm were also not changed in the dehydrated samples. This indicates the inaccessibility of these proton sites to water.
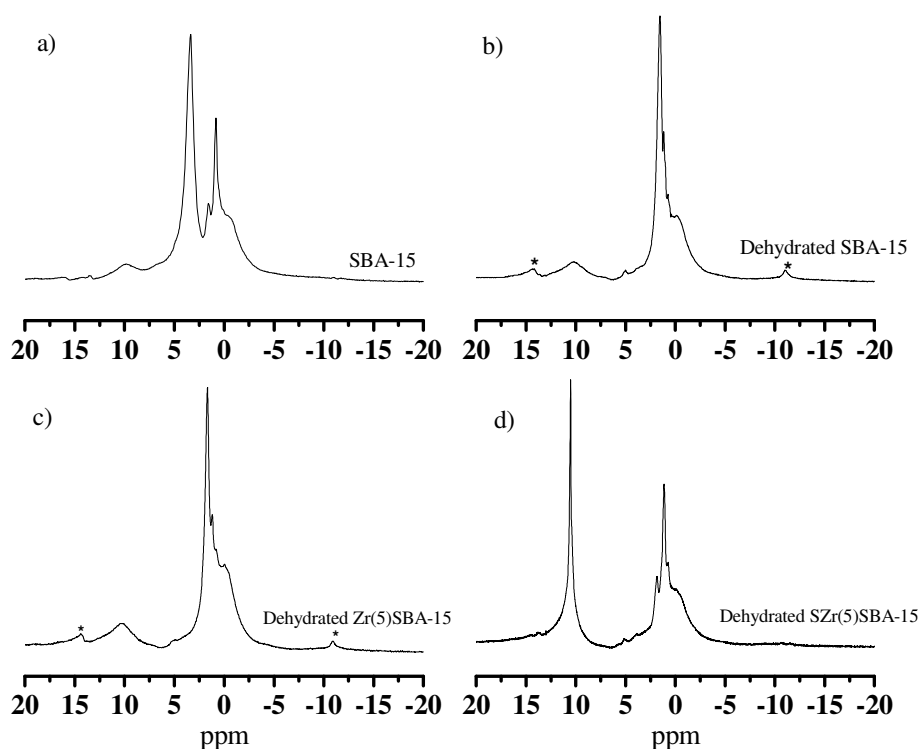
Figure 4.15 ^{1}H MAS NMR taken at AVANCE-400 with an MAS frequency of 5 kHz at 300 K for a) pure hydrated SBA-15, b) pure dehydrated SBA-15, c) dehydrated SBA-15 with 5 mol % ZrO_2 loading, d) dehydrated sulfated SBA-15 with 5 mol % ZrO_2 loading. The ppm scale is with respect to liquid TMS. * stands for the spinning side bands.

Furthermore, a relatively weak broad line at ca. 10 ppm is observed which is not altered in the modification process. This line was also not accessible to the proton exchange with OH groups and water. This strong shift can be interpreted in terms of a strong non-symmetric hydrogen bond [177, 178] to inaccessible SiOH groups in the walls of the SBA-15. The origin of the

-0.5 and 0.7 ppm lines in pure SBA-15 is not completely clear, but this uncertainty does not influence further interpretation as to be still discussed.

It was clearly observed that for ZrO_2/SBA-15 samples without sulfation the ^1H MAS NMR spectra for the dehydrated samples are practically the same as for the non-modified SBA-15 samples (Figure 4.15 b and c). However, clear changes are measured for sulfated ZrO_2/SBA-15 samples (Figure 4.15 d). An intense line appears at 10.6 ppm that was not detected in all other samples without sulfation. This line can be related to strong acid sites, which are introduced by the sulfation treatment. The effect of the ZrO_2 loading on the intensity of this line is seen in Figure 4.16. The relative intensities in the spectrum after deconvolution (Table 4.6) show that the catalyst with 25 mol % ZrO_2 loading has the highest acidity. A further increase in the ZrO_2 content causes a decrease in the relative intensity of this line.

Table 4.6 Relative intensities of the line at 10.6 ppm from the deconvoluted ^1H MAS NMR spectra for different zirconia contents[a].

ZrO_2 mol % of the Sulfated sample	0	5	15	25	30
Relative intensity (%)	0	6	7	23	15

[a]The relative intensities were estimated from the area under these lines with respect to the total spectrum.
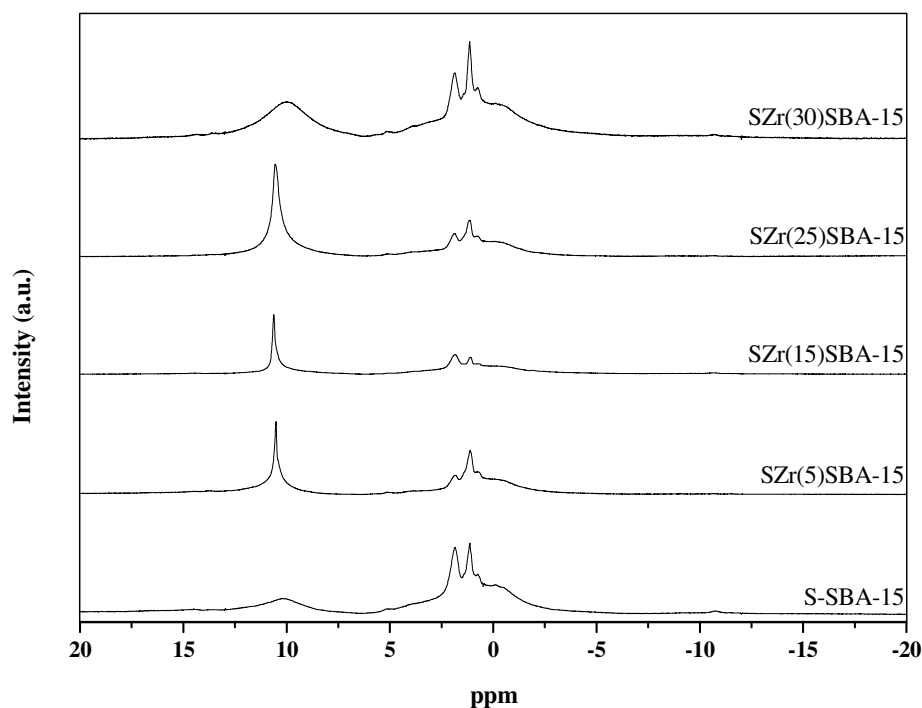
Figure 4.16 ^{1}H MAS NMR taken at Bruker AVANCE-400 with MAS frequency of 5 kHz at 300 K for dehydrated sulfated SBA-15 with 0, 5, 15, 25, and 30 mol % ZrO$_2$ loading. The ppm scale is with respect to liquid TMS.

This situation is better observed if we compare the spectra for the dehydrated sulfated samples with those for the hydrated sulfated ones at different ZrO$_2$ contents (Figure 4.17). At ZrO$_2$ levels greater than ca. 20 mol %, two intense peaks at ca. 1.2 and 3.8 ppm typical of OH shifts of crystalline ZrO$_2$ (Figure 4.17 c) are observed. These shifts are in good agreement with the shifts reported by Riemer et al. [173]. It is important to note here that at 25 % ZrO$_2$ loading the crystalline zirconia peaks also appeared in the XRD patterns, indicating the formation of ZrO$_2$ crystals (Figure 4.6). Moreover, the ^{1}H MAS NMR spectra of the hydrated samples allow a very clear conclusion about the strong acid sites: For low ZrO$_2$ content (5 mol %) only one almost symmetric line is observed at ca. 8 ppm (Figure 4.17 a). The chemical shift of this line is

slightly changed from 7.8 ppm to 8.9 ppm if the ZrO_2 content is increased to 30 mol % (Figure 4.17 a and c). It is obvious that this line corresponds to the line observed at 10.6 ppm for the dehydrated samples. The chemical shift is reduced to ca. 8 ppm due to the fast exchange between protons of the adsorbed water (and, apparently, also in the structural OH groups) on the one side and protons of the strong acid sites on the other side. If two protons in different environments described by their chemical shifts as δ_1 and δ_2 exchange faster than the NMR sampling rate, they appear in the spectrum as a single line with a chemical shift proportional to their population averaged shift as given in the following equation:

$$\delta = x_1\delta_1 + x_2\delta_2 \qquad (4.1)$$

Note that for the same reason the intensity of typical silanol lines between -0.5 to 2.3 ppm (Figure 4.17 b and d), seen after the dehydration treatment, is strongly reduced or even no more detectable in case of hydrated samples. Our measurements on hydrated and dehydrated sulfated SBA-15 samples with zirconia have clearly revealed the formation of accessible strong acidic proton sites.
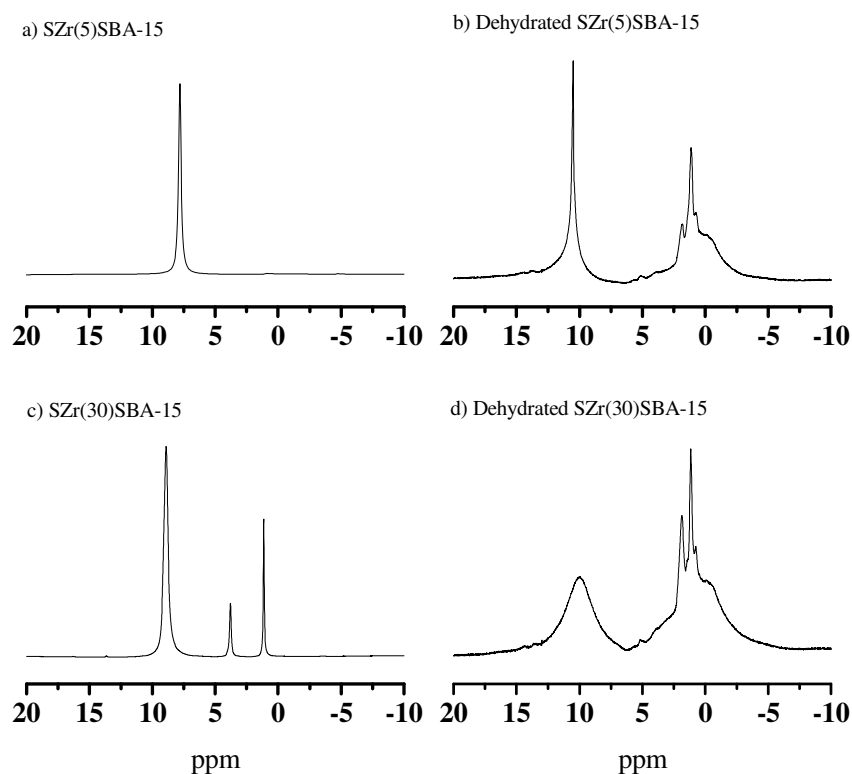
Figure 4.17 ^{1}H MAS NMR taken at Avance-400 with MAS spinning frequency of 5 kHz at 300 K for a) hydrated sulfated SBA-15 with 5% ZrO$_2$, b) dehydrated sulfated SBA-15 with 5% ZrO$_2$, c) hydrated sulfated SBA-15 with 30% ZrO$_2$, d) dehydrated sulfated SBA-15 with 30% ZrO$_2$. The ppm scale is with respect to liquid TMS.

4.3.6 ^{29}Si MAS NMR Spectroscopy

^{29}Si MAS NMR spectra of the SBA-15 and Zr(30)SBA-15 catalysts are presented in Figure 4.18. ^{29}Si NMR spectra of oxides generally exhibit three peaks for different environments for Si: isolated silanol groups (SiO)$_3$Si-OH, Q^3; geminal silanols (SiO)$_2$Si-(OH)$_2$, Q^2; and silicon in the siloxane binding environment without hydroxyl groups (SiO)$_4$Si, Q^4 [38, 179-183]. For pure SBA-15, (Figure 4.18 a), two lines were resolved at -100 and -110 ppm for Q^3

and Q^4, respectively, while the Q^2 Si line, expected at -92 ppm, could not be distinguished. In the presence of Zr, relative intensity of Q^3 line with respect to Q^4 line increased (Figure 4.18 b). The relative intensities of the two silicon environments (Q^3 and Q^4) were calculated from the ratio of the area of the corresponding peak with respect to the total area and presented in Table 4.7.

Table 4.7 ^{29}Si MAS NMR chemical shifts and relative intensity ratios Q^3/Q^4.

Catalyst	SBA-15	Zr(30)SBA-15
Chemical shift Q^3 (ppm)	-100.8	-101.9
Chemical shift Q^4 (ppm)	-110.3	-111.2
Relative intensity[a] Q^3 (%)	18	39
Relative intensity[a] Q^4 (%)	82	61
Relative intensity ratio Q^3/Q^4	0.22	0.63

[a] Relative intensities were estimated from the area under the these lines with respect to the total spectrum.

The Q^3/Q^4 ratio increases for Zr(30)SBA-15 catalysts as compared to SBA-15. This can be due to the ion modification of SBA-15 [184] or the enrichment of the surface by silica since it is thermodynamically more favourable [185]. In other words, Zr incorporated silicas can result in Q^3-like environments [186] where hydrogens in OH groups or silicons in Q^4 units are replaced by Zr, i.e. $Si(SiO)_3$-OZr. Higher concentration of Q^3 along with relatively lower surface area of Zr(30)SBA-15 suggests a more pronounced effect on the condensation of the silica walls.
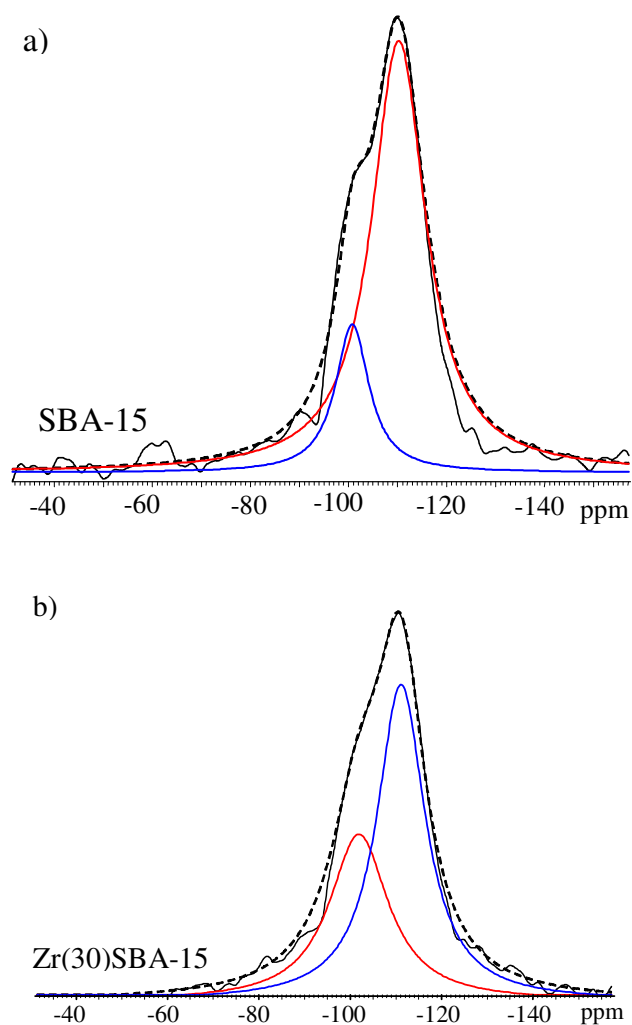
Figure 4.18 ^{29}Si MAS NMR spectra of a) SBA-15, b) Zr(30)SBA-15 taken at Bruker AVANCE-400 Spectrometer with MAS frequency of 10 kHz.

4.3.7 FT-IR Experiments

Previous FT-IR investigations prove that sulfation of zirconia enhance the strength of the bridging zirconia hydroxyl groups (i.e., Zr(OH)Zr) and eliminates the terminal ones (i.e., ZrOH) [146]. In addition, it creates a new type of Brønsted acid site, presumably protons forming multicentered or single bonds with sulfate ions. These protons are hydrogen bonded to the surface

[147]. The use of CO as probe molecule adsorbed at low temperatures has clarified various aspects of the acid sites and strength of these sites on the surface of sulfated zirconia [187].

Figure 4.19 shows the FT-IR spectra in the CO stretching region of SBA-15 after CO adsorption at 82 K. The spectra exhibit two bands at 2138 and 2157 cm^{-1}. The latter is attributed to the CO adsorbed on silanol groups. The weaker band at 2138 cm^{-1} is due to a liquid-like CO phase condensed on the surface of SBA-15.
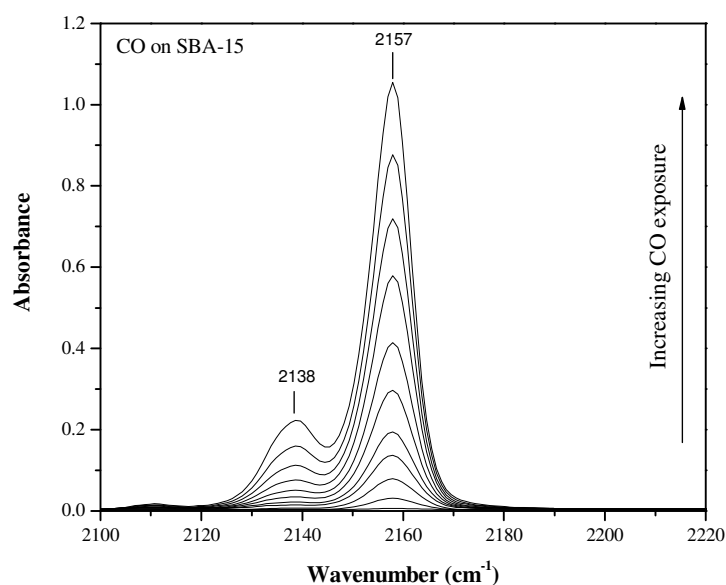
Figure 4.19 FT-IR spectra of CO adsorption at 82 K over SBA-15 in CO stretching region.

Upon the introduction of zirconia in SBA-15, an additional band is observed at 2186 cm^{-1}. The FT-IR spectra in the CO stretching region of 15 mol % zirconium included SBA-15 is shown in Figure 4.20. In addition to the bands at 2138 and 2157 cm^{-1} the inclusion of zirconia reveals an additional line at 2186 cm^{-1}. This band is assigned to Lewis acid centers due to coordinatively unsaturated Zr^{4+} centers [187]. It was observed that the increase in the exposure of the surface to CO saturated these sites earlier than the silanols,

implying that these latter sites are more strongly acidic than the silanol groups in correspondence to the larger shift of the CO frequency from the gas phase CO frequency ($\upsilon_{CO(gas\ phase)}$=2143 cm^{-1}). Further modification by sulfation of the zirconia-modified SBA-15 results in the disappearance of the band at 2186 cm^{-1} (Figure 4.21). The bands at 2138 and 2157 cm^{-1} are retained.
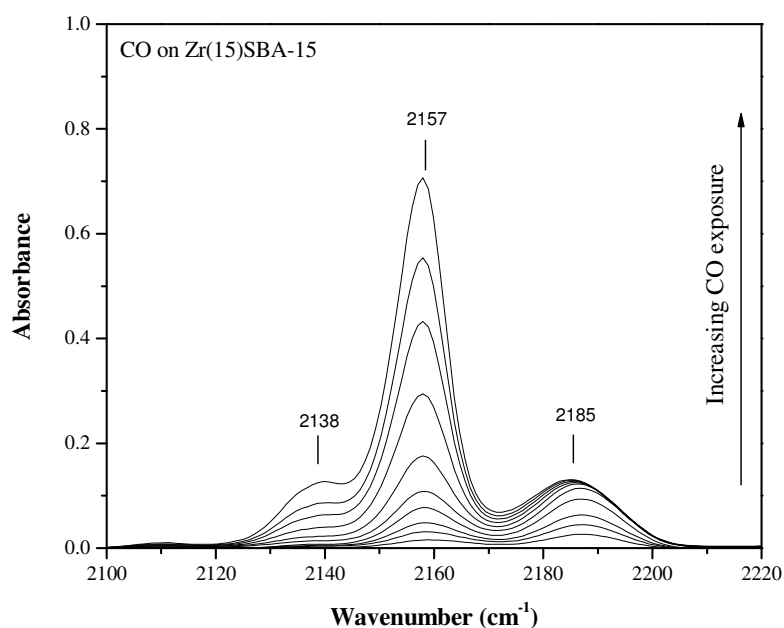
Figure 4.20 FT-IR spectra of CO adsorption at 82 K over SBA-15 with 15 mol % Zirconia loading in CO stretching region.
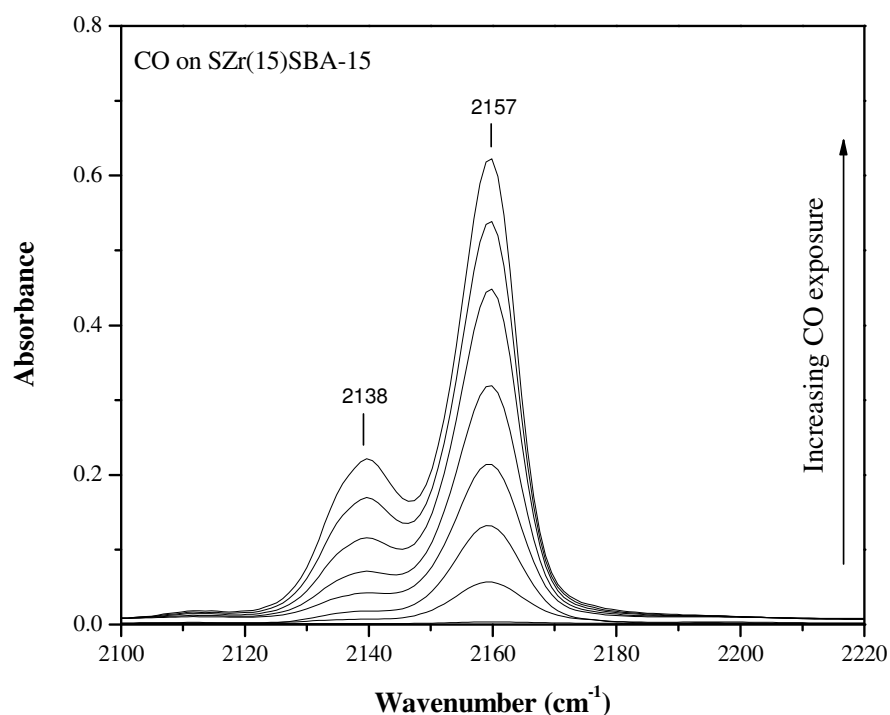
Figure 4.21 FT-IR spectra of CO adsorption at 82 K over sulfated SBA-15 with 15 mol % Zirconia loading in CO stretching region.

In Figure 4.21, the IR spectra of the sulfate modified catalyst with 15 mol % Zr loading is seen. Similar to the non-sulfated catalyst (Figure 4.20), bands at 2138 and 2157 cm^{-1}, but not at 2186 cm^{-1} are present. The band at 2138 cm^{-1} is due to weakly absorbed CO, and the band at 2157 cm^{-1} is attributed to silanol groups. The absence of band attributed to low coordinated Zr^{4+} centers is attributed to complete coverage of the Lewis acid centers by sulfate groups.

The IR band at 3794 cm^{-1} (Figure 4.22) with very low intensity is ascribed to ZrO-H, which was slightly perturbed upon CO adsorption. Its

absence in sulfated samples supports the idea that the terminal ZrOH groups are eliminated by sulfation [146].
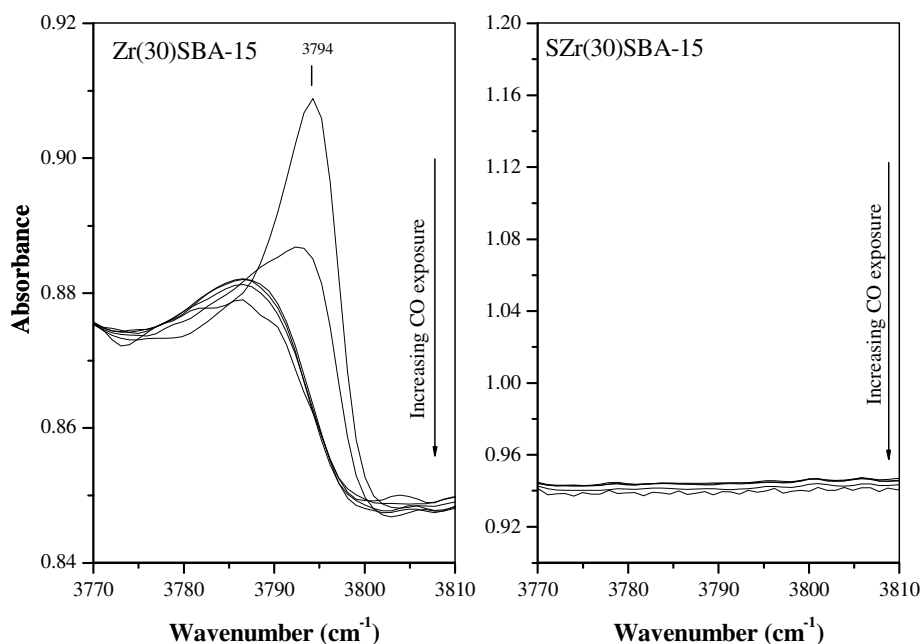
Figure 4.22 FT-IR spectra of CO adsorption at 82 K over non sulfated and sulfated 30 mol % Zr included SBA-15 in ZrOH stretching region.

Figure 4.23 shows the IR spectra in the silanol stretching region of SBA-15, Zr(30)SBA-15, and SZr(5)SBA-15catalysts. In the spectra of SBA-15 (Figure 4.23 a) the sharp line at 3747 cm^{-1} is ascribed to the non-hydrogen bonded isolated silanol groups on the surface of the silica molecular sieve. The broad tail extending towards 3400 cm^{-1} is due to the hydrogen bonded and/or geminal silanol groups. CO adsorption on isolated silanol groups weakens the hydroxyl bond and leads to a perturbed band around 3653 cm^{-1} with a frequency shift of 94 cm^{-1}.
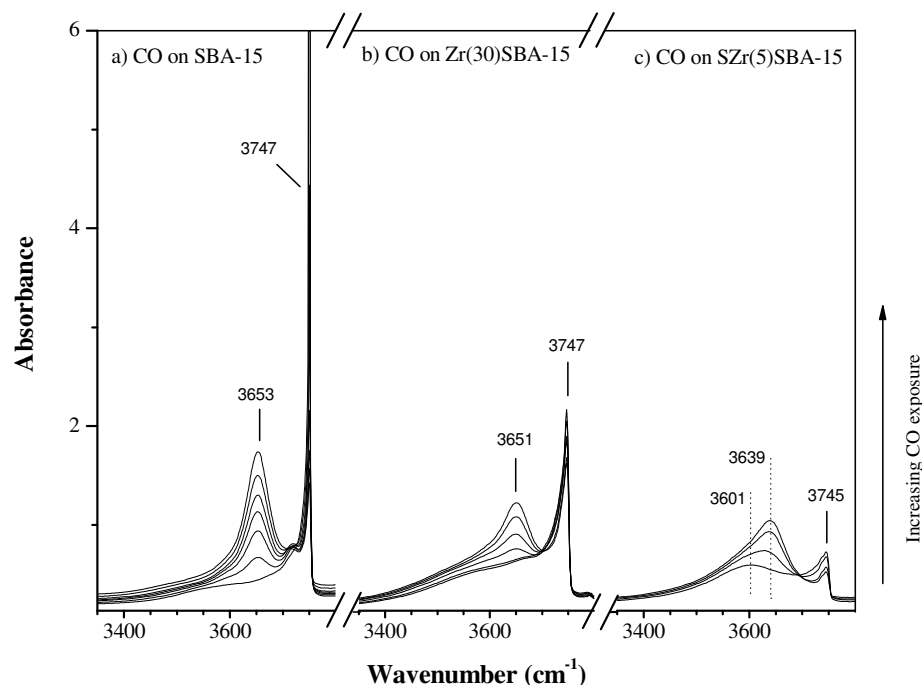
Figure 4.23 FT-IR spectra of CO adsorption at 82 K over a) SBA-15, b) SBA-15 with 30 mol % ZrO_2, and c) Sulfated SBA-15 with 5 mol % ZrO_2 in silanol stretching region.

The silanol stretching region of the 30 mol % Zr included SBA-15 (Figure 4.23 b) is similar to pure SBA-15. The isolated silanol groups are identified by the band at 3747 cm^{-1}. The tail is preserved, and its extention through 3400 cm^{-1} indicates the presence of hydrogen bonded and/or geminal silanol groups. The shift of the hydroxyl groups upon CO adsorption is similar to SBA-15 indicating that the silanol groups are still only weakly acidic.

Figure 4.23 c shows the IR spectra of the silanol region for sulfated 5 mol % Zr included SBA-15. The spectrum exhibits a band at 3747 cm^{-1} and a broad tail extending to 3400 cm^{-1} corresponding to isolated and hydrogen bonded and/or geminal silanol groups respectively, very similar to the zirconia-modified and SBA-15 catalysts. Nonetheless, the effect of CO adsorption on

the band of isolated silanol groups is different for sulfated catalysts. At low CO coverage, the perturbed hydroxyl band is located at 3601 cm^{-1} corresponding to a shift of 144 cm^{-1} for sulfated 5 mol % Zr included SBA-15 – SZr(5)SBA-15. With increasing CO coverage, the band of perturbed OH broadens and $\Delta\upsilon_{OH}$ at high CO coverage is 106 cm^{-1}. This is likely due to the presence of both weakly acidic sites ($\Delta\upsilon_{OH}$ = 94 cm^{-1}) and more strongly acidic sites ($\Delta\upsilon_{OH}$ = 144 cm^{-1}). A shift of 144 cm^{-1} is very close to the shift (139 cm^{-1}) reported earlier for conventional sulfated zirconia catalysts and SZr-SBA-15 catalysts are slightly more acidic [187].

We interpret the presence of more acidic silanol groups in terms of hydrogen bonding to the Brønsted acid proton connected to the bisulfate group. This is in agreement with the model proposed by Adeeva et. al. [147]. In this structural model, proton interacts with proximate oxygen. In our catalyst, zirconia is finely dispersed in the silica framework and it is thus reasonable to suggest that the acid proton of the bisulfate group interacts with proximate silanol groups. Thus, a chemical shift of 144 cm^{-1} can be explained by hydrogen bonding of the acidic proton of the bisulfate group not only with the adjacent zirconia but also with the silanol in close proximity. The increased acidity of these sites is indicated by the preferential interaction of CO with these sites over the weaker acidic silanol groups at low CO coverages. Since these centers are more acidic than the isolated silanol groups, CO is first adsorbed on these sites followed by the adsorption on the remaining silanol groups. However, the protons of the silanol groups are weaker due to the hydrogen bonding between the proton of the bisulfate group and the oxygen in the silanol.

The specific IR bands ascribable to the bisulfate OH groups are difficult to detect due to their hydrogen bonding to the surface. In the IR spectra of conventionally prepared sulfated zirconia, the band at 3639 cm^{-1} is accepted to originate from the acidic hydroxyl groups [187].

The presence of bisulfate groups is also evident from the influence of CO adsorption on the S=O stretching band. Figure 4.24 shows the IR spectra of the S=O stretching region for sulfated 5 and 30 mol % Zr included SBA-15. Upon CO adsorption, peak at 1407 cm^{-1} was blue shifted by 26 cm^{-1}. This shift suggests an increase of the S=O bond strength and is attributed to the interaction of carbon monoxide with the proton interacting with the bisulfate group. Weakening of the SO−H bond upon CO adsorption leads to an increase in S=OH bond strength. This provides a strong indication for the presence of protonic sites connected to the bisulfate groups indirectly. Indeed, direct observation of the strong Brønsted acid protons in sulfated zirconia catalysts is not straightforward, likely because of the strong hydrogen bonding to adjacent surface groups.
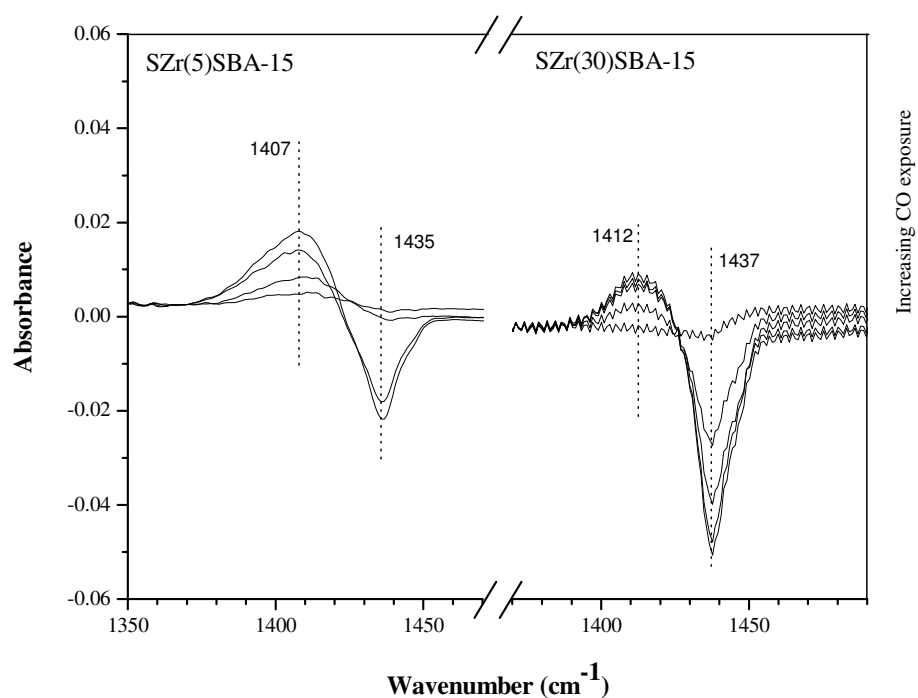

Figure 4.24 FT-IR spectra of CO adsorption at 82 K over sulfated Zr-SBA-15 catalysts in SO stretching region a) 5 mol % Zr b) 30 mol % Zr.

4.3.8 TPD Experiments

TPD of alkylamines is a way to quantify acidic site densities. Alkyl ammonium ions form by protonation of amines at Brønsted sites and decompose into the corresponding alkene and NH_3 in a narrow temperature range through a reaction similar to the Hoffman elimination [188]. Thus, isopropylamine (IPAm) can be utilized by its decomposition into propene to quantify the Brønsted sites.

TPD of isopropylamine decomposition are shown in Figure 4.25. During the TPD of non modified SBA-15, no propene desorption peaks were observed. In the zirconia included catalysts, the IPAm decomposition was seen between 310 to 360 °C having a maximum at 340 °C. In sulfated catalysts the decomposition interval decreases to lower temperatures, between 290-340 °C peaking around 312 °C. Thus, the sulfation treatment clearly introduces strong acidity to the structure. Within the sulfated catalysts, the maximum decomposition rate ranges between 310-316 °C but does not show a trend. In Table 4.8 the total amounts of isopropylamine decomposition is given for different catalysts. The total amount of IPAm decomposed increases with the introduction of zirconia, and further increase is seen with sulfation treatment.

The IPAm decomposition has a maximum (0.5 mmol/g cat.) with sulfated 15 mol % Zr/SBA-15 catalyst. This indicates that zirconium is distributed finely within the structure up to this loading. Further increase does not introduce additional acid sites, conversely leads to an agglomeration of zirconium precursor to form zirconia crystals and thus the formation of bulk zirconium results in a lower number of available sites per gram of the catalyst.
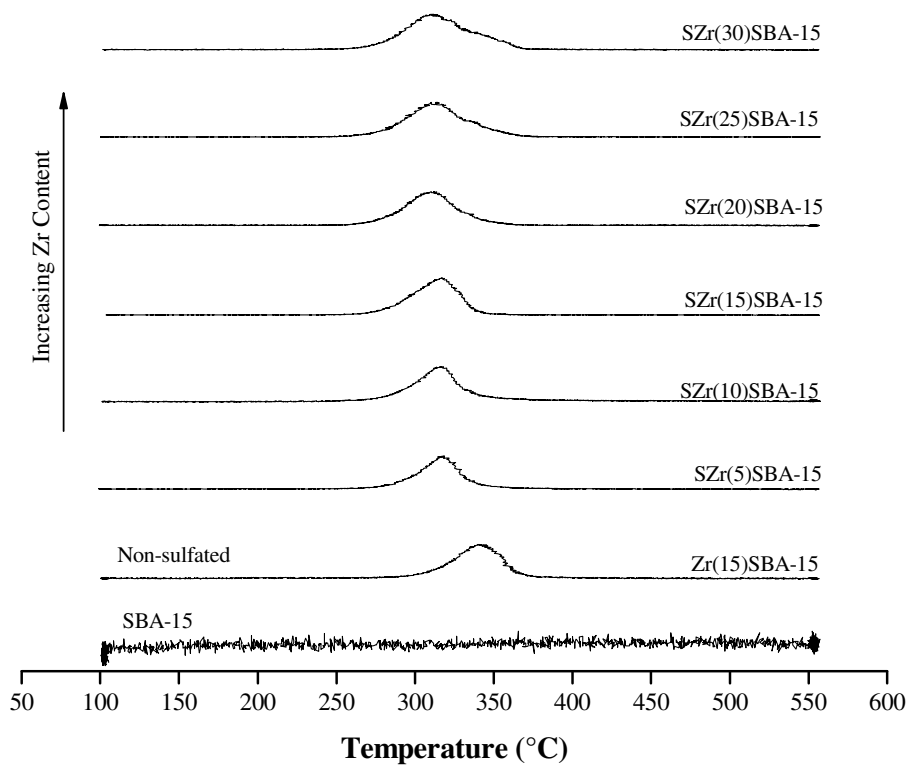
Figure 4.25 TPD curves of isopropylamine decomposition.

Table 4.8 IPAm decomposition amounts for SBA-15, Zirconia modified SBA-15 and Sulfated ZrO_2 included SBA-15 catalysts.

Catalyst	Zr (wt. %)	S (wt. %)	IPA decomposed (mmol/g cat.)
SBA-15	0	0	0.00
Zr(5)SBA-15	4.3	0	0.09
SZr(5)SBA-15	4.3	3.5	0.26
SZr(10)SBA-15	3.7	N/A	0.14
SZr(15)SBA-15	5.2	3.4	0.50
SZr(20)SBA-15	8.9	N/A	0.37
SZr(25)SBA-15	10.8	N/A	0.39
SZr(30)SBA-15	13.4	3.1	0.28

It is important to note here that the maximum acidity was observed for 8.5 wt % Zr included catalyst in ^{1}H MAS NMR experiments and 5.2 wt. % Zr included catalyst for TPD analysis (Table 4.9). The contradiction could be explained by comparing the actual zirconium amounts in the catalysts. In TPD experiments the maximum corresponded to a 5.2 wt. % Zr and the acidity decreased when the Zr content became 8.9%. In ^{1}H MAS NMR measurements maximum corresponded to 8.5 wt. % Zr, which is within the range of 5.2-8.9 wt. % Zr.

Table 4.9 The Zr contents of the catalysts and the corresponding IPAm decomposed amounts and relative intensities of ^{1}H MAS NMR line at 10 ppm.

Catalyst	Zr (wt. %)	IPAm decomposed (mmol/g)	Zr (wt. %)	Rel. Intensity of ^{1}H NMR line at 10 ppm (%)
SBA-15	0	0.00	0	0
Zr(5)SBA-15	-	0.09	-	0
SZr(5)SBA-15	4.3	0.26	2.0	6
SZr(10)SBA-15	3.7	0.14	-	-
SZr(15)SBA-15	5.2	0.50	4.8	7
SZr(20)SBA-15	8.9	0.37	-	-
SZr(25)SBA-15	10.8	0.39	8.5	23
SZr(30)SBA-15	13.4	0.28	15.2	15

4.4 SUMMARY OF THE CHARACTERIZATION STUDIES

In this section the preparation and the acid characteristics of sulfated zirconia included SBA-15 catalysts were reported. The measurements on hydrated and dehydrated sulfated zirconia included SBA-15 samples clearly revealed the formation of accessible strong Brønsted acid sites. The fine distribution of zirconia in SBA-15 structure was achieved up to 25 mol % ZrO_2

included catalyst at which the highest acidity was observed with a BET surface area of 246 m^2/g.

The zirconia included SBA-15 has a fine distribution of zirconia in the structure, by the formation of terminal, and low coordinated Zr^{4+} Lewis acid sites. Further sulfation eliminates the terminal groups, and Lewis centers to create a new type of acidic protons bonding with sulfate anions. Since the zirconium is distributed finely within the framework of SBA-15, isolated silanol group hydrogen bonded to the adjacent bisulfate-zirconium site is a plausible model. The chemical shift of 144 cm^{-1} in silanol region indicates the acidity enhancement due to sulfated zirconia modification of the SBA-15 catalyst.

CHAPTER 5

METHANE BROMINATION OVER SULFATED ZIRCONIA IN SBA-15

5.1 INTRODUCTION

Cross-coupling between CH_2Br_2 and CH_3Br was seen in the higher output of aromatics and subsequent coke when both species are present in the reaction medium for hydrocarbon synthesis. It was concluded that CH_2Br_2 condenses predominantly to absorbed carbon in the absence of CH_3Br. Because of favorable product distribution under conditions of low CH_2Br_2 and high CH_3Br, it is important to obtain high selectivity for CH_3Br in the methane bromination reaction. At high reaction temperatures (500 °C) and high conversions (70%) CH_3Br selectivity under homogeneous conditions were about 62% [23]. Olah [16, 17] proposed selective bromination for the activation of methane in the presence of super acid catalysts, i.e. Lewis acid halide-oxyhalide catalysts. He obtained methane conversion of 14 % with $TaOF_3/Al_2O_3$ and 20 % with $SbOF_3/Al_2O_3$ with high CH_3Br selectivity (99%) at 200 °C and 250 °C.

In this part of the study, it was demonstrated that sulfated zirconia included SBA-15 catalyst provides CH_3Br selectivity (99%) at 340 °C with 69% methane conversion. The bromination temperatures were reduced from 500 °C in gas phase to 340 °C in heterogeneous phase with high methane

conversions (69%) providing the selectivity for CH_3Br (99%). The results were examined in more detail in the following sections.

5.2 EXPERIMENTAL

5.2.1 Reaction Tests

The schematic representation of the reaction setup is given in Figure 5.1 and the photographs in Appendix C (Figure C.51). Methane (CH_4, 99.98 % pure) was fed to the reactor at the desired amounts by use of a mass flow controller (MKS Instruments).
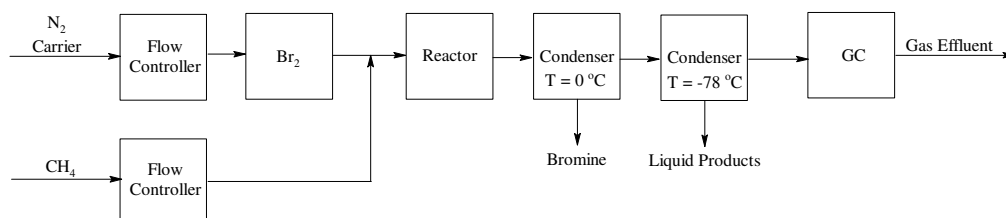
Figure 5.1 Schematic representation of the reaction setup.

Liquid bromine was stored in a container (Figure C.52), which is a quartz bottle with a narrow neck (1 mm ID). The tip of the bottle was mounted to the inside of a horizontally oriented cylindrical quartz tube. The tip was bended towards the opposite direction of the flow. Nitrogen was used as the carrier gas, and its flow was controlled by a mass flow controller. The flow of the carrier gas (N_2) through the cylindrical quartz tube allows the carrier to drag the bromine vapor coming out of the bottle through the neck. This is a

modified Stefan tube, which allows the bromine to be fed to the reactor by diffusion through the bromine container. 0.6-0.9 ml of Br_2 (liquid) was placed in the container, which lasts 5 h during the reaction ($F_{Br_2} = 7.76x10^{-3}$ mol/h). Later they are mixed with methane, and are fed to the reactor with a rough estimate of the ratio of Br_2:CH_4 = 10:1.

0.2 g catalyst was placed in quartz reactors, 0.4 cm ID, supported by quartz wool at both ends. The reactor was placed in a home made tubular furnace. The system was run for 3 h to achieve steady state which was continuously monitored by the gas chromatograph in terms of gas composition.

Homogeneous gas phase kinetics were monitored at two different space times using two reactors with ID = 0.1 and 1.0 cm. The reactor with 1.0 cm ID was filled with glass beads OD = 0.3 cm to provide a level of mixing.

Table 5.1 The properties of the reactors.

#	Diameter (cm)	Length (cm)	Volume (ml)	Void fraction	Catalyst
1	0.1	18	0.14	1	-
2	1.0	18	14.1	0.7	-
3	0.4	18	1.45	0.1	SBA-15
4	0.4	18	1.45	0.1	$SZrO_2$/SBA-15

A condenser operating at the freezing point of water (~0 °C) was mounted at the exit of the reactor to collect the unconverted bromine vapor. The liquid products i.e. CH_3Br, was collected in the second condenser operated at -78 °C achieved by acetone dry ice mixture. The analysis of the exit gases were performed by a GC (Varian 3900) equipped with a flame ionization detector (FID) and a capillary column (Varian FactorFour[TM], 15m x 0.25 mm ID, df=0.25 µm).

5.2.2 Liquid NMR

About 1 ml of the product was dissolved in ca. 5 ml of $CDCl_3$ and the liquid ^1H NMR experiments were performed in a 400 MHz Bruker AVANCE spectrometer. The ppm scale was with respect to liquid TMS.

5.3 RESULTS AND DISCUSSION

5.3.1 Reaction Tests

The experiments of the reaction of CH_4 and Br_2 with three different reactors (properties are given in Table 5.1) were performed within the temperature interval of 300-400 °C.

The results with the first reactor (cylindrical quartz tube with inside diameter of 0.1cm) revealed that detectable amounts of product were only formed at temperatures as high as 380 °C. The reactions at different temperatures were performed at CH_4 and N_2 flow rates of 0.0034 ml/s and 0.16 ml/s consecutively, which corresponds to a residence time of 0.86 s. The methane conversion is within the limits of the fluctuations of the observable methane amounts by GC. Therefore for these experimental conditions, conversion could not be calculated since methane conversion is as low as the detection limits.

In the experiments on the reactor of quartz tube with 1.0 cm ID (filled with glass beads), the experiments were conducted at CH_4 and N_2 flow rates of 0.0034 ml/s and 0.16 ml/s respectively, which corresponds to a residence time of 60.6 s, almost 70 times greater than the first reactor. The maximum methane conversion calculated in this reactor was 8.3% (Figure 5.2).
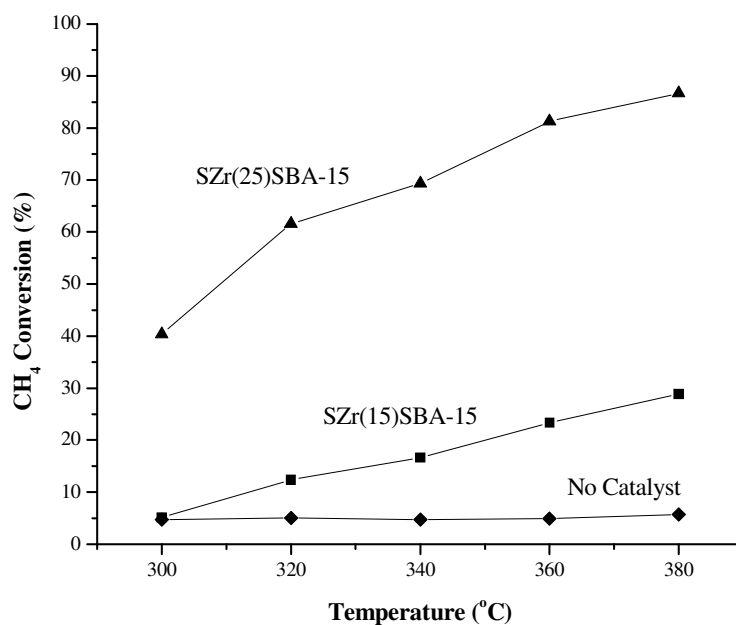
Figure 5.2 Methane conversions as a function of temperature over different catalysts and homogeneous reaction results were also shown.

Finally, the reactor (0.4 cm ID) was filled with 0.0801 g of SBA-15 with a pore volume of 1.198 cm^3/g and ~0.2 g of Zr-SBA-15 and SZr-SBA-15 catalysts. The corresponding residence time is at ca. 0.6 s. Then, the reaction was performed at different temperatures. The CH_4 and N_2 flow rates were kept at similar levels with the reactions run without any catalysts, 0.0036 and 0.16 ml/s. The increase in the reaction temperature resulted in an increase in the conversion of methane; however it was as low as 4% for the reactor with pure SBA-15 at 380 °C. Over the zirconia included catalysts the conversions were similar conversions with SBA-15 (2.8%, over Zr(15)SBA-15 at 380 °C).

For the reaction over the sulfated catalyst – SZr(15)SBA-15, methane conversions were quite high as compared to homogeneous or SBA-15 reactions at 340 °C. The highest conversion observed was as high as 29% at 380 °C.

The brominated products were analyzed by liquid NMR (Section 5.3.2) and only CH_3Br formation was observed. The high product selectivity (>99%) was attained over SZr(25)SBA-15, SBA-15 and homogeneous reaction (Figure 5.3). The conversions of methane to CH_3Br over the sulfated catalysts were higher than the reaction in the homogeneous gas phase, over SBA-15 and Zr-SBA-15. The highest conversion (69% at 340 °C) over SZr(25)SBA-15 was observed with high CH_3Br selectivity (>99%).

Table 5.2 Methane conversion and methyl bromide selectivity

Catalyst	Br_2:CH_4	GHSV (mL/gh)	T (°C)	CH_4 Conversion (%)	CH_3Br Select. (%)
In This Study					
SZr(25)SBA-15	10:1	3000	340	69	99
SZr(15)SBA-15	10:1	3000	340	14	99
No catalyst	10:1	60 s	340	8	99
Olah et. al.					
$SbOF_3$/Al_2O_3	1:5	100	200	20	99
$TaOF_3$/Al_2O_3	1:15	50	250	14	99
Pt/Al_2O_3	1:2	300	200	8	99
Lorkovic et. al.					
No catalyst	1:10	0.3 s	500	70	62

The results of the reaction tests at 340 °C were summarized and compared with literature in Table 5.2. It was seen that the methane conversions were quite high over the sulfated zirconia catalyst (69%) and the selectivity of the CH_3Br is 99%. The use of catalyst improves the conversion from 8% to 69%. The reaction temperature 340 °C is reasonable as compared to the methanol to olefins route (~350 °C). As far as the implementation of the process to a large scale production facility are concerned, higher temperatures (500 °C) are not desired – the case in homogeneous gas phase reactions – due to the operating costs as well as the selectivity problems. The improvement in the methane conversion from 8% to 69% provided by the use of SZr-SBA-15

at lower temperatures (340 °C) should reduce the operation costs in case of a large scale production.

5.3.2 Liquid NMR

Methane bromination reaction may yield brominated products, such as, CH_3Br, and CH_2Br_2. About 10 ml of product was collected after a reaction of 5 hours at 340 °C. After all runs the liquid was analyzed by the liquid ^{1}H NMR. The ^{1}H NMR spectra of the products were given in Figure 5.3. The single intense line was observed at 2.15 ppm. According to literature [189] CH_3Br and CH_2Br_2 can be distinguished by the lines at 2.68 and 4.95 ppm w.r.t. TMS respectively. Thus, the single line observed at 2.15 ppm can be attributed to CH_3Br.

According to liquid ^{1}H NMR results (Figure 5.3), only methyl bromide was produced. This result contradicts with our homogeneous gas phase conversion calculations [132]. However, the experimental results are in coincidence with the product selectivity that was observed over strong superacid catalysts reported by Olah [16].
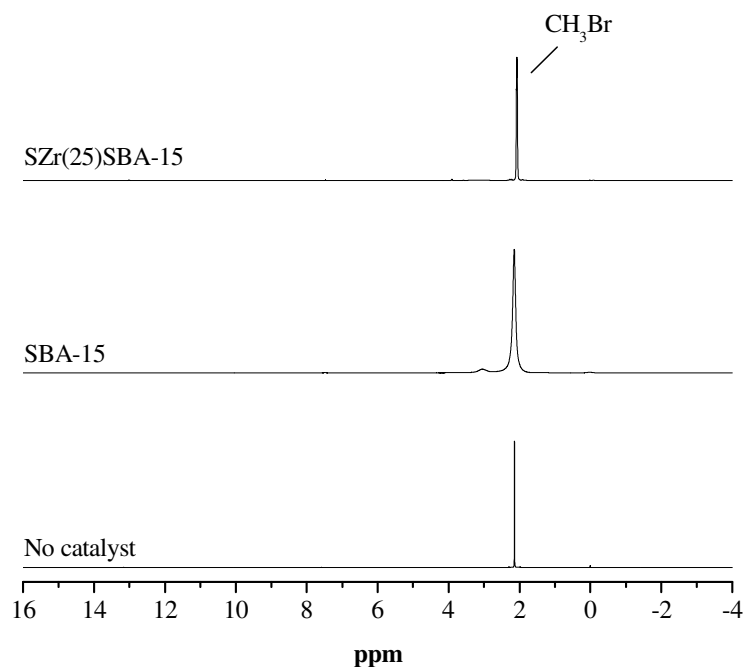
Figure 5.3 Liquid ^{1}H NMR of the products dissolved in CDCl$_3$ and taken at Bruker AVANCE-400 after the methane bromination reaction with no catalyst, SBA-15 and Sulfated SBA-15 with 25 mol % ZrO$_2$.

If the gas phase kinetics of bromination were investigated (Equation 3.1-3.6), it was seen that the propagation steps involve the formation of CH$_3$• radicals from methane (Equation 3.1). The next step is the formation of CH$_3$Br. It can be concluded that these steps occur similarly on the strong Brønsted acid sites of the catalyst. The next step in the gas phase bromination was the formation of CH$_2$Br• radical which lead to the formation of CH$_2$Br$_2$. The selectivity towards CH$_3$Br infers that the formation of CH$_2$Br• radical is not favored in the presence of strong Brønsted acid sites on the surface of the catalyst and instead CH$_3$• radicals was formed.

5.4 SUMMARY OF THE BROMINATION REACTION TESTS

Single product (CH_3Br) was obtained at relatively high methane conversions (69%) with the proved proton donor strong acidic catalyst with relatively highest acidity (Sulfated 25 mol %ZrO_2/SBA-15). It is a very promising result for the cost effective replacement of syn-gas methane conversion route.

CHAPTER 6

SUMMARY

Halogenation was proposed as an alternative for methane conversion to higher hydrocarbons by Benson [18], and Olah [16] who proposed the catalytic chlorination and bromination of methane over superacid catalysts. The overall method is a two step process for the conversion of methane into valuable chemicals. In the first step, bromine (chlorine) is used to convert methane into an intermediate compound $CH_{4-x}Br_x$ at moderate temperatures. Second, the conversion of brominated (chlorinated) compound into liquid fuels can be achieved. Bromination revealed to be the most suitable halogen and the selective production of methyl bromide is crucial in this route according to the studies of Olah [16] and Lorkovic et. al [25].

In this study, first the homogenous gas phase reactions of methane and bromine were modeled. The optimum reaction conditions for the methane bromination were obtained by a reactor model depending on the kinetic data available in literature. It was determined that, methane conversions above 90% accompanied by high CH_2Br_2 selectivity above 90% at 330 °C at a residence time of 3 s are possible in gas phase methane bromination.

As far as the catalyst is concerned, sulfated zirconia is known as a strong acid due to its high catalytic activity in the isomerization of small hydrocarbon molecules at low temperatures. The relatively small surface area of the SZ limits its applications. The combination of the advantages of the mesoporous molecular sieve and sulfated zirconia should greatly expand the

catalytic activity. Therefore SZ included in SBA-15 type catalysts were prepared at different zirconia loadings (5-30 mol % ZrO_2). In the preparation of the sulfated zirconia modified SBA-15, zirconia was introduced in the form of $ZrOCl_2 \cdot 8H_2O$ during the synthesis of SBA-15 to obtain a better dispersion. Sulfation was carried out after calcination by treatment of the surface with sulfuric acid. Catalysts were characterized by ICP, XRD, N_2 adsorption (BET), TEM, ^{1}H and ^{29}Si MAS NMR, CO adsorption FT-IR and IPAm TPD techniques. The small angle XRD results showed that zirconia crystals were formed after 8.5 wt. % loading, and TEM images revealed that mesoporous structure was preserved up to 4.8 wt. % ZrO_2 loading. The sulfated catalyst with 8.5 % ZrO_2 has a BET surface area of 246 m^2/g, which is quite high as compared to conventional SZ. ^{1}H MAS NMR spectra revealed a strong chemical shift at ca. 10 ppm with the introduction of zirconia associated with the strong acidity of the sulfated zirconia. The intensity of this acidic line increases up to a certain limit, implying that there is an optimum zirconia loading for the maximum acidity. According to ^{1}H MAS NMR results 8.5 wt. % sulfated zirconia showed the maximum acidity. Furthermore, the acidic properties of sulfated zirconia modified SBA-15 were investigated by means of FT-IR and TPD analysis. FT-IR analysis of CO adsorbed at 82 K revealed the presence of Brønsted and Lewis acid sites in these catalysts. Brønsted acid sites were only observed in sulfate modified catalysts. CO adsorption induced a ~100 cm^{-1} red shift of the isolated SiO-H band in non-sulfated samples. The shift increased to ~140 cm^{-1} for sulfated samples suggesting hydrogen bonding between the proton of the bisulfate and the silanol group. The acidic proton of the bisulfate group was also identified by a blue shift in S=O band. For siliceous SBA-15, no decomposition of adsorbed i-propylamine (IPAm) was observed in agreement with its weak acidity. In contrast, zirconia-containing SBA-15 shows clear acidity as evidenced from the i-propylamine decomposition. Following sulfation, the temperature of decomposition decreased from 340 to 310 °C. This indicated increased acidity of the sulfated

catalysts. Maximum acidity was observed for a catalyst containing 5.2 wt. % Zr with a 0.5 mmol/gcat. IPAm decomposed. It is important to note here that, 0-30 mol % ZrO_2 loaded SBA-15 catalysts were synthesized in a different sets and the IR and TPD experiments were performed by using the catalysts from the second set, which shows the maximum acidity for 5.2 wt. % Zr loaded catalyst.

The reaction experiments were performed in tubular quartz packed bed reactor in the temperature range between 300-400 °C. The products were analyzed by a gas chromatograph and methane conversions at corresponding reaction conditions were calculated. By the use of a condenser at the exit of the reactor, products were collected and the liquid ^{1}H NMR spectra revealed the selectivity of the brominated products. The result showed that the CH_3Br can be selectively produced (>99%). Methane conversion was as low as 8% in a plug flow reactor without any catalyst, however it attained a maximum of 69% conversion by the use of the most acidic catalyst, namely 25 mol % sulfated zirconia included SBA-15.

CHAPTER 7

RECOMMENDATIONS

In this study we have shown that the combination of sulfated zirconia and SBA-15 revealed strong acidic property. In addition it was seen that, the selective conversion of methane with bromine was feasible in terms of kinetics, which is critical for the production of higher hydrocarbons through halogenation. However some points should be considered in more detail, which could be summarized as follows.

The long range orders of the mesostructure of zirconia included SBA-15 catalysts were affected by the sulfation of the catalyst, probably due to the leaching problem. The disorder after the sulfation treatment could be improved by controlled sulfation of the catalyst. Very low concentration of sulfuric acid can be flushed over the catalyst or the SO_3 in gas phase could be used to sulfate the sample. If the problem was solved and the long range order would preserved a great improvement would be achieved for both SBA-15 and sulfated zirconia, one lacks pore volume and surface area and the other lacks active centers.

Another question was the nature of the Zr species in the catalyst; whether they are in ion form or in oxide form. The XANES studies should clarify the problem. The fraction of zirconia in the pores and the extra framework could be the subject of further study. The high dispersion of the zirconia was observed by XRD analysis and Zr could not be distinguished in TEM images at lower loadings. This infers that a high portion is in the

mesopores; however a detailed TEM/EDX analysis would be beneficial for direct evidence.

The actual loadings of zirconium were lower than the intended amounts in catalysts. In order to increase the metal loading in SBA-15 another precursor such as zirconium propoxide could be used during the synthesis with a control of the pH of the solution.

The reaction system did not allow the accurate control of the amount of bromine feed. Therefore the bromine feed to the reactor was not more than an estimate. The further improvement would be to design a new system with a better control of the bromine feed. Another improvement could be the use of longer capillary column in GC or a mass spectrometer, which allow the detection of brominated products.

As far as the industrial application of the halogenation is concerned the system should be free of any leakage. Bromine, HBr and CH_3Br should be kept in the system. The recycling of the products is very important. Methyl bromide was used as an agricultural soil and structural fumigant to control a wide variety of pests. However, it is ozone depleting substance and its production and distribution was abandoned by the Montreal protocol with CFCs. Therefore it is critical to keep the system free of leakage. It is a difficult task to achieve; however if the huge capital investments to syn-gas synthesis plants are taken into account, it does not seem impossible.

REFERENCES

1. Hubbert M. K.; "Nuclear Energy and the Fossil Fuels", in Spring Meeting of the Southern District Division of Production American Petroleum Institute, San Antonio, Texas, March 7-9, 1956.

2. Ohta T., "Sources, Systems and Frontier Conversion", Pregamon Press, New York, 1994.

3. Ayala M., Torres E.; Applied Catalysis A: General, 272(1-2), 1-13, 2004.

4. Gesser H. D., Hunter N. R.; Catalysis Today, 42(3), 183-189, 1998.

5. Roberts C. B., Elbashir N. O.; Fuel Processing Technology, 83(1-3), 1-9, 2003.

6. Gesser H. D., Hunter N. R., Prakash C. B.; Chemical Reviews, 85(4), 235-244, 1985.

7. Choudhary T. V., Aksoylu E., Goodman D. W.; Chemical Reviews, 45(1), 151–203, 2003.

8. Xu Y. D., Bao X. H., Lin L. W.; Journal of Catalysis, 216(1-2), 386-395, 2003.

9. Weckhuysen B. M., Wang D. J., Rosynek M. P., Lunsford J. H.; Journal of Catalysis, 175(2), 338-346, 1998.

10. Xu Y. D., Lin L. W.; Applied Catalysis A: General, 188(1-2), 53-67, 1999.

11. Periana R. A., Taube D. J., Gamble S., Taube H., Satoh T., Fujii H.; Science, 280(5363), 560-564, 1998.

12. Yoshida H., Chaskar M. G., Kato Y., Hattori T.; Journal of Photochemistry and Photobiology a-Chemistry, 160(1-2), 47-53, 2003.

13. Taylor C. E.; Catalysis Today, 84(1-2), 9-15, 2003.

14. Okumoto M., Mizuno A.; Catalysis Today, 71(1-2), 211-217, 2001.

15. Olah G. A.; US Patent 4,523,040; 1985.

16. Olah G. A.; Accounts Of Chemical Research, 20(11), 422-428, 1987.

17. Olah G. A., Gupta B., Farina M., Felberg J. D., Ip W. M., Husain A., Karpeles R., Lammertsma K., Melhotra A. K., Trivedi N. J.; Journal Of The American Chemical Society, 107(24), 7097-7105, 1985.

18. Benson S. W.; US Patent 4,199,533; 1980.

19. Weissman M., Benson S. W.; International Journal of Chemical Kinetics, 16(4), 307-333, 1984.

20. Zhou X. P., Lorkovic I. M., Stucky G. D., Ford P. C., Sherman J. H., Grosso P.; US Patent 6,472,572; 2002.

21. Gas Reaction Technologies, Gas Reaction Technologies Inc. http://www.grt-inc.com; Access Date: 16.09.2007

22. Lorkovic I., Noy M., Weiss M., Sherman J., McFarland E., Stucky G. D., Ford P. C.; Chemical Communications, (5), 566-567, 2004.

23. Lorkovic I. M., Noy M. L., Schenck W. A., Belon C., Weiss M., Sun S. L., Sherman J. H., McFarland E. W., Stucky G. D., Ford P. C.; Catalysis Today, 98(4), 589-594, 2004.

24. Lorkovic I. M., Sun S. L., Gadewar S., Breed A., Macala G. S., Sardar A., Cross S. E., Sherman J. H., Stucky G. D., Ford P. C.; Journal Of Physical Chemistry A, 110(28), 8695-8700, 2006.

25. Lorkovic I. M., Yilmaz A., Yilmaz G. A., Zhou X. P., Laverman L. E., Sun S. L., Schaefer D. J., Weiss M., Noy M. L., Cutler C. I., Sherman J. H., McFarland E. W., Stucky G. D., Ford P. C.; Catalysis Today, 98(1-2), 317-322, 2004.

26. Zhou X. P., Yilmaz A., Yilmaz G. A., Lorkovic I. M., Laverman L. E., Weiss M., Sherman J. H., McFarland E. W., Stucky G. D., Ford P. C.; Chemical Communications, (18), 2294-2295, 2003.

27. Corma A.; Chemical Reviews, 97(6), 2373-2419, 1997.

28. Beck J. S., Chu C.T.-W., Johnson I.D., Kresge C.T., Leonowicz M.E., Roth W.J., Vartuli J.W.; WO Patent 91/11390; 1991.

29. Xiao F. S.; Topics In Catalysis, 35(1-2), 9-24, 2005.

30. Taguchi A., Schuth F.; Microporous and Mesoporous Materials, 77(1), 1-45, 2005.

31. Vera C. R., Pieck C. L., Shimizu K., Parera J. M.; Applied Catalysis A-General, 230(1-2), 137-151, 2002.

32. Yang X. B., Jentoft R. E., Jentoft F. C.; Catalysis Letters, 106(3-4), 195-203, 2006.

33. Hua W. M., Yue Y. H., Gao Z.; Journal of Molecular Catalysis a-Chemical, 170(1-2), 195-202, 2001.

34. Breda A., Signoretto M., Ghedini E., Pinna F., Cruciani G.; Applied Catalysis A-General, 308, 216-222, 2006.

35. Landau M. V., Titelman L., Vradman L., Wilson P.; Chemical Communications, (5), 594-595, 2003.

36. Chen C. L., Li T., Cheng S. F., Xu N. P., Mou C. Y.; Catalysis Letters, 78(1-4), 223-229, 2002.

37. Du Y. C., Sun Y. Y., Di Y., Zhao L., Liu S., Xiao F. S.; Journal Of Porous Materials, 13(2), 163-171, 2006.

38. Zhang W. H., Lu J. Q., Han B., Li M. J., Xiu J. H., Ying P. L., Li C.; Chemistry Of Materials, 14(8), 3413-3421, 2002.

39. Yue Y. H., Gedeon A., Bonardet J. L., Melosh N., D'Espinose J. B., Fraissard J.; Chemical Communications, (19), 1967-1968, 1999.

40. "World Energy Outlook 2007", International Energy Agency, 2007.

41. "Annual Energy Review 2006", Energy Information Administration, US Department of Energy, 2007.

42. "Key World Energy Statistics", International Energy Agency, 2007.

43. "BP Statistical Review of World Energy June 2007", British Petroleum, 2007.

44. Raiper R.; http://www.omninerd.com/2006/05/17/articles/52; Access Date: 15.09.2007

45. Natural Gas Organization, http://www.naturalgas.org; Access Date: 15.09.2007

46. Internet Encyclopedia, http://en.wikipedia.org/wiki/Methane_hydrate; Access Date: 15.09.2007

47. Olah G. A., Molnár A., "Hydrocarbon Chemistry", 2nd ed.; Wiley Interscience, New York, 2003.

48. Robert H. P., Green D. W.; in "Perry's Chemical Engineers' Handbook", McGraw-Hill Inc., New York, pp 27/21-25, 1999.

49. Bakkerud P. K.; Catalysis Today, 106(1-4), 30-33, 2005.

50. Aasberg-Petersen K., Christensen T. S., Nielsen C. S., Dybkjaer I.; Fuel Processing Technology, 83(1-3), 253-261, 2003.

51. Lunsford J. H.; Catalysis Today, 63(2-4), 165-174, 2000.

52. Hickman D. A., Schmidt L. D.; Science, 259(5093), 343-346, 1993.

53. Wilhelm D. J., Simbeck D. R., Karp A. D., Dickenson R. L.; Fuel Processing Technology, 71(1-3), 139-148, 2001.

54. Sabatier P., Senderens J. B.; Compt. Rend., 134, 514, 1902.

55. Fischer F., Tropsch H.; Brennstoff-Chem., 4, 276, 1923.

56. Fischer F., Tropsch H.; Ber. Dtsch. Chem. Ges., 59, 830, 1926.

57. Fischer F., Tropsch H.; Brennstoff-Chem., 7, 97, 1926.

58. Thomas J. M., Thomas W. J., "Principles and Practice of Heterogeneous Catalysis", VCH Verlagsgesellschaft mbH, Weinheim, 1997.

59. Ohtsuka Y., Takahashi Y., Noguchi M., Arai T., Takasaki S., Tsubouchi N., Wang Y.; Catalysis Today 89, 419-429, 2004.

60. Sethuraman R., Bakhshi N. N., Katikaneni S. P., Idem R. O.; Fuel Processing Technology, 73, 197-222, 2001.

61. Natta G.; in "Catalysis", Emmet R. H. (Editor); Reinhold, New York, Vol. 3, p 349, 1955.

62. Internet Encyclopedia, http://en.wikipedia.org/wiki/Methanol; Access Date: 24.09.2007

63. Kieboom A. P. G., Moulijn J. A., Sheldon R. A., Van Leeuwen P. W. N. M.; in "Studies in Surface Science and Catalysis 123 Catalysis: An Integrated Approach", Santen V. A., Van Leeuwen P. W. N. M., Moulijn J. A., Averill B. A. (Editors); 2nd ed.; Elsevier, Amsterdam, Vol. 123, pp 29-80, 2000.

64. Methyl alcohol, Chemlink Ltd., http://chemlink.com.au/index.html; Access Date: 23.09.2007

65. Svelle S., Joensen F., Nerlov J., Olsbye U., Lillerud K. P., Kolboe S., Bjorgen M.; Journal of the American Chemical Society, 128(46), 14770-14771, 2006.

66. Svelle S., Bjorgen M., Kolboe S., Kuck D., Letzel M., Olsbye U., Sekiguchi O., Uggerud E.; Catalysis Letters, 109(1-2), 25-35, 2006.

67. Olsbye U., Bjorgen M., Svelle S., Lillerud K. P., Kolboe S.; Catalysis Today, 106(1-4), 108-111, 2005.

68. Bjorgen M., Olsbye U., Svelle S., Kolboe S.; Catalysis Letters, 93(1-2), 37-40, 2004.

69. Bjorgen M., Olsbye U., Petersen D., Kolboe S.; Journal of Catalysis, 221(1), 1-10, 2004.

70. Chang C. D., Lang W. H., Silvestri A. J.; US Patent 4,062,905; 1977.

71. Smart L. E., Moore E. A., "Solid State Chemistry: An Introduction", 2nd ed.; Chapman & Hall, London, 1995.

72. Santen V. A., Neurock M., "Molecular Heterogeneous Catalysis A conceptual and Computational Approach", WILEY-VCH Verlag GmbH & Co. KGaA, Weinheim, 2006.

73. Kaiser S. W.; US Patent 4,499,327; 1985.

74. Chen J. Q., Bozzano A., Glover B., Fuglerud T., Kvisle S.; Catalysis Today, 106(1-4), 103-107, 2005.

75. Sasol Ltd., www.sasol.com; Access Date: 22.09.2007

76. Maiden C. J.; in "Studies in Surface Science and Catalysis 36 Methane Conversion", Bibby D. M., Chang C. D., Howe R. F., Yurchak S. (Editors); Elsevier, Amsterdam, Vol. 36, pp 1-16, 1987.

77. Shell SMDS Technology and Process, http://www.shell.com/home/content2/my-en/about_shell/smds/smds_process.html; Access Date: 25.09.2007

78. Sasol Chevron Ltd., http://sasolchevron.com/default.htm; Access Date: 25.09.2007

79. Brown T. L., LeMay H. E., Bursten B. E., "Chemistry The Central Science", 7th ed.; Prentice-Hall, New Jersey, 1997.

80. Solomons G., Fryhle C., "Organic Chemistry", 7th ed.; John Wiley & Sons, Inc., New York, 1998.

81. Amenomiya Y., Birss V. I., Goledzinowski M., Galuszka J., Sanger A. R.; Catalysis Reviews-Science and Engineering, 32(3), 163-227, 1990.

82. Scurrell M. S.; Applied Catalysis, 32(1-2), 1-22, 1987.

83. Lunsford J. H.; Angewandte Chemie-International Edition in English, 34, 970-980, 1995.

84. Verma S. S.; Energy Conversion and Management, 43, 1999-2008, 2002.

85. Crabtree R. H.; Chemical Reviews, 95(4), 987-1007, 1995.

86. Kieboom A. P. G., Moulijn J. A., Van Leeuwen P. W. N. M., Santen V. A.; in "Studies in Surface Science and Catalysis 123 Catalysis: An Integrated Approach", Santen V. A., Van Leeuwen P. W. N. M., Moulijn J. A., Averill B. A. (Editors); 2nd ed.; Elsevier, Amsterdam, Vol. 123, pp 1-28, 2000.

87. Otsuka K., Wang Y.; Applied Catalysis A: General 222, 145-161, 2001.

88. Aoki K., Ohmae M., Nanba T., Takeishi K., Azuma N., Ueno A., Ohfune H., Hayashi H., Udagawa Y.; Catalysis Today, 45, 29-33, 1998.

89. de Lucas A., Valverde J. L., Rodriguez L., Sanchez P., Garcia M. T.; Applied Catalysis A: General, 203, 81-90, 2000.

90. Han S., Martenak D. J., Palermo R. E., Pearson J. A., Walsh D. E.; Journal of Catalysis, 148(1), 134-137, 1994.

91. Foster N. R.; Applied Catalysis, 85, 1-9, 1985.

92. Arena F., Parmaliana A.; Accounts of Chemical Research, 36(12), 867-875, 2003.

93. Wang Y., Otsuka K.; Journal Of Molecular Catalysis A-Chemical, 111, 341-356, 1996.

94. Wang D. J., Lunsford J. H., Rosynek M. P.; Journal of Catalysis, 169(1), 347-358, 1997.

95. Wang L. S., Tao L. X., Xie M. S., Xu G. F., Huang J. S., Xu Y. D.; Catalysis Letters, 21(1-2), 35-41, 1993.

96. Solymosi F., Cserenyi J., Szoke A., Bansagi T., Oszko A.; Journal of Catalysis, 165(2), 150-161, 1997.

97. Amin N. A. S., Anggoro D. D.; Fuel, 83, 487-494, 2004.

98. Peng J. J., Deng Y. Q.; Applied Catalysis A: General, 201(2), L55-L57, 2000.

99. Lin M., Sen A.; Nature, 368(6472), 613-615, 1994.

100. Raja R., Ratnasamy P.; Applied Catalysis A: General 158, L7-L15, 1997.

101. Hoyano J. K., McMaster A. D., Graham W. A. G.; Journal of the American Chemical Society, 105(24), 7190-7191, 1983.

102. Shilov A. E., Shul'pin G. B.; Chemical Reviews, 97(8), 2879-2932, 1997.

103. Wolf D.; Angewandte Chemie-International Edition in English, 37(24), 3351-3353, 1998.

104. Periana R. A., Taube D. J., Evitt E. R., Loffler D. G., Wentrcek P. R., Voss G., Masuda T.; Science, 259(5093), 340-343, 1993.

105. Labinger J. A., Bercaw J. E.; Nature, 417(6888), 507-514, 2002.

106. Taylor C. E., Noceti R. P.; Catalysis Today, 55, 259–267, 2000.

107. Huang W., Xie K.-C., Wang J.-P., Gao Z.-H., Yin L.-H., Zhu Q.-M.; Journal of Catalysis, 201, 100-104, 2001.

108. Kado S., Sekine Y., Fujimoto K.; Chemical Communications, 2485-&, 1999.

109. Onoe K., Fujie A., Yamaguchi T., Hatano Y.; Fuel, 76, 281, 1997.

110. Heintze M., Magureanu M.; Journal of Catalysis 206, 91–97, 2002.

111. Tanashev Y. Y., Fedoseev V. I., Aristov Y. I., Pushkarev V. V., Avdeeva L. B., Zaikovskii V. I., Parmon V. N.; Catalysis Today, 42, 333-336, 1998.

112. Thanychotpaiboon K., Chavadej S., Caldwell T. A., Lobban L. L., Mallinson R. G.; Reaction Kinetics and Catalysis, 44, 2252, 1998.

113. Kado S., Urasaki K., Sekine Y., Fujimoto K., Nozaki T., Okazaki K.; Fuel, 82, 2291-2297, 2003.

114. Zhang Y.-P., Li Y., Wang Y., Liu C.-J., Eliasson B.; Fuel Processing Technology, 83, 101-109, 2003.

115. Granada A., Karra S. B., Senkan S. M.; Industrial & Engineering Chemical Research, 26(9), 1901-1905, 1987.

116. Karra S. B., Senkan S. M.; Industrial & Engineering Chemical Research, 27(7), 1163-1168, 1988.

117. Romannikov V. N., Ione K. G.; Kinetics and Catalysis, 25(1), 75-80, 1984.

118. Svelle S., Aravinthan S., Bjorgen M., Lillerud K. P., Kolboe S., Dahl I. M., Olsbye U.; Journal of Catalysis, 241(2), 243-254, 2006.

119. Olah G. A., Doggweiler H., Felberg J. D., Frohlich S., Grdina M. J., Karpeles R., Keumi T., Inaba S., Ip W. M., Lammertsma K., Salem G., Tabor D. C.; Journal of the American Chemical Society, 106(7), 2143-2149, 1984.

120. Olah G. A.; US Patent 4,373,109; 1983.

121. Osterwalder N., Stark W. J.; Chemphyschem, 8(2), 297-303, 2007.

122. Reid R. C., Prausnitz J. M., Sherwood T. K., "The Properties of Gases and Liquids", 3rd ed.; Mc-Graw Hill, New York, 1987.

123. Kistiakowsky G. B., Van Artsdalen E. R.; Journal of Chemical Physics, 12(12), 469-478, 1944.

124. Amphlett J. C., Whittle E.; Transactions of the Faraday Society, 64(548P), 2130-2142, 1968.

125. Fettis G. C., Knox J. H.; in "Progress in Reaction Kinetics and Mechanism", Porter G. (Editor); Pergamon Press, New York, Vol. 2, p 1, 1964.

126. Poutsma M. L.; in "Free Radicals", Kochi J. K. (Editor); John Wiley & Sons, New York, Vol. 2, p 159, 1973.

127. Gordon A. R., Barnes C. J.; Chemical Physics, 1(1), 692-695, 1933.

128. Bodenstein M., Lutkemeyer H.; Zeitsch. F. Physik. Chemie, 114(1), 208-212, 1924.

129. Yadav G. D., Nair J. J.; Microporous and Mesoporous Materials, 33(1-3), 1-48, 1999.

130. Wang J. H., Mou C. Y.; Applied Catalysis A-General, 286(1), 128-136, 2005.

131. Risch M., Wolf E. E.; Applied Catalysis A: General, 206(2), 283-293, 2001.

132. Degirmenci V., Uner D., Yilmaz A.; Catalysis Today, 106(1-4), 252-255, 2005.

133. Olindo R., Li X. B., Lercher J. A.; Chemie Ingenieur Technik, 78(8), 1053-1060, 2006.

134. Stepanov A. G., Luzgin M. V., Arzumanov S. S., Wang W., Hunger M., Freude D.; Catalysis Letters, 101(3-4), 181-185, 2005.

135. Marcus R. L., Gonzalez R. D., Kugler E. L., Auroux A.; Chemical Engineering Communications, 190(12), 1601-1619, 2003.

136. Yang X., Jentoft F. C., Jentoft R. E., Girgsdies F., Ressler T.; Catalysis Letters, 81(1-2), 25-31, 2002.

137. Moreno J. A., Poncelet G.; Journal Of Catalysis, 203(2), 453-465, 2001.

138. Duchet J. C., Guillaume D., Monnier A., Dujardin C., Gilson J. P., van Gestel J., Szabo G., Nascimento P.; Journal Of Catalysis, 198(2), 328-337, 2001.

139. Risch M., Wolf E. E.; Catalysis Today, 62(2-3), 255-268, 2000.

140. Li X. B., Nagaoka K., Olindo R., Lercher J. A.; Journal Of Catalysis, 238(1), 39-45, 2006.

141. Kanougi T., Atoguchi T., Yao S.; Journal of Molecular Catalysis A-Chemical, 177(2), 289-298, 2002.

142. Yamaguchi T.; Applied Catalysis, 61(1), 1-25, 1990.

143. Arata K., Hino M.; Materials Chemistry and Physics, 26(3-4), 213-237, 1990.

144. Bensitel M., Saur O., Lavalley J. C., Morrow B. A.; Materials Chemistry And Physics, 19(1-2), 147-156, 1988.

145. Clearfield A., Serrette G. P. D., Khazisyed A. H.; Catalysis Today, 20(2), 295-312, 1994.

146. Kustov L. M., Kazansky V. B., Figueras F., Tichit D.; Journal of Catalysis, 150(1), 143-149, 1994.

147. Adeeva V., Dehaan J. W., Janchen J., Lei G. D., Schunemann V., Vandeven L. J. M., Sachtler W. M. H., Vansanten R. A.; Journal of Catalysis, 151(2), 364-372, 1995.

148. Song X. M., Sayari A.; Catalysis Reviews-Science and Engineering, 38(3), 329-412, 1996.

149. Davis B. H., Keogh R. A., Srinivasan R.; Catalysis Today, 20(2), 219-256, 1994.

150. Adeeva V., Lei G. D., Sachtler W. M. H.; Catalysis Letters, 33(1-2), 135-143, 1995.

151. Liu H., Adeeva V., Lei G. D., Sachtler W. M. H.; Journal Of Molecular Catalysis A-Chemical, 100(1-3), 35-48, 1995.

152. Comelli R. A., Vera C. R., Parera J. M.; Journal of Catalysis, 151(1), 96-101, 1995.

153. Kresge C. T., Leonowicz M. E., Roth W. J., Vartuli J. C., Beck J. S.; Nature, 359(6397), 710-712, 1992.

154. Sayari A.; Chemistry of Materials, 8(8), 1840-1852, 1996.

155. Beck J. S., Vartuli J. C., Roth W. J., Leonowicz M. E., Kresge C. T., Schmitt K. D., Chu C. T. W., Olson D. H., Sheppard E. W., McCullen S. B., Higgins J. B., Schlenker J. L.; Journal of the American Chemical Society, 114(27), 10834-10843, 1992.

156. Sun Y. Y., Yuan L., Ma S. Q., Han Y., Zhao L., Wang W., Chen C. L., Xiao F. S.; Applied Catalysis A: General, 268(1-2), 17-24, 2004.

157. Chen C. L., Li T., Cheng S. F., Lin H. P., Bhongale C. J., Mou C. Y.; Microporous And Mesoporous Materials, 50(2-3), 201-208, 2001.

158. Ciesla U., Schacht S., Stucky G. D., Unger K. K., Schuth F.; Angewandte Chemie-International Edition in English, 35(5), 541-543, 1996.

159. Schuth F.; Berichte Der Bunsen-Gesellschaft-Physical Chemistry Chemical Physics, 99(11), 1306-1315, 1995.

160. Knowles J. A., Hudson M. J.; Journal of the Chemical Society-Chemical Communications, (20), 2083-2084, 1995.

161. Hudson M. J., Knowles J. A.; Journal of Materials Chemistry, 6(1), 89-95, 1996.

162. Landau M. V., Vradman L., Wang X. G., Titelman L.; Microporous And Mesoporous Materials, 78(2-3), 117-129, 2005.

163. Wu Z. G., Zhao Y. X., Liu D. S.; Microporous and Mesoporous Materials, 68(1-3), 127-132, 2004.

164. Trebosc J., Wiench J. W., Huh S., Lin V. S. Y., Pruski M.; Journal of the American Chemical Society, 127(9), 3057-3068, 2005.

165. Alba M. D., Becerro A. I., Klinowski J.; Journal of the Chemical Society-Faraday Transactions, 92(5), 849-854, 1996.

166. Pfeifer H., Freude D., Hunger M.; Zeolites, 5(5), 274, 1985.

167. Brunner E.; Habilitation Thesis, Leipzig University, Leipzig, 1995.

168. Brunner E.; Catalysis Today, 38(3), 361-376, 1997.

169. Zhao D. Y., Feng J. L., Huo Q. S., Melosh N., Fredrickson G. H., Chmelka B. F., Stucky G. D.; Science, 279(5350), 548-552, 1998.

170. Zhao D. Y., Huo Q. S., Feng J. L., Chmelka B. F., Stucky G. D.; Journal Of The American Chemical Society, 120(24), 6024-6036, 1998.

171. Pruski M., Kelzenberg J. C., Gerstein B. C., King T. S.; Journal of the American Chemical Society, 112(11), 4232-4240, 1990.

172. Brunner E.; Journal of the Chemical Society-Faraday Transactions, 86(23), 3957-3960, 1990.

173. Riemer T., Spielbauer D., Hunger M., Mekhemer G. A. H., Knozinger H.; Journal of the Chemical Society-Chemical Communications, (10), 1181-1182, 1994.

174. Hu J. Z., Kwak J. H., Herrera J. E., Wang Y., Peden C. H. F.; Solid State Nuclear Magnetic Resonance, 27(3), 200-205, 2005.

175. Hunger M., Schenk U., Breuninger M., Glaser R., Weitkamp J.; Microporous and Mesoporous Materials, 27(2-3), 261-271, 1999.

176. Hunger M., Ernst S., Steuernagel S., Weitkamp J.; Microporous Materials, 6(5-6), 349-353, 1996.

177. Emmler T., Gieschler S., Limbach H. H., Buntkowsky G.; Journal of Molecular Structure, 700(1-3), 29-38, 2004.

178. Erdem O. F., Michel D.; Journal of Physical Chemistry B, 109(24), 12054-12061, 2005.

179. Nieminen V., Karhu H., Kumar N., Heinmaa I., Ek P., Samoson A., Salmi T., Murzin D. Y.; Physical Chemistry Chemical Physics, 6(15), 4062-4069, 2004.

180. Wang J. C., Liu Q.; Microporous And Mesoporous Materials, 83(1-3), 225-232, 2005.

181. Vinu A., Srinivasu P., Miyahara M., Ariga K.; Journal Of Physical Chemistry B, 110(2), 801-806, 2006.

182. Hu L. H., Ji S. F., Xiao T. C., Guo C. X., Wu P. Y., Nie P. Y.; Journal Of Physical Chemistry B, 111(14), 3599-3608, 2007.

183. Li F. X., Yu F., Li Y. L., Li R. F., Xie K. C.; Microporous And Mesoporous Materials, 101(1-2), 250-255, 2007.

184. Orlov A., Zhai Q. Z., Klinowski J.; Journal Of Materials Science, 41(8), 2187-2193, 2006.

185. Gao X. T., Wachs I. E.; Catalysis Today, 51(2), 233-254, 1999.

186. Davis R. J., Liu Z. F.; Chemistry Of Materials, 9(11), 2311-2324, 1997.

187. Manoilova O. V., Olindo R., Arean C. O., Lercher J. A.; Catalysis Communications, 8, 865-870, 2007.

188. Palkhiwala A. G., Gorte R. J.; Catalysis Letters, 57, 19–23, 1999.

189. Lacey M. J., Macdonal C., Pross A., Shannon J. S.; Australian Journal of Chemistry, 23(7), 1421-&, 1970.

APPENDIX A

FREE ENERGY AND ENTHALPY CALCULATIONS

Constants for variable temperature heat capacities for reactants and products:

$$C_{ppBr2} := \begin{pmatrix} 33.86 \\ 0.01125 \\ -1.192 \cdot 10^{-5} \\ 4.534 \cdot 10^{-9} \end{pmatrix} \quad C_{ppCH4} := \begin{pmatrix} 19.875 \\ 5.021 \cdot 10^{-2} \\ 1.268 \cdot 10^{-5} \\ -11.004 \cdot 10^{-9} \end{pmatrix}$$

$$C_{ppCH3Br} := \begin{pmatrix} 14.43 \\ 0.1091 \\ -5.401 \cdot 10^{-5} \\ 1.0 \cdot 10^{-8} \end{pmatrix} \quad C_{ppCH2Br2} := \begin{pmatrix} 25.0 \\ 0.2517 \\ -1.833 \cdot 10^{-4} \\ 5.646 \cdot 10^{-8} \end{pmatrix} \quad C_{ppHBr} := \begin{pmatrix} 30.65 \\ -9.462 \cdot 10^{-3} \\ 1.722 \cdot 10^{-5} \\ -6.238 \cdot 10^{-9} \end{pmatrix}$$

Temperature dependency of the heat capacities for reactants and products:

$$C_{pHBr}(T) := \left(C_{ppHBr\,0}\right) + \left(C_{ppHBr\,1}\right) \cdot T + \left(C_{ppHBr\,2}\right) \cdot T^2 + \left(C_{ppHBr\,3}\right) \cdot T^3$$

$$C_{pBr2}(T) := \left(C_{ppBr2\,0}\right) + \left(C_{ppBr2\,1}\right) \cdot T + \left(C_{ppBr2\,2}\right) \cdot T^2 + \left(C_{ppBr2\,3}\right) \cdot T^3$$

$$C_{pCH3Br}(T) := \left(C_{ppCH3Br\,0}\right) + \left(C_{ppCH3Br\,1}\right) \cdot T + \left(C_{ppCH3Br\,2}\right) \cdot T^2 + \left(C_{ppCH3Br\,3}\right) \cdot T^3$$

$$C_{pCH4}(T) := \left(C_{ppCH4\,0}\right) + \left(C_{ppCH4\,1}\right) \cdot T + \left(C_{ppCH4\,2}\right) \cdot T^2 + \left(C_{ppCH4\,3}\right) \cdot T^3$$

$$C_{pCH2Br2}(T) := \left(C_{ppCH2Br2\,0}\right) + \left(C_{ppCH2Br2\,1}\right) \cdot T + \left(C_{ppCH2Br2\,2}\right) \cdot T^2 + \left(C_{ppCH2Br2\,3}\right) \cdot T^3$$

Bromination reactions:

1. $CH_4 + Br_2 \longrightarrow CH_3Br + HBr$
2. $CH_3Br + Br_2 \longrightarrow CH_2Br_2 + HBr$
3. $CH_2Br_2 + Br_2 \longrightarrow CHBr_3 + HBr$

Standart Gibbs' Free enegies and the Enthalpies of the reactions:

$$\Delta H_{0rxn1} := -28.3 \cdot 10^3 \qquad \Delta H_{0rxn2} := -70.6 \cdot 10^3 \qquad \Delta H_{0rxn3} := -11.3 \cdot 10^3$$

$$\Delta G_{0rxn1} := -32.5 \cdot 10^3 \qquad \Delta G_{0rxn2} := -40.79 \cdot 10^3 \qquad \Delta G_{0rxn3} := -37.91 \cdot 10^3$$

Gas Constant:

$$R := 8.314$$

Standard Temperature in Kelvin:

$$T_0 := 298.15$$

Enthalpies of reactions at different temperatures:

$$\Delta H_{rxn1}(T) := 10^{-3} \left[\Delta H_{0rxn1} + \int_{298.15}^{T} \left(C_{pCH3Br}(t) + C_{pHBr}(t) - C_{pCH4}(t) - C_{pBr2}(t) \right) dt \right]$$

$$\Delta H_{rxn2}(T) := 10^{-3} \left[\Delta H_{0rxn2} + \int_{298.15}^{T} \left(C_{pCH2Br2}(t) + C_{pHBr}(t) - C_{pCH3Br}(t) - C_{pBr2}(t) \right) dt \right]$$

$$\Delta H_{rxn3}(T) := \Delta H_{0rxn3} \cdot 10^{-3} \qquad \text{....Constant} \Delta H_{rxn} \text{ assumption}$$

Logarithm of the equilibrium constants at standard states:

$$\ln K1_0 := \frac{-\Delta G_{0rxn1}}{R \cdot T_0} \qquad \ln K2_0 := \frac{-\Delta G_{0rxn2}}{R \cdot T_0} \qquad \ln K3_0 := \frac{-\Delta G_{0rxn3}}{R \cdot T_0}$$

Calculation of equilibrium constants of the reactions at different temperatures according to van't Hoff equation:

$$K_1(T) := e^{\ln K1_0 + \frac{1}{R} \cdot \int_{298}^{T} \frac{\Delta H_{0rxn1} + \int_{298.15}^{T} \left(C_{pCH3Br}(t) + C_{pHBr}(t) - C_{pCH4}(t) - C_{pBr2}(t)\right) dt}{T^2} \, dT}$$

$$K_2(T) := e^{\ln K2_0 + \frac{1}{R} \cdot \int_{298}^{T} \frac{\Delta H_{0rxn2} + \int_{298.15}^{T} \left(C_{pCH2Br2}(t) + C_{pHBr}(t) - C_{pCH3Br}(t) - C_{pBr2}(t)\right) dt}{T^2} \, dT}$$

$$K_3(T) := e^{\left[\ln K3_0 - \frac{\Delta H_{0rxn3}}{R} \cdot \left(\frac{1}{T} - \frac{1}{T_0}\right)\right]}$$

Gibbs' Free Energies of the reactions at different temperatures:

$$\Delta G_{rxn1}(T) := -\left(R \cdot T \cdot \ln\left(K_1(T)\right) \cdot 10^{-3}\right)$$

$$\Delta G_{rxn2}(T) := -\left(R \cdot T \cdot \ln\left(K_2(T)\right) \cdot 10^{-3}\right)$$

$$\Delta G_{rxn3}(T) := -\left(R \cdot T \cdot \ln\left(K_3(T)\right) \cdot 10^{-3}\right)$$

APPENDIX B

MATLAB PROGRAM CODE FOR CONVERSION CALCULATIONS

```
1    function v
2
3    CAo=input('initial concentration of methane:');
4    Q=input('initial bromine to methane ratio:');
5    T1=input('Initial Temperature :');
6    T2=input('Final Temperature :');
7    TStep=input('increment in temperature :');
8    t1=input('initial residence time :');
9    t2=input('final residence time :');
10   tstep=input('increment in residence time :');
11   for t=t1:tstep:t2
12       ttj=((t-t1)/tstep)+1;
13       tj=round(ttj);
14       eex=0;
15       xx1=0.0001;
16       for T=T1:TStep:T2
17               j=(T-T1)/TStep+1;
18               TT(j)=T;
19               k1(j,tj)=6*(10^13)*exp(-76060/(8.314*(T+273)));
20               k2(j,tj)=1.67*(10^13)*exp(-66320/(8.314*(T+273)));
```

```
21          K(j,tj)=2*(10^-36)*exp(0.085*(T+273));
22          %tj
23          XA(j,tj)=1.0;
24          x2(j,tj)=0.0000001;
25          for ex=eex:0.001:0.999
26                  %ex
27                      for x1=xx1:0.0001:0.9999
28                          if abs(k1(j,tj)*t*(1-x1)*sqrt(K(j,tj)*(Q-x1-
       ex)*CAo)-x1)<0.01
29                                  XA(j,tj)=x1;
30                                  xx1=XA(j,tj);
31                                  break
32                          end
33                      end
34                      x(j,tj)=k1(j,tj)*t*CAo*(1-
       XA(j,tj))*sqrt(K(j,tj)*CAo*(Q-  XA(j,tj))));
35                      xx(j,tj)=1+k2(j,tj)*t*sqrt(K(j,tj)*CAo*(Q-XA(j,tj)));
36                      xx2(j,tj)=CAo*XA(j,tj)-x(j,tj)/xx(j,tj);
37                      if abs(xx2(j,tj)-ex)<0.01
38                          x2(j,tj)=xx2(j,tj);
39                          if x2(j,tj)<0.0
40                                  x2(j,tj)=0.000001;
41                          end
42                          eex=x2(j,tj);
43                          break
44                      end
45          end
46          XA;
47          x2;
48          CD(j,tj)=CAo*XA(j,tj)-x2(j,tj);
```

```
49        CA(j,tj)=CAo*(1-XA(j,tj));
50        CC(j,tj)=CAo*XA(j,tj)+x2(j,tj);
51        %CB(j,tj)=CAo*(Q-XA(j,tj));
52        CB(j,tj)=CAo*(Q-XA(j,tj))-x2(j,tj);
53        yield(j,tj)=CD(j,tj)/(Q*CAo)*100;
54        Ovsel(j,tj)=CD(j,tj)/(CAo*XA(j,tj))*100;
55        Rsel(j,tj)=CD(j,tj)/x2(j,tj);
56        Psel(j,tj)=(k1(j,tj)*CA(j,tj)*sqrt(K(j,tj)*CB(j,tj))-
   (k2(j,tj)*CD(j,tj)*sqrt(K(j,tj)*CB(j,tj))))/(k2(j,tj)*CD(j,tj)*sqrt(K(j,tj)*CB
   (j,tj)));
57        %PPsel(j,tj)=(k1(j,tj)*CA(j,tj)*sqrt(K(j,tj)*CBB(j,tj))-
   (k2(j,tj)*CD(j,tj)*sqrt(K(j,tj)*CBB(j,tj))))/(k2(j,tj)*CD(j,tj)*sqrt(K(j,tj)*C
   BB(j,tj)));
58     end
59     XA
60   end
61   %XA
62   %x2
63   figure;
64   plot(TT,CD(:,1),'r',TT,x2(:,1),'g',TT,CA(:,1),'b',TT,CB(:,1),'c')
65   title('Concentration of Species for Initial Residence Time vs. T')
66   legend('CH3Br','CH2Br2','CH4','Br2',1)
67   grid on
68   figure;
69   plot(TT,CD(:,2),'r',TT,x2(:,2),'g',TT,CA(:,2),'b',TT,CB(:,2),'c')
70   title('Concentration of Species for Second Residence Timevs. T')
71   legend('CH3Br','CH2Br2','CH4','Br2',1)
72   grid on
73   figure;
74   plot(TT,CD(:,3),'r',TT,x2(:,3),'g',TT,CA(:,3),'b',TT,CB(:,3),'c')
```

```
75   title('Concentration of Species for Third Residence Time vs. T')

76   legend('CH3Br','CH2Br2','CH4','Br2',1)

77   grid on

78   igure;

79   plot(TT,CD(:,4),'r',TT,x2(:,4),'g',TT,CA(:,4),'b',TT,CB(:,4),'c')

80   title('Concentration of Species for Fourth Residence Timevs. T')

81   legend('CH3Br','CH2Br2','CH4','Br2',1)

82   grid on

83   figure;

84   plot(TT,Ovsel(:,1),'r',TT,Ovsel(:,2),'g',TT,Ovsel(:,3),'b',TT,Ovsel(:,4),'c')

85   title('% Overall Selectivity vs. T for Different Residence Times')

86   legend('t1','t2','t3','t4',1)

87   grid on

88   figure;

89   plot(TT,yield(:,1),'r',TT,yield(:,2),'g',TT,yield(:,3),'b',TT,yield(:,4),'c')

90   title('% Yield vs. T for Different Residence Times')

91   legend('t1','t2','t3','t4',2)

92   grid on

93   figure;

94   plot(TT,Rsel(:,1),'r',TT,Rsel(:,2),'g',TT,Rsel(:,3),'b',TT,Rsel(:,4),'c')

95   title('Relative Selectivity vs. T for Different Residence Time')

96   legend('t1','t2','t3','t4',1)

97   grid on

98   figure

99   plot(TT,Psel(:,1),'r',TT,Psel(:,2),'g',TT,Psel(:,3),'b',TT,Psel (:,4),'c')

100  title('Point Selectivity vs. T for Different Residence Time')

101  legend('t1','t2','t3','t4',1)

102  grid on

103  figure

104  plot(TT,100*XA(:,1),'r',TT,100*XA(:,2),'g',TT,100*XA(:,
```

```
    3),'b',TT,100*XA(:,4),'c')
105 title('Conversion of CH4 vs. T for Different Residence Time')
106 legend('t1','t2','t3','t4',2)
107 grid on
108
```

APPENDIX C

FIGURES
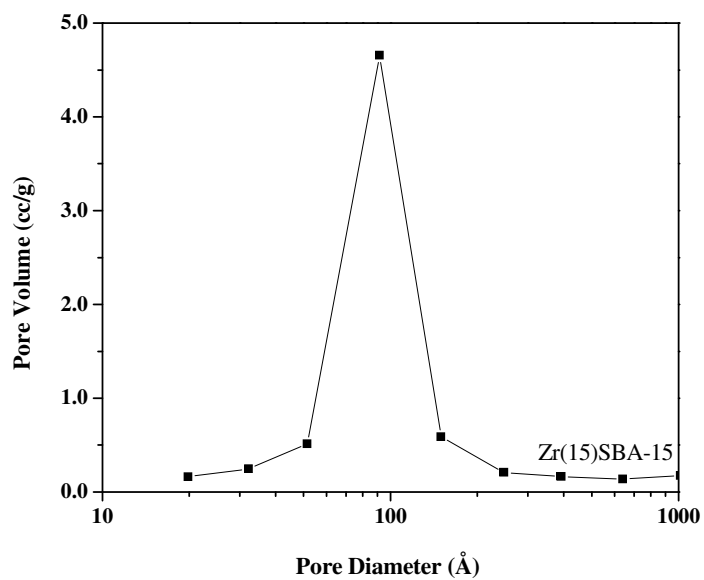
Figure C.1 BJH adsorption pore size distribution of 15 mol % zirconia included SBA-15.
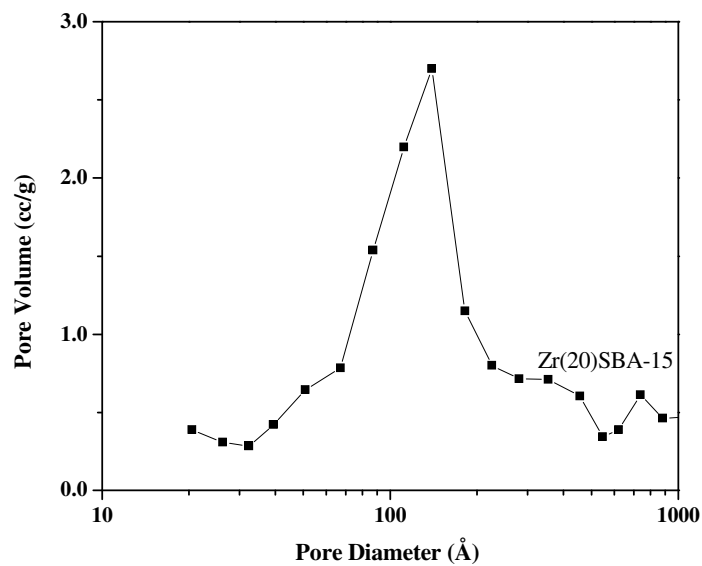
Figure C.2 BJH adsorption pore size distribution of 20 mol % zirconia included SBA-15.
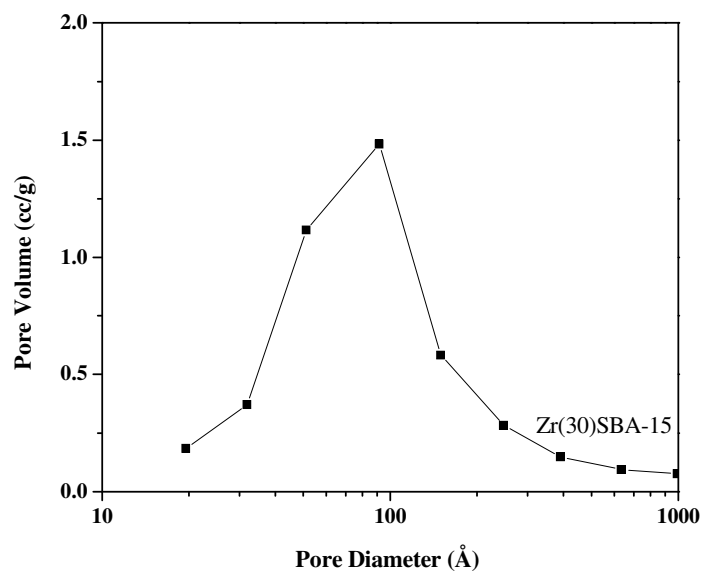
Figure C.3 BJH adsorption pore size distribution of 30 mol % zirconia included SBA-15.
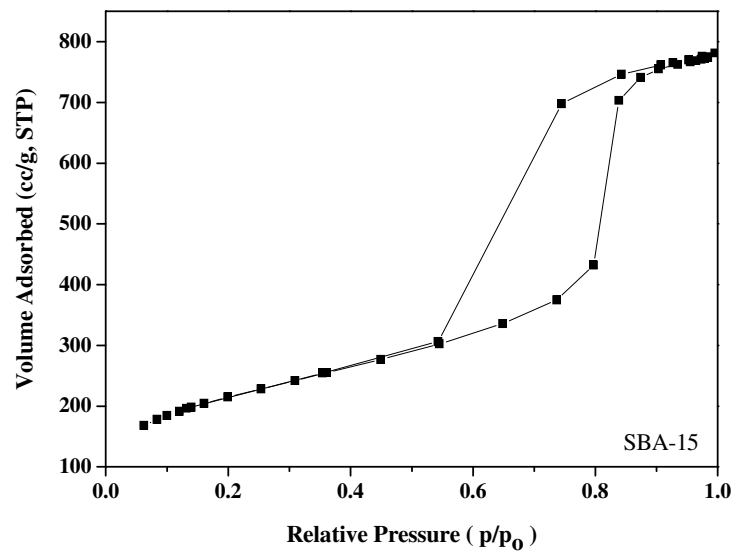
Figure C.4 Nitrogen adsorption-desorption isotherms of SBA-15.
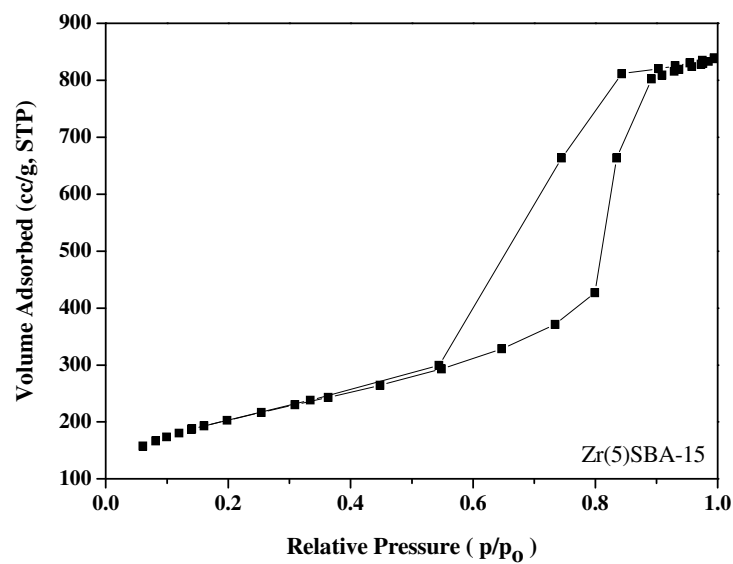
Figure C.5 Nitrogen adsorption-desorption isotherms of 5 mol % zirconia included SBA-15.
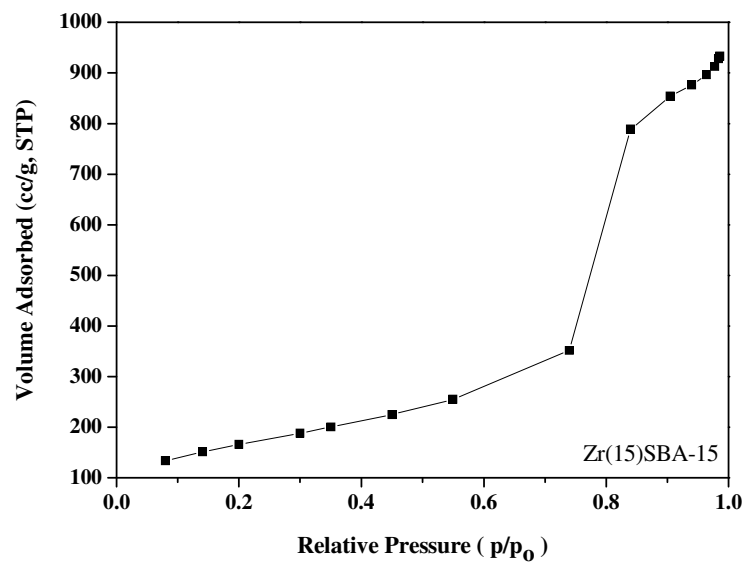
Figure C.6 Nitrogen adsorption isotherm of 15 mol % zirconia included SBA-15.
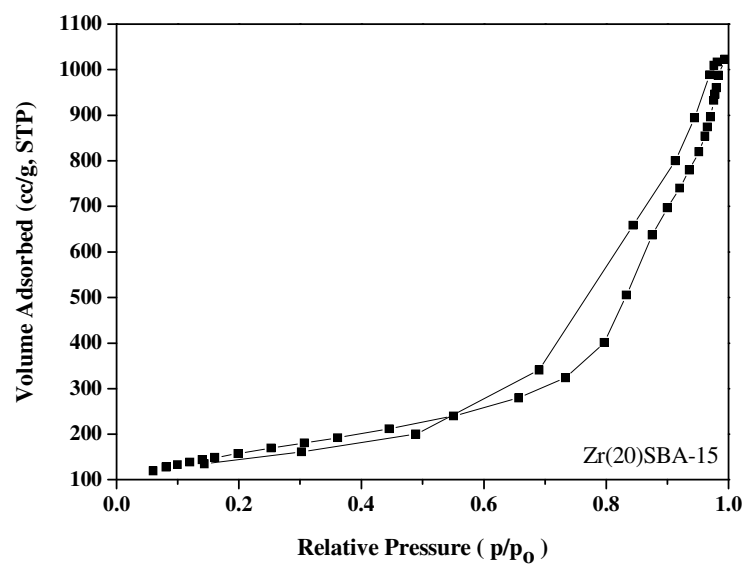
Figure C.7 Nitrogen adsorption-desorption isotherms of 20 mol % zirconia included SBA-15.
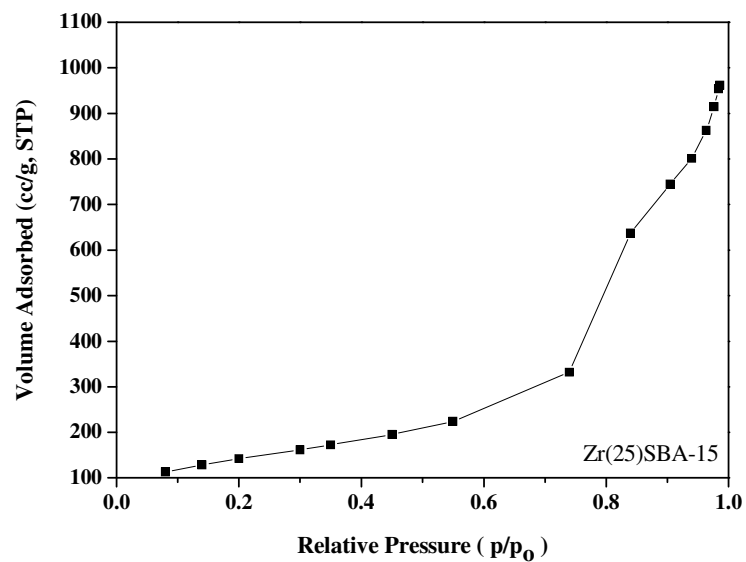
Figure C.8 Nitrogen adsorption isotherm of 25 mol % zirconia included SBA-15.
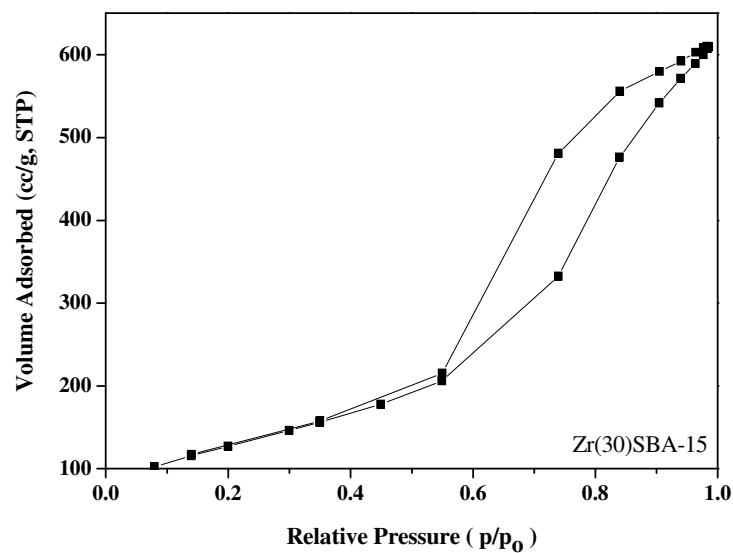
Figure C.9 Nitrogen adsorption-desorption isotherms of 30 mol % zirconia included SBA-15.
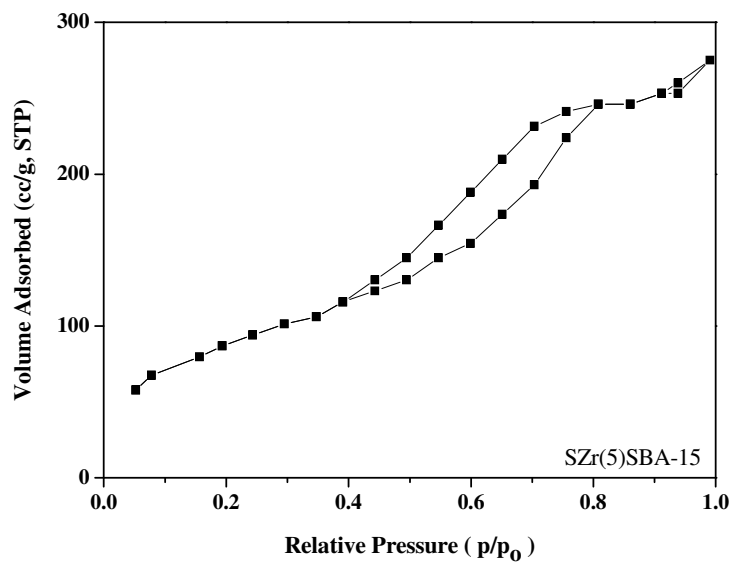
Figure C.10 Nitrogen adsorption-desorption isotherms of sulfated 5 mol % zirconia included SBA-15.
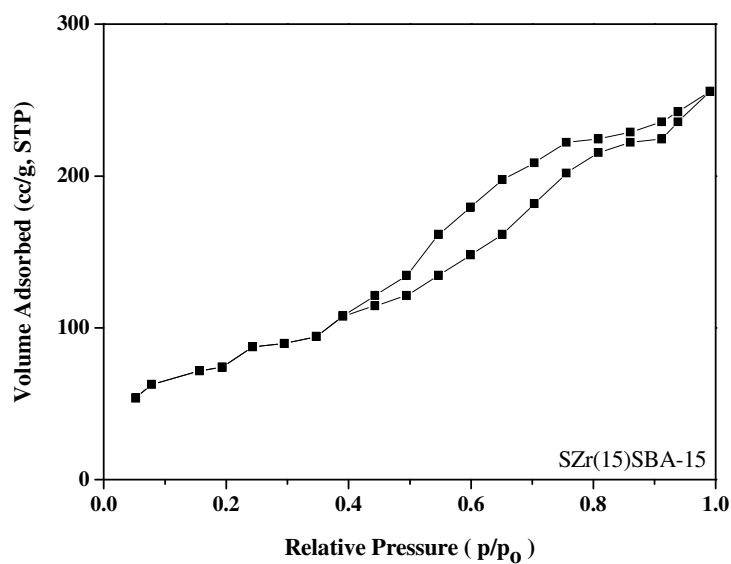
Figure C.11 Nitrogen adsorption-desorption isotherms of sulfated 15 mol % zirconia included SBA-15.
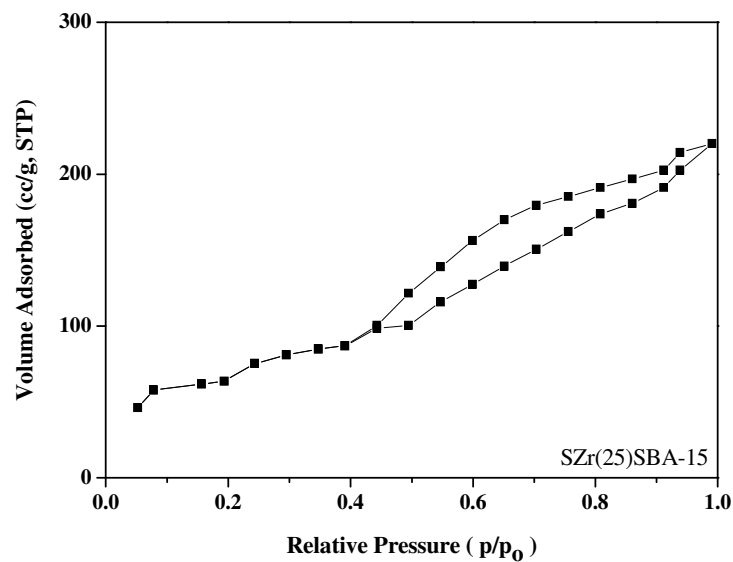
Figure C.12 Nitrogen adsorption-desorption isotherms of sulfated 25 mol % zirconia included SBA-15.
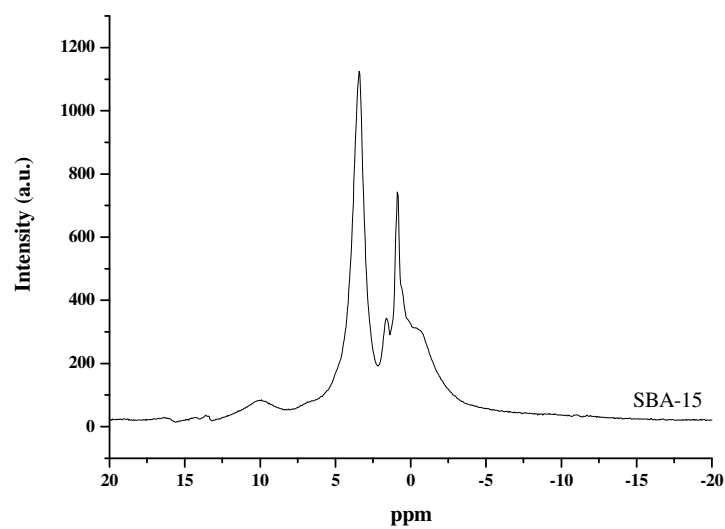
Figure C.13 ^{1}H MAS NMR Spectra of SBA-15 taken at Bruker AVANCE-400 with MAS frequency of 5 kHz at 300 K. The ppm scale is with respect to liquid TMS.
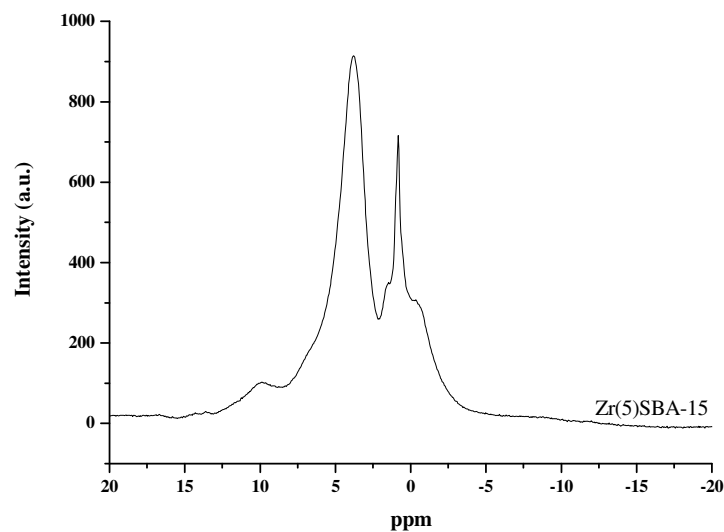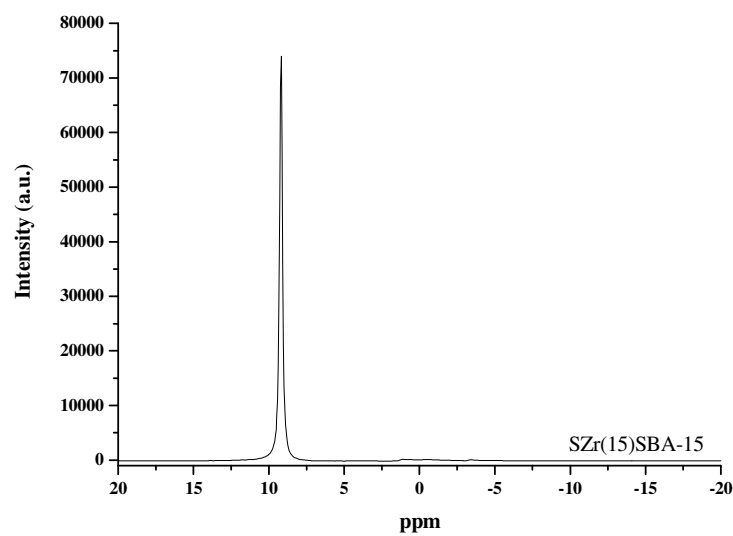
Figure C.14 ^{1}H MAS NMR Spectra of 5 mol % ZrO$_2$ included SBA-15 catalyst taken at Bruker AVANCE-400 with MAS frequency of 5 kHz at 300 K. The ppm scale is with respect to liquid TMS.
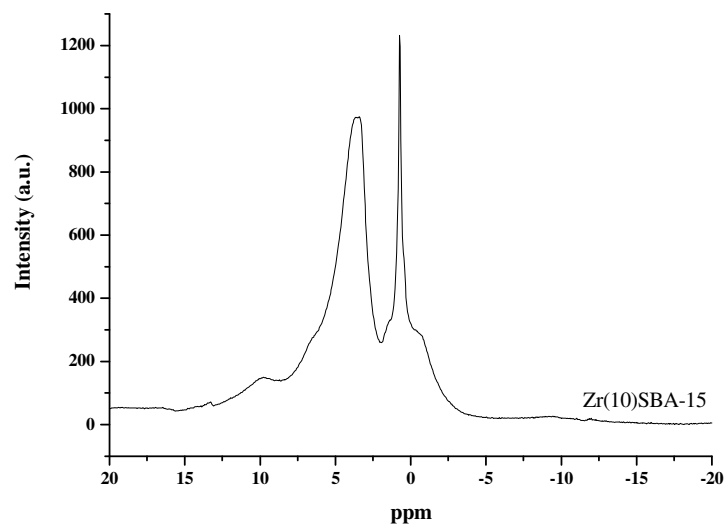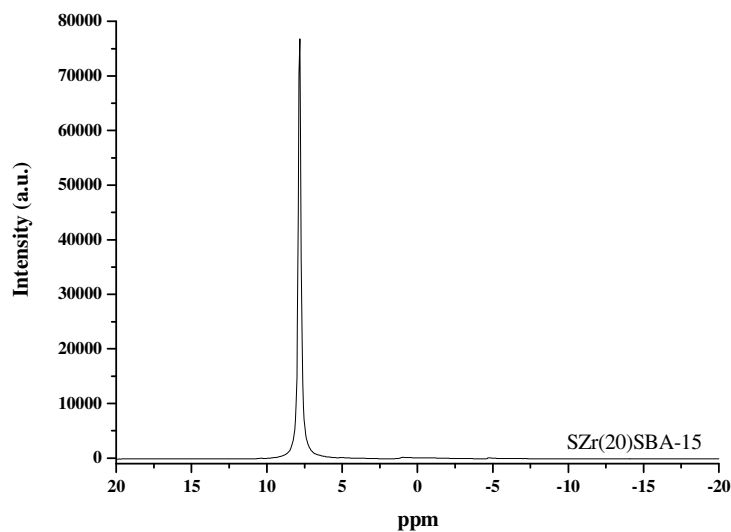

Figure C.15 ^{1}H MAS NMR Spectra of 10 mol % ZrO$_2$ included SBA-15 catalyst taken at Bruker AVANCE-400 with MAS frequency of 5 kHz at 300 K. The ppm scale is with respect to liquid TMS.
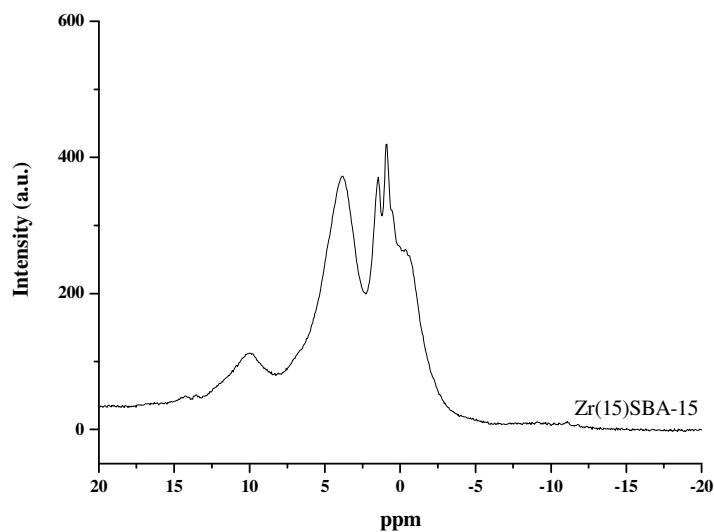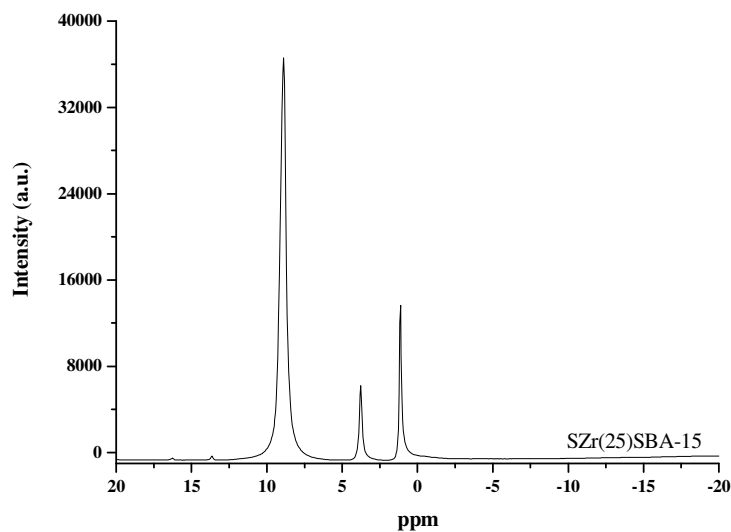
Figure C.16 ^{1}H MAS NMR Spectra of 15 mol % ZrO$_2$ included SBA-15 catalyst taken at Bruker AVANCE-400 with MAS frequency of 5 kHz at 300 K. The ppm scale is with respect to liquid TMS.
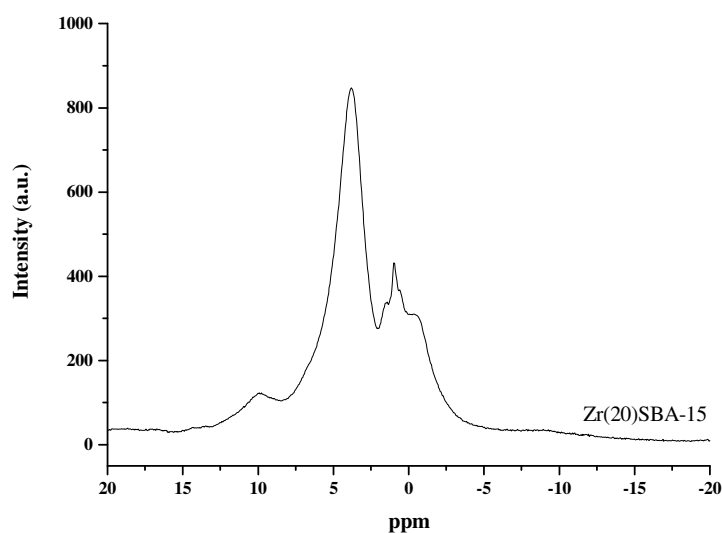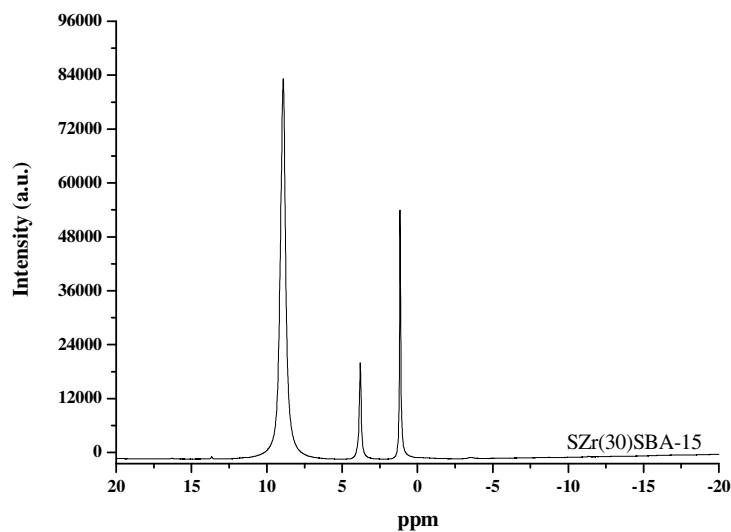

Figure C.17 ^{1}H MAS NMR Spectra of 20 mol % ZrO$_2$ included SBA-15 catalyst taken at Bruker AVANCE-400 with MAS frequency of 5 kHz at 300 K. The ppm scale is with respect to liquid TMS.
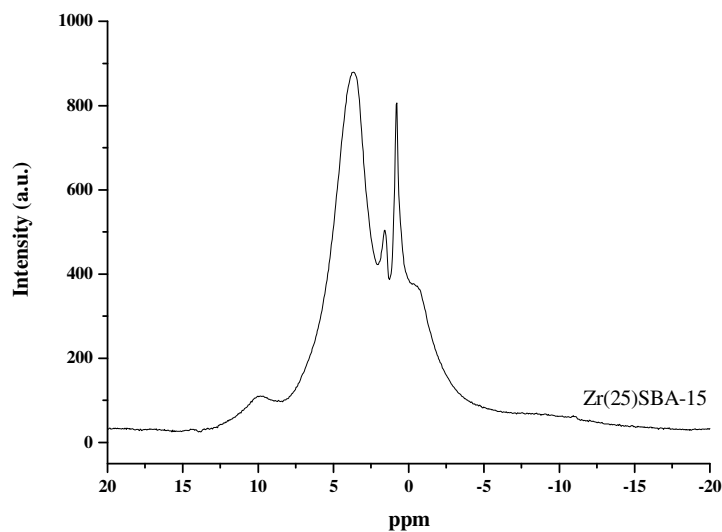
Figure C.18 ^{1}H MAS NMR Spectra of 25 mol % ZrO_2 included SBA-15 catalyst taken at Bruker AVANCE-400 with MAS frequency of 5 kHz at 300 K. The ppm scale is with respect to liquid TMS.
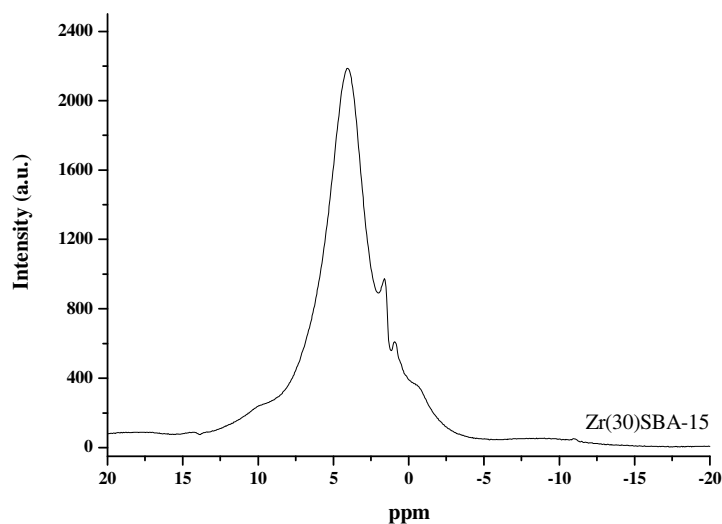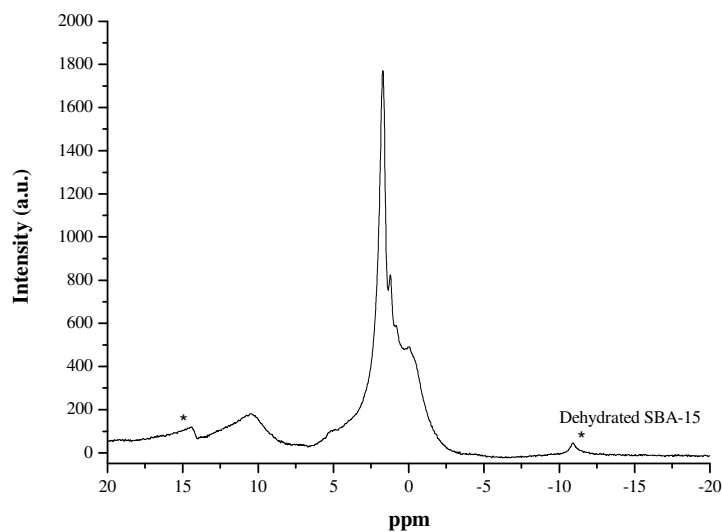

Figure C.19 ^{1}H MAS NMR Spectra of 30 mol % ZrO_2 included SBA-15 catalyst taken at Bruker AVANCE-400 with MAS frequency of 5 kHz at 300 K. The ppm scale is with respect to liquid TMS.
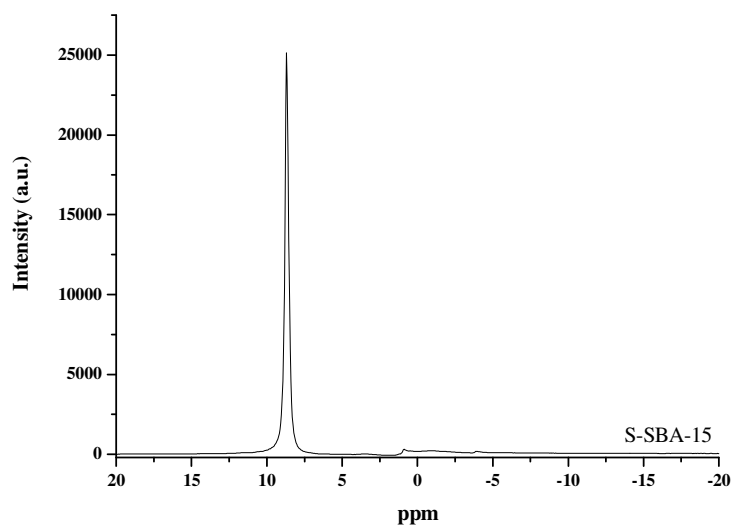
Figure C.20 ^{1}H MAS NMR Spectra of sulfated SBA-15 catalyst taken at Bruker AVANCE-400 with MAS frequency of 5 kHz at 300 K. The ppm scale is with respect to liquid TMS.
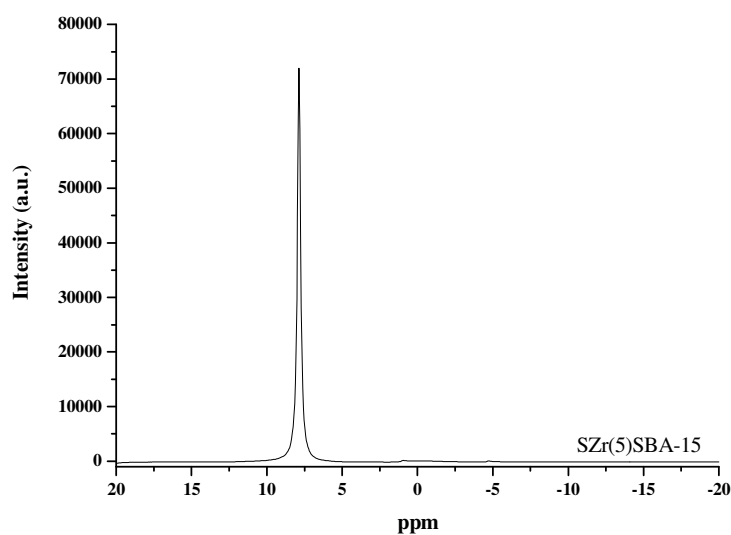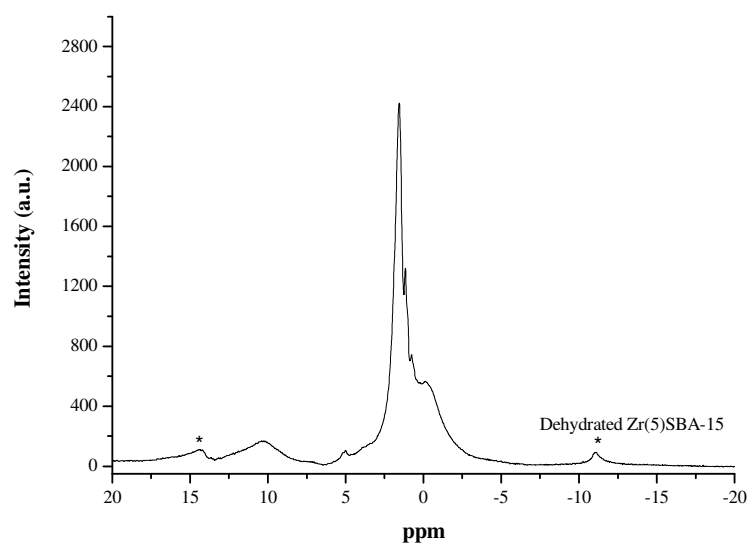

Figure C.21 ^{1}H MAS NMR Spectra of sulfated 5 mol % ZrO_2 included SBA-15 catalyst taken at Bruker AVANCE-400 with MAS frequency of 5 kHz at 300 K. The ppm scale is with respect to liquid TMS.
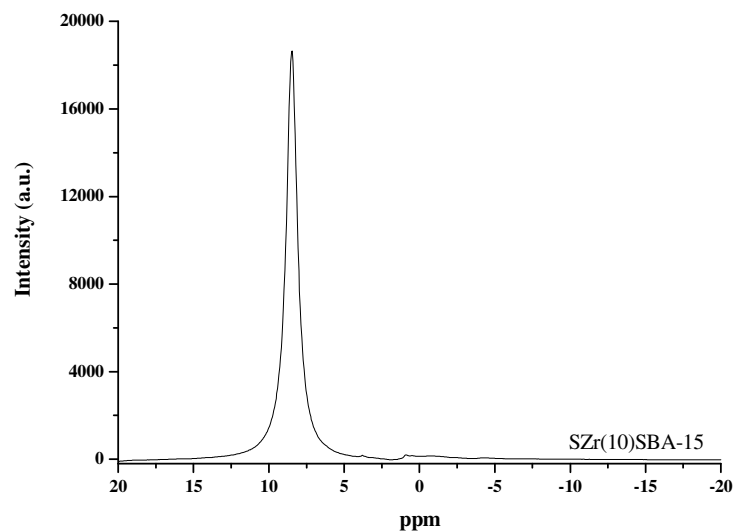
Figure C.22 ^{1}H MAS NMR Spectra of sulfated 10 mol % ZrO$_2$ included SBA-15 catalyst taken at Bruker AVANCE-400 with MAS frequency of 5 kHz at 300 K. The ppm scale is with respect to liquid TMS.
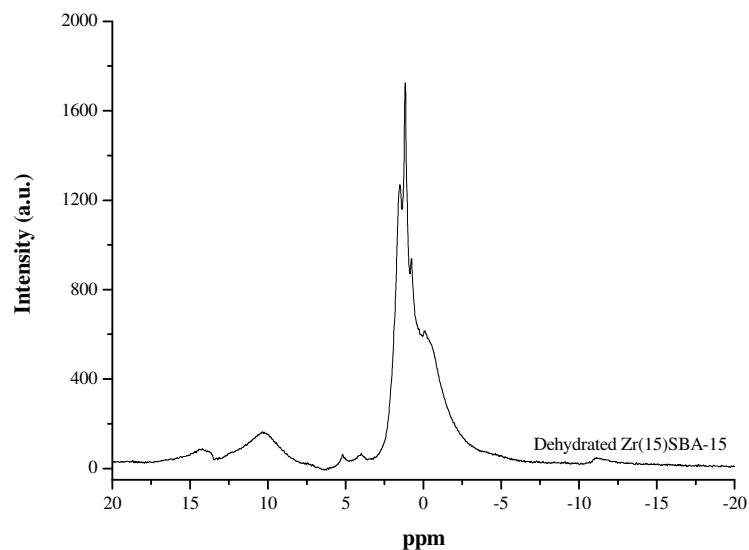

Figure C.23 ^{1}H MAS NMR Spectra of sulfated 15 mol % ZrO$_2$ included SBA-15 catalyst taken at Bruker AVANCE-400 with MAS frequency of 5 kHz at 300 K. The ppm scale is with respect to liquid TMS.

Figure C.24 ^{1}H MAS NMR Spectra of sulfated 20 mol % ZrO$_2$ included SBA-15 catalyst taken at Bruker AVANCE-400 with MAS frequency of 5 kHz at 300 K. The ppm scale is with respect to liquid TMS.
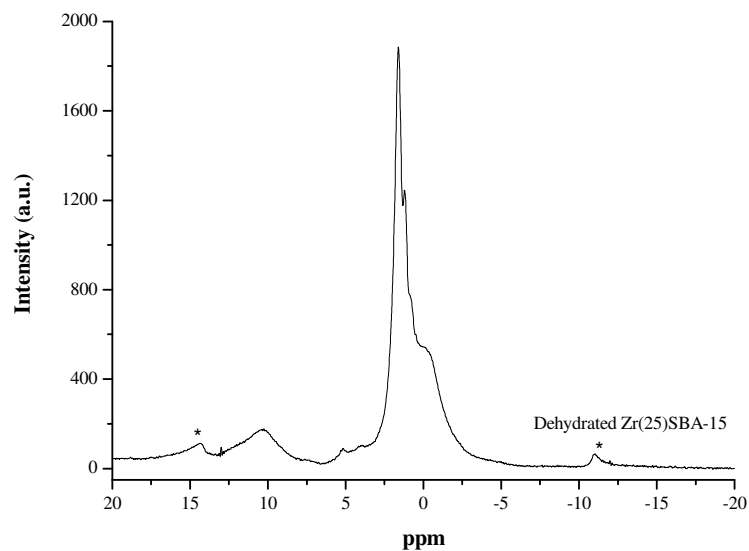

Figure C.25 ^{1}H MAS NMR Spectra of sulfated 25 mol % ZrO$_2$ included SBA-15 catalyst taken at Bruker AVANCE-400 with MAS frequency of 5 kHz at 300 K. The ppm scale is with respect to liquid TMS.

Figure C.26 ^{1}H MAS NMR Spectra of sulfated 30 mol % ZrO_2 included SBA-15 catalyst taken at Bruker AVANCE-400 with MAS frequency of 5 kHz at 300 K. The ppm scale is with respect to liquid TMS.

Figure C.27 ^{1}H MAS NMR Spectra of dehydrated SBA-15 catalyst taken at Bruker AVANCE-400 with MAS frequency of 5 kHz at 300 K. The ppm scale is with respect to liquid TMS. * stands for spinning side bands.
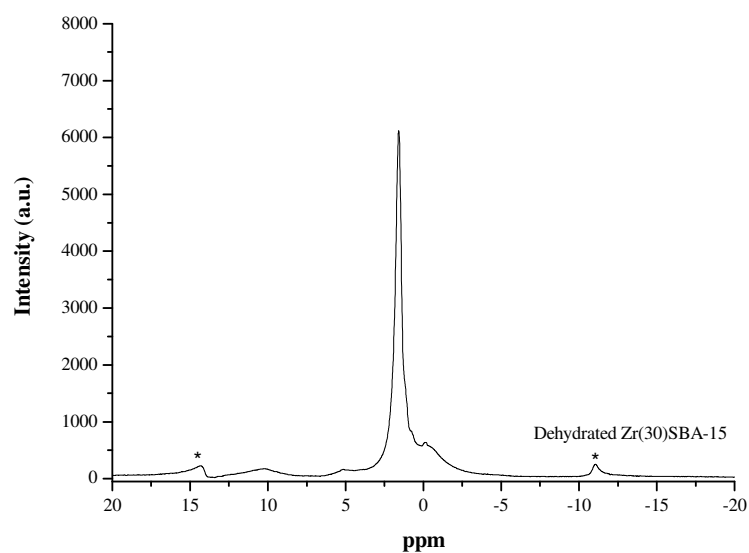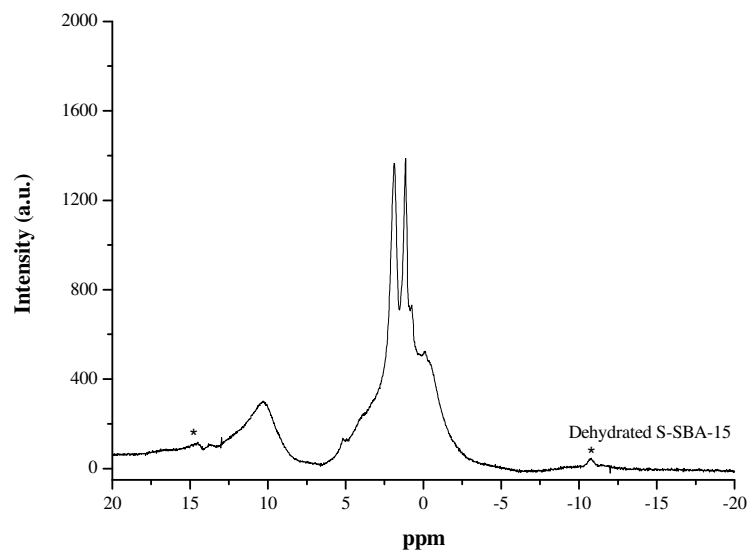
Figure C.28 ^{1}H MAS NMR Spectra of dehydrated 5 mol % ZrO$_2$ included SBA-15 catalyst taken at Bruker AVANCE-400 with MAS frequency of 5 kHz at 300 K. The ppm scale is with respect to liquid TMS. * stands for spinning side bands.
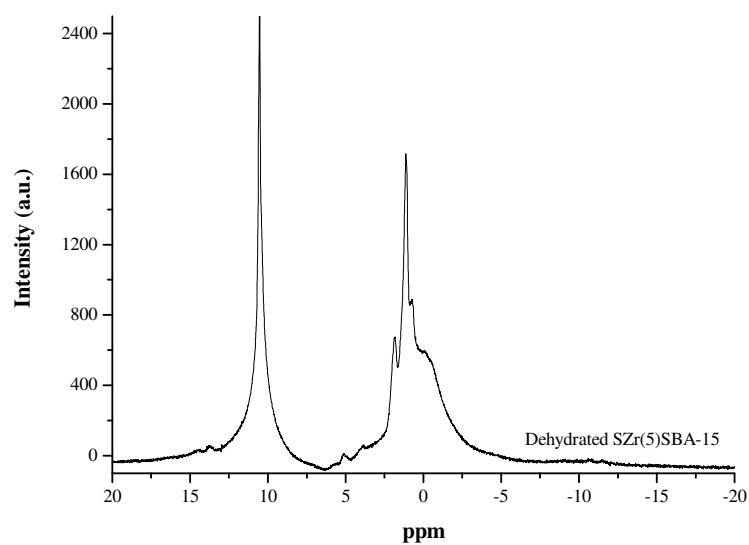

Figure C.29 ^{1}H MAS NMR Spectra of dehydrated 15 mol % ZrO$_2$ included SBA-15 catalyst taken at Bruker AVANCE-400 with MAS frequency of 5 kHz at 300 K. The ppm scale is with respect to liquid TMS.

Figure C.30 ^{1}H MAS NMR Spectra of dehydrated 25 mol % ZrO$_2$ included SBA-15 catalyst taken at Bruker AVANCE-400 with MAS frequency of 5 kHz at 300 K. The ppm scale is with respect to liquid TMS. * stands for spinning side bands.
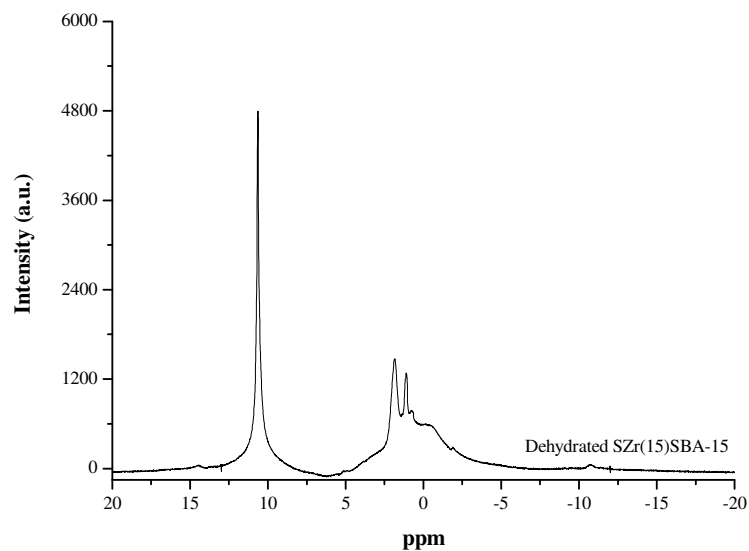

Figure C.31 ^{1}H MAS NMR Spectra of dehydrated 30 mol % ZrO$_2$ included SBA-15 catalyst taken at Bruker AVANCE-400 with MAS frequency of 5 kHz at 300 K. The ppm scale is with respect to liquid TMS. * stands for spinning side bands.
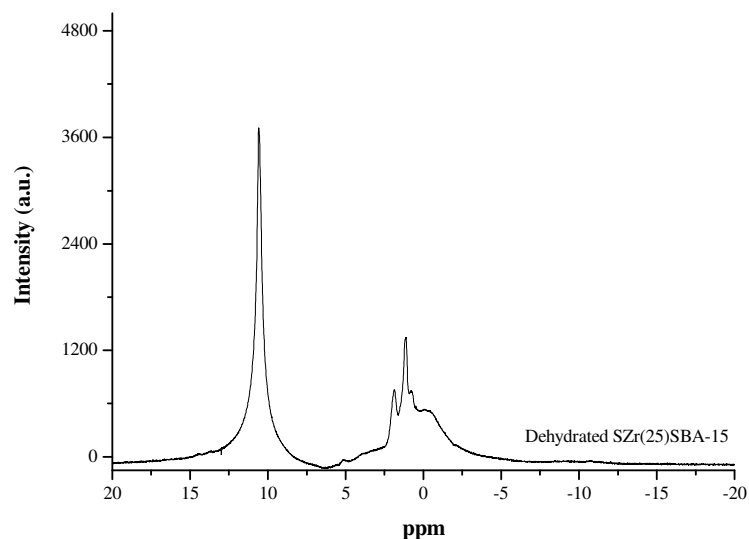
Figure C.32 ^{1}H MAS NMR Spectra of dehydrated sulfated SBA-15 catalyst taken at Bruker AVANCE-400 with MAS frequency of 5 kHz at 300 K. The ppm scale is with respect to liquid TMS. * stands for spinning side bands.

Figure C.33 ^{1}H MAS NMR Spectra of dehydrated sulfated 5 mol % ZrO_2 included SBA-15 catalyst taken at Bruker AVANCE-400 with MAS frequency of 5 kHz at 300 K. The ppm scale is with respect to liquid TMS.
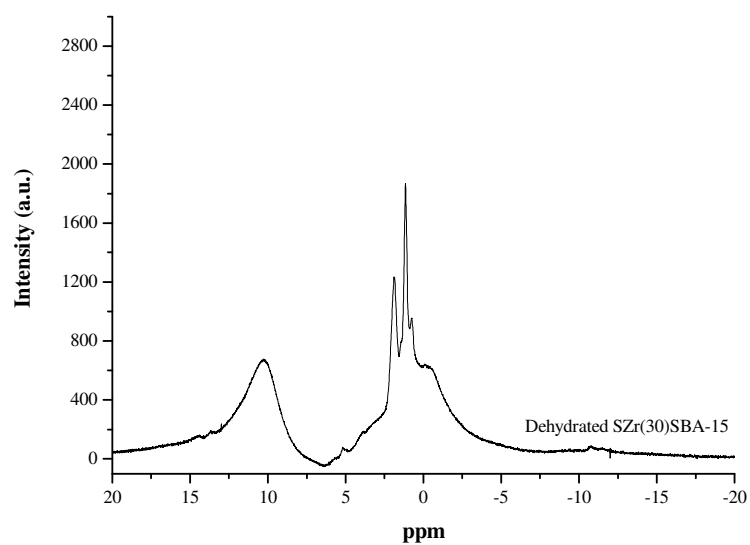
Figure C.34 ^{1}H MAS NMR Spectra of dehydrated sulfated 15 mol % ZrO$_2$ included SBA-15 catalyst taken at Bruker AVANCE-400 with MAS frequency of 5 kHz at 300 K. The ppm scale is with respect to liquid TMS.

Figure C.35 ^{1}H MAS NMR Spectra of dehydrated sulfated 25 mol % ZrO$_2$ included SBA-15 catalyst taken at Bruker AVANCE-400 with MAS frequency of 5 kHz at 300 K. The ppm scale is with respect to liquid TMS.

Figure C.36 ^{1}H MAS NMR Spectra of dehydrated sulfated 30 mol % ZrO$_2$ included SBA-15 catalyst taken at Bruker AVANCE-400 with MAS frequency of 5 kHz at 300 K. The ppm scale is with respect to liquid TMS.
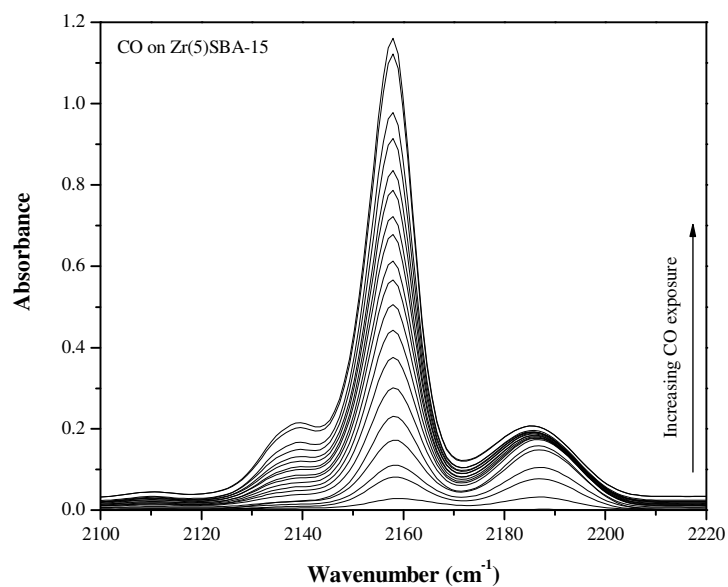

Figure C.37 FT-IR spectra of CO adsorption at 82 K over SBA-15 with 5 mol % Zirconia loading in CO stretching region.
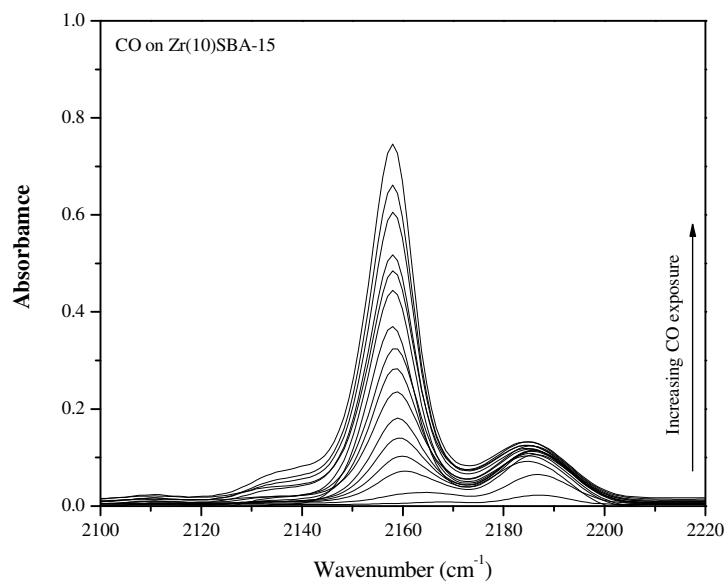
Figure C.38 FT-IR spectra of CO adsorption at 82 K over SBA-15 with 10 mol % Zirconia loading in CO stretching region.
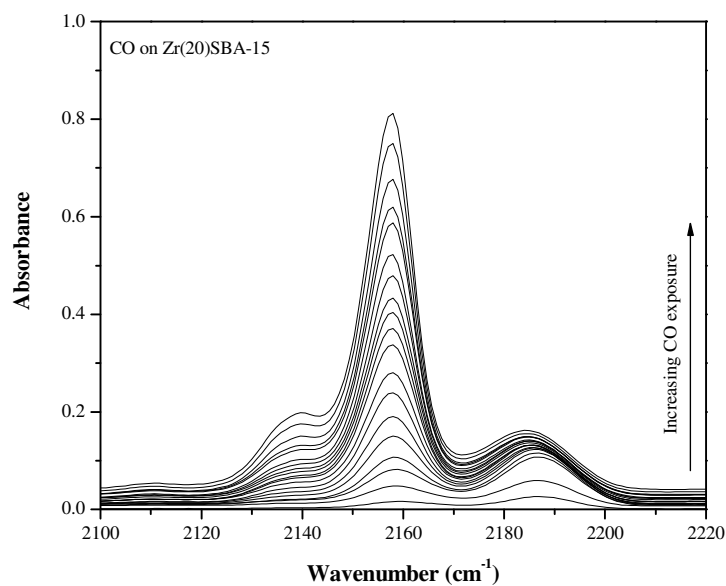

Figure C.39 FT-IR spectra of CO adsorption at 82 K over SBA-15 with 20 mol % Zirconia loading in CO stretching region.
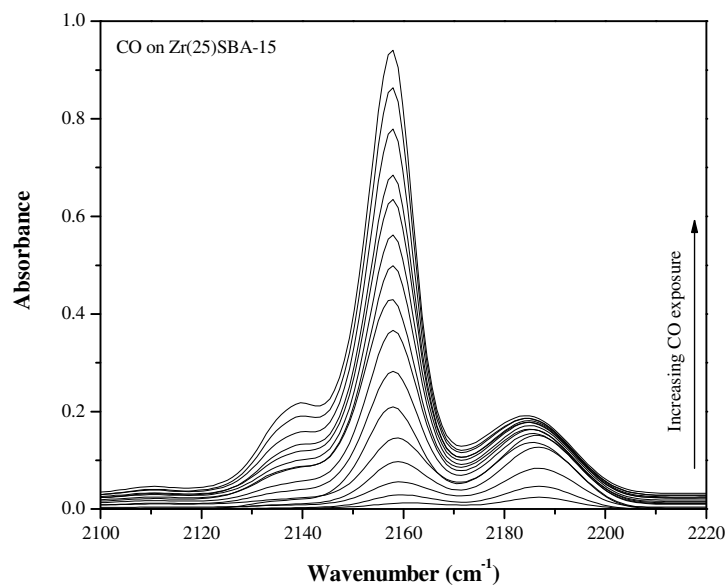
Figure C.40 FT-IR spectra of CO adsorption at 82 K over SBA-15 with 25 mol % Zirconia loading in CO stretching region.
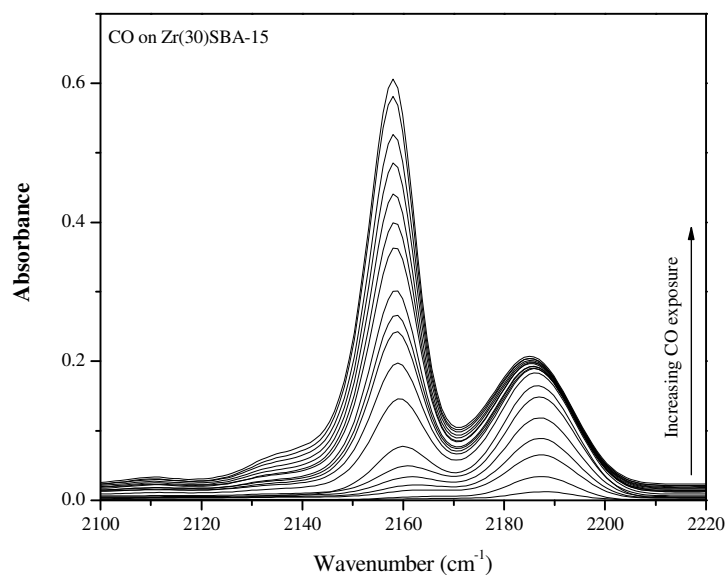

Figure C.41 FT-IR spectra of CO adsorption at 82 K over SBA-15 with 30 mol % Zirconia loading in CO stretching region.
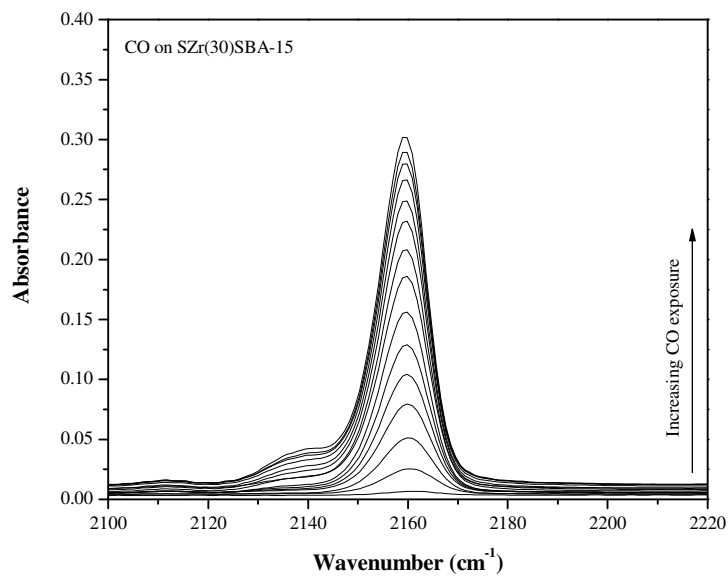
Figure C.42 FT-IR spectra of CO adsorption at 82 K over sulfated SBA-15 with 5 mol % Zirconia loading in CO stretching region.
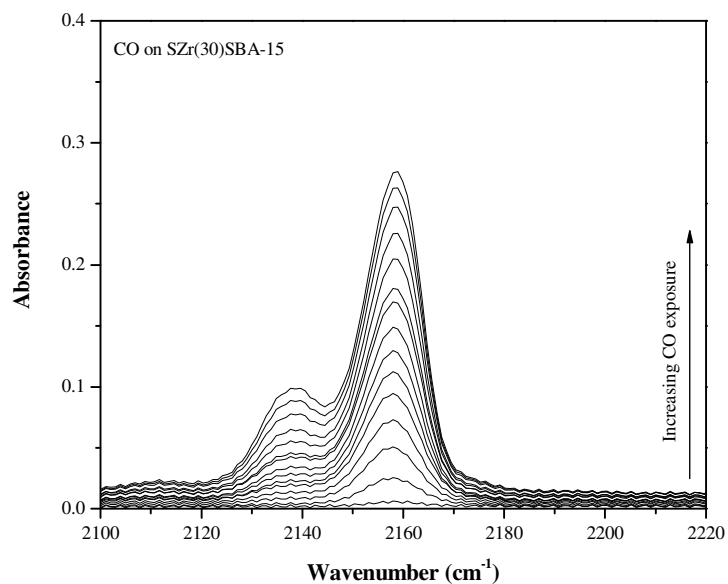

Figure C.43 FT-IR spectra of CO adsorption at 82 K over sulfated SBA-15 with 30 mol % Zirconia loading in CO stretching region.

Figure C.44 FT-IR spectra of CO adsorption at 82 K over SBA-15 with 5 mol % ZrO_2 in silanol stretching region.

Figure C.45 FT-IR spectra of CO adsorption at 82 K over SBA-15 with 10 mol % ZrO_2 in silanol stretching region.

Figure C.46 FT-IR spectra of CO adsorption at 82 K over SBA-15 with 15 mol % ZrO_2 in silanol stretching region.

Figure C.47 FT-IR spectra of CO adsorption at 82 K over SBA-15 with 20 mol % ZrO_2 in silanol stretching region.
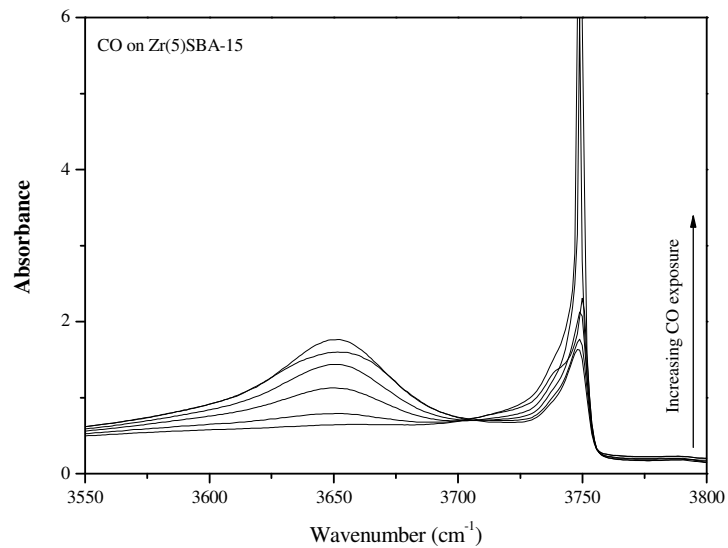
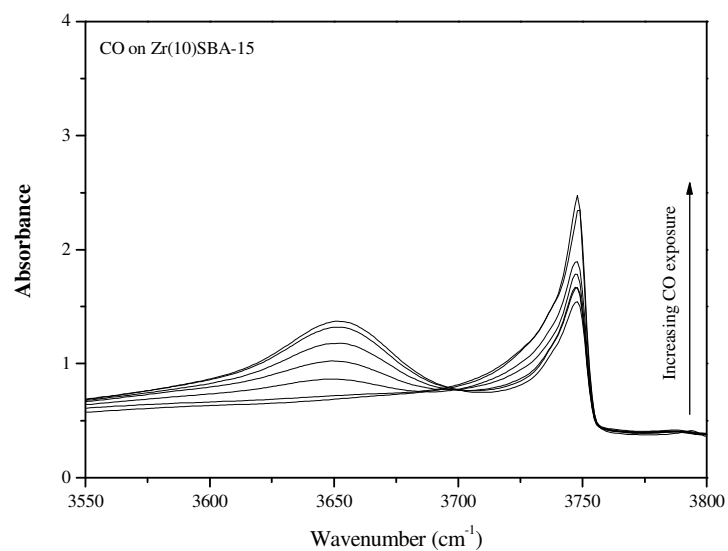Figure C.48 FT-IR spectra of CO adsorption at 82 K over SBA-15 with 25 mol % ZrO$_2$ in silanol stretching region.
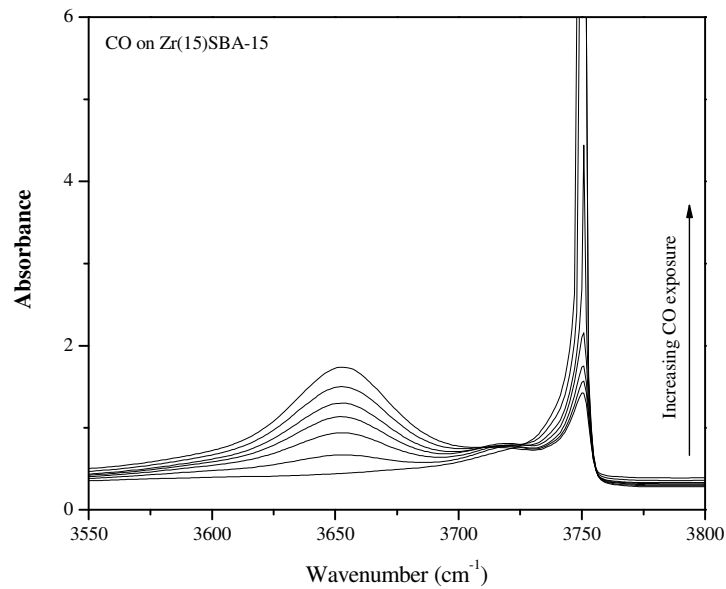

Figure C.49 FT-IR spectra of CO adsorption at 82 K over sulfated SBA-15 with 15 mol % ZrO$_2$ in silanol stretching region.
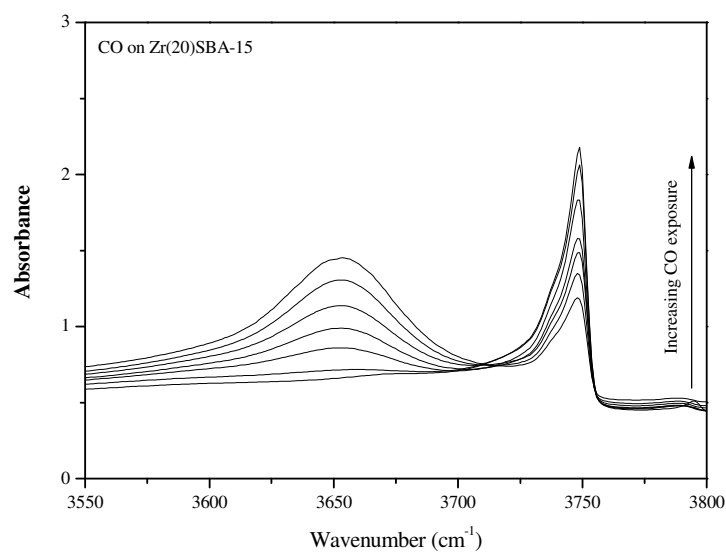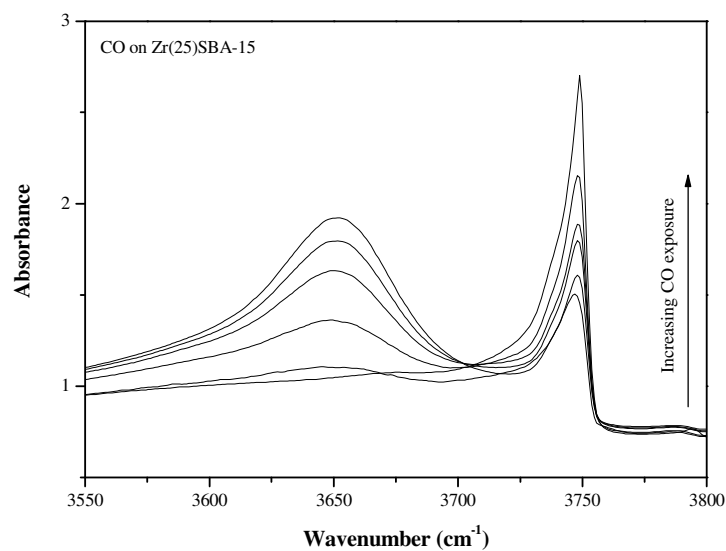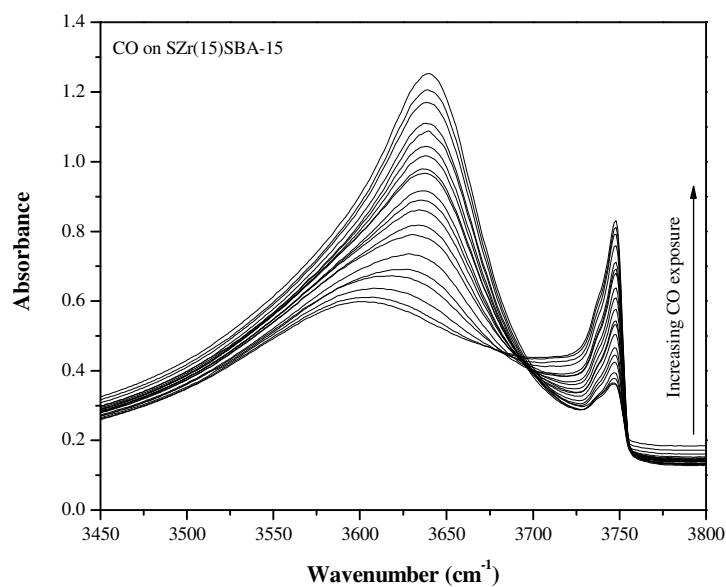
Figure C.50 FT-IR spectra of CO adsorption at 82 K over sulfated SBA-15 with 30 mol % ZrO_2 in silanol stretching region.

Figure C.51 Experimental setup.
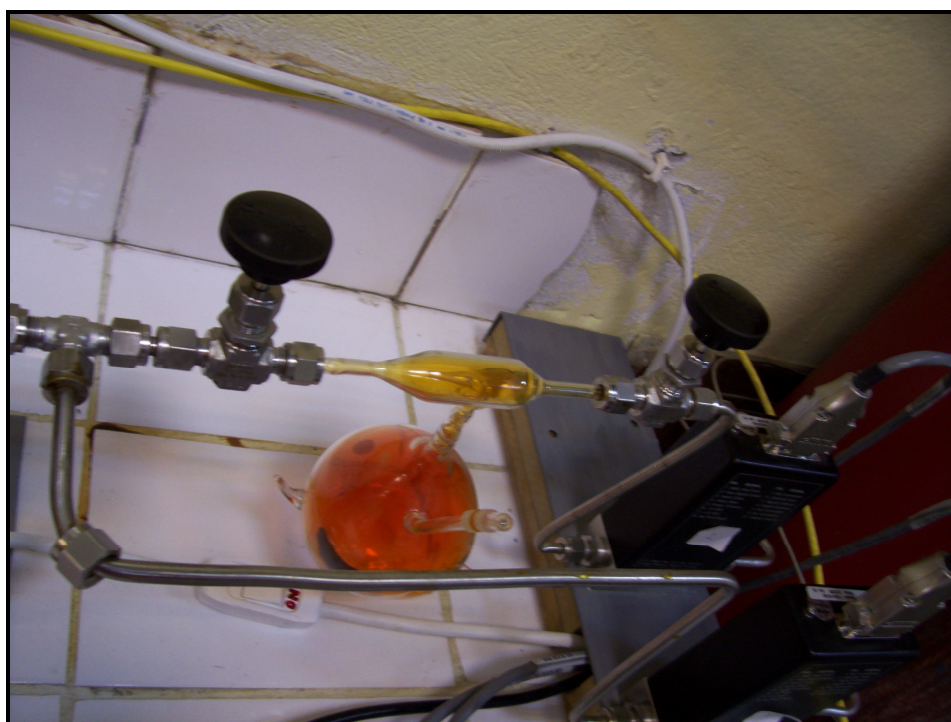
Figure C.52 Bromine feed apparatus.

APPENDIX D

UNIT CONVERSIONS

Table D.1 Energy conversion factors.

	TJ	Gcal	Mtoe	MBtu	GWh
1 TJ =	1	238.8	2.388×10^{-5}	947.8	0.2778
1 Gcal =	4.1868×10^{-3}	1	10^{-7}	3.988	1.163×10^{-3}
1 Mtoe =	4.1868×10^{4}	10^{7}	1	3.988×10^{7}	11630
1 MBtu =	1.051×10^{-3}	0.252	2.52×10^{-8}	1	2.931×10^{-4}
1 GWh =	3.6	860	8.6×10^{-5}	3412	1

Table D.2 Conversion factors for volume.

	gal (US)	gal (UK)	bbl	ft^3	l	m^3
1 gal (US) =	1	0.8327	0.02381	0.1337	3.785	0.0038
1 gal (UK) =	1.201	1	0.02859	0.1605	4.546	0.0045
1 barrel (bbl) =	42.0	34.97	1	5.615	159.0	0.159
1 ft^3 =	7.48	6.229	0.1781	1	28.3	0.0283
1 liter (l) =	0.2642	0.220	0.0063	0.0353	1	0.001
1 m^3 =	264.2	220.0	6.289	35.3147	1000	1

CURRICULUM VITAE

Volkan Değirmenci
Middle East Technical University
Department of Chemical Engineering
06531 Ankara/Turkey

Phone: +90 312 210 43 61
Fax: +90 312 210 26 00
E-mail: degirmencivolkan@gmail.com

PERSONAL INFORMATION

Nationality: Turkish (TC)
Gender: Male
Date and Place of Birth: 23 June 1980, Çanakkale

EDUCATION

Degree	Institution	Year of Graduation
Ph. D.	METU	
	Chemical Engineering	2007
B. Sc.	METU	
	Chemical Engineering	2003
High School	Çanakkale Milli Piyango	
	Anatolian High School	1998

WORK EXPERIENCE

Year	Place	Enrollment
2001 July	Akçansa Cement Industry	Internship
2002 August	Kalebodur Ceramic Tile Industry	Internship

HONORS and AWARDS

2004 – 2007	Ph.D. Scholarship, TUBİTAK
2003 December	Unilever Lipton Ice Tea Idea Trophy, Marketing Project Competition, Turkey Finalist Group Member

MEMBERSHIPS

2006 -   Catalysis Society of Turkey
1998 - 2007   Middle East Technical University Turkish Folklore Club

FOREIGN LANGUAGES

Advanced English, Beginner German and Italian

PROFESSIONAL

Year
2007 April - June, Visiting Scientist;
    Technical University of Eindhoven, Department of Chemical
    Engineering and Chemistry, Molecular Heterogeneous Catalysis,
    The Netherlands
    *"Surface characterizations of sulfated zirconia included SBA-15
    materials by low temperature CO adsorption FT-IR and iso-
    propylamine decomposition TPD studies"*

2006 January, Visiting Scientist;
    University of Leipzig, Department of Experimental Physics II, Leipzig,
    Germany
    **"*Surface characterizations of sulfated zirconia included SBA-15
    materials by ^{1}H MAS NMR"***

PUBLICATIONS

Refereed Journals:

1. V. Degirmenci, A. Yilmaz, D. Uner, E. J. M. Hensen, R. A. V. Santen, *"FT-IR and TPD investigations of sulfated zirconia included SBA-15"*, *In preparation*

2. V. Degirmenci, A. Yilmaz, D. Uner, *"Heterogeneous Kinetics of Methane Bromination over S-ZrO$_2$/SBA-15 catalysts"*, *In preparation*

3. V. Degirmenci, Ö.F. Erdem, O. Ergun, A. Yilmaz, D. Michel, D. Uner, *"Synthesis and NMR characterization of Titanium and Zirconium oxides Incorporated in SBA-15"*, Topics in Catalysis, 2007, *Accepted*

4. B. Akca, M. Can, V. Degirmenci, A. Yilmaz, D. Uner, "*Single step synthesis of mesoporous Co-Pb/SBA-15 catalysts*", Studies in Surface Science and Catalysis, 172 (2007) 317.

5. V. Degirmenci, Ö.F. Erdem, A. Yilmaz, D. Michel, D. Uner, "*Sulfated Zirconia in SBA-15 Structures with Strong Brønsted Acidity as Observed by ^1H MAS NMR Spectroscopy*", Catalysis Letters, 115 (2007*)* 79.

6. V. Degirmenci, A. Yilmaz, D. Uner, "*Methane to higher hydrocarbons via halogenation*", Catalysis Today, 106 (2005) 252.

International Conference Presentations:

1. V. Degirmenci, A. Yilmaz, D. Uner, Ö.F. Erdem, D. Michel, E.J.M. Hensen, R.A.V. Santen, "Selective methane bromination over sulfated zirconia structures in SBA-15 Structures", EuropaCat-VIII Catalysis: From theory to industrial practice, August 26-31, 2007, Turku, Finland, *Oral Presentation*.

2. V. Degirmenci, Ö.F. Erdem, A. Yilmaz, D. Michel, D. Uner, "Sulfated zirconia in mesoporous silica frame for the methatesis of halogenated methane molecules", Fifth Tokyo Conference on Advanced Catalytic Science and Technology, July 23-28, 2006, Tokyo, Japan, *Poster Presentation*.

3. B. Akca, V. Degirmenci, A. Yilmaz, D. Uner, "Preparation and Characterization of Pb and Co Incorporated Mesoporous SBA-15", International Workshop on Nanostructured Materials, June 21-23, 2006, Antalya, Turkey, *Poster Presentation*.

4. V. Degirmenci, A. Yilmaz, D. Uner, "Methane to higher hydrocarbons via halogenation", Gas-Fuel 05, November 14-16, 2005, Brugge Belgium, *Oral Presentation*.

5. V. Degirmenci, A. Yilmaz, D. Uner, "Methane Activation over SO_4^{2-}/ZrO_2 Modified SBA-15", EuropaCat -VII Catalysis: a key to a richer and cleaner society, August 28 – September 1, 2005, Sofia, Bulgaria, *Poster Presentation*.

6. V. Degirmenci, A. Yilmaz, D. Uner, "Methane Activation by Halogenation", North American Catalysis Society 19th North American

Catalysis Meeting, May 22-27, 2005, Philadelphia, Pennsylvania, USA, *Poster Presentation*.

National Conference Presentations:

1. <u>V. Degirmenci</u>, Ö.F. Erdem, A. Yilmaz, D. Michel, D. Uner, "Acidic Mesoporous Sulfated Zirconia Structures for Methane Coupling via Bromination" First National Catalysis Conference (NCC-1), January 17-20, 2007, METU Northern Cyprus Campus, Güzelyurt, *Oral Presentation*.

2. <u>V. Degirmenci</u>, Ö.F. Erdem, A. Yilmaz, D. Michel, D. Uner, "Metan Aktivasyonu için SBA-15 Tipi Nanogözenekli Malzemelerin SO_4^{2-}/ZrO_2 ile Modifiye Edilmesi", 7th National Chemical Engineering Conference, September 5-8, 2006, Anadolu University, Eskişehir, Turkey, *Poster Presentation*.

3. <u>V. Degirmenci</u>, A. Yilmaz, D. Uner, "Metan Halojenlenmesi Tepkimesinin Kinetik ve Termodinamiğinin Kuramsal İncelemesi", 6th National Chemical Engineering Conference, September 7-10, 2004, Ege University, İzmir, Turkey, *Poster Presentation*.

Summer Schools:

1. "*Solid State NMR and Recent Developments*", October 30 – November 1, 2007, Middle East Technical University Central Laboratory, Ankara, Turkey.

2. First Anatolian School on Catalysis (ASC-I), September 25 – October 6, 2006, Middle East Technical University, Ankara, Turkey, (Workshop I: *Master class Catalysis*. Workshop II: *Computational Catalysis*.)

3. 4th EFCATS School on Catalysis, "*Catalyst Design - From Molecular to Industrial Level*", September 20-24, 2006, Tsars Village (suburb of St. Petersburg), Russia.